الجمهورية الجزائرية الديمقراطية الشعبية
People's Democratic Republic of Algeria
وزارة التعليم العالي والبحث العلمي
Ministry of Higher Education and Scientific Research

Mohamed Khider University - Biskra
Faculty of Architecture, Urbanism, Civil Engineering and Hydraulic
Department: Civil and Hydraulic Engineering
Ref. :.....

جا معـة محـمد خيضـر بسكـــرة
كلية الهندسة المعمارية و العمران والهندسة المدنية و الر ي
قسـم: الهـنـدسـة الـمـدنـيـة والـــري
الـمرجع:.....

Thesis submitted for the
diploma of

Doctorate in :

Public Works

Speciality (Option) :

Roads and engineering structures

Fiber valorization in cementitious materials. Application in high-performance structural concretes for the validation of Dynamic Interaction Tests.

Presented by :

Imed GUEHLOUZ

Publicly defended on : 00/00/2025

In front of a jury composed of:

Remadna Mohamed Saddek	**Professor**	**Chair**	University of Biskra
Ben khadda Ben ammar	**MC-A**	**Supervisor**	University of Biskra
Ahmed Abderraouf Belkadi	**MC-A**	**Co-supervisor**	University of BBA
Taallah Bachir	**Professor**	**Examinateur**	University of Biskra
Kessal Oussama	**MC-A**	**Examinateur**	University of BBA
Mezghiche Bouzidi	**MC-A**	**Invite**	University of Biskra

الجمهورية الجزائرية الديمقراطية الشعبية
République Algérienne Démocratique et Populaire
وزارة التعليم العالي والبحث العلمي
Ministère de l'enseignement supérieur et de la recherche scientifique

Université Mohamed Khider – Biskra
Faculté d'architecture, d'urbanisme, de génie civil et d'hydraulique
Département : Génie Civil Et Hydraulique
Ref. :.....

جامعة محمد خيضر بسكرة
كلية الهندسة المعمارية و العمران والهندسة المدنية و الري
قسم: الهندسة المدنية والري
المرجع:.....

Mémoire en vue de l'obtention
Du diplôme de
Doctorat en :
Travaux Publics
Speciality (Option) :
Voies et Ouvrages d'Art

Valorisation des fibres dans des matériaux cimentaires. Application dans les bétons structurels à haute performance pour la validation des Essais d'interaction dynamique.

Présentée par :

Imed GUEHLOUZ

Soutenue publiquement le : 00/00/2025

Devant le jury composé de :

Remadna Mohamed Saddek	**Professor**	**Président**	University of Biskra
Ben Khadda Ben Ammar	**MC-A**	**Rapporteur**	University of Biskra
Ahmed Abderraouf Belkadi	**MC-A**	**Rapporteur**	University of BBA
Taallah Bachir	**Professor**	**Examinateur**	University of Biskra
Kessal Oussama	**MC-A**	**Examinateur**	University of BBA
Mezghiche Bouzidi	**MC-A**	**Invité**	University of Biskra

Dedication

To my beloved family and cherished friends, this journey would not have been possible without you.

To my father, Khamisi, whose steadfast strength and quiet encouragement have been my anchor through every storm thank you for showing me what it means to persevere with grace. To my mother, Fatiha, whose boundless love and unwavering belief in me turned every obstacle into opportunity.

To my wife, whose resilience and laughter have been my guiding light this journey would not exist without your unwavering support. To my son aous and my daughter Iline, whose curiosity and joy remind me daily why this work matters you are my joy and my greatest inspiration.

To my sisters, Samia, Bouchra, Ahlam, Khadidja, and Aya El Rahman, whose fierce loyalty and shared memories have been my refuge thank you for your laughter and light and I could not have asked for a better companion on this journey. To their children, Tasnim, Raounak, Yazan, Djouri, Ousaid, Mouhamed,wassim whose vibrant spirits fill our lives with hope you are the legacy I strive to honor.

And to my friends, whose camaraderie and late-night encouragement proved that even solitude is shared when hearts are aligned thank you for walking this path beside me. This thesis is a testament to your collective strength, and I am forever grateful for the privilege of carrying your love with me.

Acknowledgements

This thesis is thanks to those who have provided unwavering support and guidance throughout my academic journey. Their contributions have been invaluable and have profoundly shaped the completion of this work.I extend my deepest gratitude to my family, whose love and encouragement have been a constant source of strength. Their belief in my abilities and their unwavering support have been instrumental in my pursuit of this academic milestone. .I would also like to express my profound appreciation to my advisors, BEN KHADDA ben ammar ,and AHMED ABDERRAOUF belkhadi, whose expertise, patience, and mentorship have been invaluable throughout this research. Their guidance has not only shaped this thesis but has also contributed significantly to my professional development. I am deeply thankful for their unwavering commitment to my success.Finally, I acknowledge the contributions of my colleagues My thanks and recognition are addressed to HAMZA soualhi , BOUALEM boukazata ,HICHEM alioui,HALIM amroun,AMIROUCHE berkouch, HANI boutalbi,and MOUHAMED tamim whose camaraderie and collaborative spirit have enriched my academic experience. Their insights and support have been invaluable, and I am grateful for the many meaningful conversations and shared moments of discovery.Thank you all for your unwavering support and encouragement. This achievement is as much yours as it is mine.and for Institutions and Organizations.

I am grateful to the University of bourj bouararidj for providing a stimulating academic environment and access to essential resources. Special thanks to the Department of civil engeneering for their support and the laboratoire staff for their assistance.

I thank all the teams of the laboratories (Cergy), Hydraulic Development and Environment Laboratory (LAHE) (Biskra) and Public Works Laboratory of the East (LTPE Setif) who supported me in carrying out my research work.

I thank all the members of the administration of the University of Biskra who helped me in all my efforts.

To my committee members, I am profoundly thankful for your constructive feedback, thoughtful questions, and rigorous examination of my work. Your expertise and engagement have significantly enhanced the quality of this thesis and have provided me with invaluable insights that will inform my future research.

Abstract

This thesis investigates the impact of various fiber types on the mechanical properties, durability, and microstructural characteristics of High-Performance Concrete (HPC). The study aims to optimize fiber-reinforced HPC formulations for enhanced structural performance and sustainability. Nine concrete mixtures incorporating flax and polypropylene fibers were prepared and tested at different dosages and lengths. The mechanical properties, including compressive strength, flexural tensile strength, and split tensile strength, were evaluated alongside durability indicators such as porosity, capillary absorption, and thermal conductivity. Advanced techniques like Digital Image Correlation (DIC) and Scanning Electron Microscopy (SEM) were employed to analyze deformation behavior and microstructural integrity. Key findings indicate that fiber reinforcement significantly enhances the mechanical properties and durability of HPC, with optimal results observed at specific fiber dosages and lengths. For instance, including 0.3% flax fibers of 30 mm length (FF3030) improved compressive strength and reduced deformation under load. The study also highlights the importance of fiber surface treatment in enhancing matrix-fiber adhesion, as demonstrated by the alkaline treatment of flax fibers. While the research provides valuable insights into fiber-reinforced HPC optimization, limitations such as focusing on specific fiber types and the need for long-term durability studies are acknowledged. Future work should explore a broader range of fibers and investigate the long-term performance of fiber-reinforced HPC in real-world applications.

Keyword : Cementitious composites, plant fibers, synthetic fibers, formulation, mechanical behavior, durability, sustainable development.

ملخص

تتناول هذه الأطروحة دراسة المركبات الأسمنتية المتمثلة في الخرسانة عالية الأداء(HPC) ، مع التركيز على تقييم تأثير إضافة أنواع مختلفة من الألياف لتحسين السلوك الميكانيكي والديمومة .يهدف البحث إلى تحسين تركيب الخرسانة عالية الأداء المدعمة بالألياف، وتحديداً الألياف النباتية (الكتان) والألياف الاصطناعية (البولي بروبيلين)، بهدف تعزيز الأداء الإنشائي ودعم مبادئ التنمية المستدامة.

لتحقيق ذلك، تم تحضير ودراسة تسع خلطات خرسانية، تضمنت إضافة ألياف الكتان والبولي بروبيلين بجرعات وأطوال مختلفة. شملت الدراسة تقييمًا شاملاً للخصائص الميكانيكية (مقاومة الانضغاط، الشد بالانثناء، والشد الانشطاري)، بالإضافة إلى مؤشرات الديمومة (المسامية، الامتصاص الشعري، والموصلية الحرارية). كما تم توظيف تقنيات متقدمة مثل ارتباط الصور الرقمي (DIC) والمجهر الإلكتروني الماسح (SEM) لتحليل سلوك التشوه والبنية المجهرية للمواد.

أظهرت النتائج الرئيسية أن تدعيم الخرسانة بالألياف يعزز بشكل ملحوظ من خصائصها الميكانيكية وديمومتها، حيث لوحظت أفضل النتائج عند استخدام جرعات وأطوال محددة. على سبيل المثال، أدى دمج 0.3% من ألياف الكتان بطول 30 مم (FF3030)إلى تحسين مقاومة الانضغاط وتقليل التشوه تحت الحمل. كما أبرزت الدراسة أهمية المعالجة السطحية للألياف، وتحديدًا المعالجة القلوية لألياف الكتان، في تحسين التصاقها بالمصفوفة الأسمنتية.

ورغم أن البحث يقدم رؤى قيمة لتحسين الخرسانة عالية الأداء المدعمة بالألياف، إلا أنه يقر بوجود محددات، مثل التركيز على أنواع معينة من الألياف والحاجة إلى دراسات ديمومة طويلة الأمد. ويوصي العمل المستقبلي باستكشاف نطاق أوسع من الألياف ودراسة الأداء طويل الأمد لهذه المركبات الأسمنتية في تطبيقات واقعية.

الكلمات المفتاحية : المركبات الأسمنتية، الألياف النباتية، الألياف الاصطناعية، التركيب، السلوك الميكانيكي، الديمومة، التنمية المستدامة.

Résume

Cette thèse étudie l'impact de différents types de fibres sur les propriétés mécaniques, la durabilité et les caractéristiques microstructurales du béton à haute performance (HPC). L'étude vise à optimiser les formulations de HPC renforcées par des fibres pour améliorer les performances structurelles et la durabilité. Neuf mélanges de béton incorporant des fibres de lin et de polypropylène ont été préparés et testés à différents dosages et longueurs. Les propriétés mécaniques, notamment la résistance à la compression, la résistance à la traction par flexion et la résistance à la traction par fendage, ont été évaluées parallèlement à des indicateurs de durabilité tels que la porosité, l'absorption capillaire et la conductivité thermique. Des techniques avancées telles que la corrélation d'images numériques (DIC) et la microscopie électronique à balayage (SEM) ont été utilisées pour analyser le comportement de déformation et l'intégrité microstructurale. Les principales conclusions indiquent que le renforcement par des fibres améliore considérablement les propriétés mécaniques et la durabilité des HPC, avec des résultats optimaux observés pour des dosages et des longueurs de fibres spécifiques. Par exemple, l'inclusion de 0,3 % de fibres de lin d'une longueur de 30 mm (FF3030) a amélioré la résistance à la compression et réduit la déformation sous charge. L'étude souligne également l'importance du traitement de surface des fibres dans l'amélioration de l'adhésion matrice-fibre, comme le montre le traitement alcalin des fibres de lin. Bien que la recherche fournisse des informations précieuses sur l'optimisation des HPC renforcés par des fibres, des limites telles que la focalisation sur des types de fibres spécifiques et la nécessité d'études de durabilité à long terme sont reconnues. Les travaux futurs devraient explorer une gamme plus large de fibres et étudier les performances à long terme des HPC renforcés par des fibres dans des applications réelles.

Mots clés : Les composites cimentaires, Fibres végétales, Fibres synthétiques, Formulation, comportement mécanique, Durabilité, Développement durable.

Table of Contents

List of figures

List of tables

List of Abbreviations

HPC	Reference Mixture.
FF	flax fibers.
PP	polypropylene fibers.
FF1515	An HPC mix incorporating 0.15% (by weight of cement) of 15mm flax fibers.
FF1530	An HPC mix containing 0.30% (by weight of cement) of 15mm flax fibers.
FF1550	An HPC mix with 0.50% (by weight of cement) of 15mm flax fibers.
FF3015	An HPC mix incorporating 0.15% (by weight of cement) of 30mm flax fibers.
FF3030	An HPC mix containing 0.30% (by weight of cement) of 30mm flax fibers.
FF3050	An HPC mix with 0.50% (by weight of cement) of 30mm flax fibers.
PP1215	Contains 0.15% (by weight of cement) of 12mm polypropylene fibers.
PP1230	Contains 0.30% (by weight of cement) of 12mm polypropylene fibers.
DIC	Digital image correlate.
HPC	High-Performance Concretes.
ACI	The American Concrete Institute's standard method for regular concrete.
W	Water.
B	Binder.
SCMs	Concretes incorporating supplementary cementitious materials.
ITZ	Interfacial transition zone.
EDS	Energy-dispersive X-ray spectroscopy.
CSH	Calcium silicate hydrate.

UHPC Ultra-High-Performance Concrete.

IGH High-rise buildings.

BO Ordinary concretes .

HPFRC High-performance fiber-reinforced concrete.

SET Sand equivalent

σ Stress.

ρ Density.

φ Porosity.

ω Velocity.

M Torque

CT Computed Tomography

General Introduction

GENERAL INTRODUCTION

High-performance concrete (HPC) has become indispensable in modern construction, offering unparalleled mechanical strength, durability, and workability that address the demands of critical infrastructure projects, from high-rise buildings to marine structures. Its advanced properties, high compressive strength, reduced permeability, and resistance to chemical attack make it a cornerstone of resilient engineering. However, HPC faces persistent challenges that limit its full potential, particularly in long-term performance and sustainability. Among these, shrinkage-induced cracking, permeability, and environmental degradation pose significant threats to structural integrity and service life. These issues are compounded by the material's high cement content and low water-binder ratio, which exacerbate autogenous and drying shrinkage, leading to microcracking and reduced durability.

Researchers have explored innovative reinforcement strategies to mitigate these limitations, with fiber reinforcement emerging as a promising solution. Fibers, including natural (e.g., flax) and synthetic (e.g., polypropylene) variants, enhance HPC's mechanical resilience refers to the ability of the High-Performance Concrete (HPC) to absorb and dissipate energy when subjected to mechanical stress, thereby resisting catastrophic failure and maintaining its structural integrity. by bridging microcracks and optimizing stress distribution. Flax fibers, in particular, offer a sustainable alternative, combining high tensile strength with eco-friendly attributes, while polypropylene fibers provide chemical resistance and crack control. However, integrating these fibers into HPC requires meticulous optimization, as factors like fiber type, length, dosage, and surface treatment critically influence performance. Alkali treatment, for instance, chemically modifies fiber surfaces to improve adhesion to the cementitious matrix, reducing degradation in alkaline environments and enhancing durability.

This study investigates the impact of flax and polypropylene fibers, with varying lengths (15–30 mm for flax and 12 mm for polypropylene) and dosages (0.15%–0.50% by cement weight), on the mechanical properties, shrinkage behavior, and durability of HPC. A critical focus is placed on the role of alkali treatment in optimizing fiber-matrix interaction and mitigating shrinkage-related defects. Digital Image Correlation (DIC) technology is cutting-edge. Noncontact optical measurement tools provide nuanced insights into deformation and strain behavior, offering real-time, full-field analysis of mechanical responses.

The research objectives are multifaceted: (1) to evaluate the influence of fiber type, length, and dosage on HPC's compressive, tensile, and flexural strengths; (2) to assess the efficacy of alkali treatment in enhancing fiber-matrix adhesion and reducing shrinkage-induced cracking; (3) to leverage DIC technology to characterize strain distribution and deformation mechanisms under mechanical stress; and (4) to analyze the techno-economic and environmental implications of fiber-reinforced HPC. This study aims to advance the understanding of fiber-reinforced HPC by addressing these objectives and offering actionable insights for designing sustainable, high-performance materials that balance mechanical robustness with long-term durability. The findings hold implications for reducing environmental footprints, enhancing structural resilience, and aligning with global efforts to promote resource efficiency in infrastructure development.

Chapter 01

State of the art on high-performance concretes (HPC)

Chapter 01

STATE OF THE ART ON HIGH-PERFORMANCE CONCRETES (HPC)

1.1. Introduction

Concrete is the world's most widely used construction material, playing a critical role in infrastructure development [1]. The increasing demands for stronger, more durable, and sustainable structures have driven the evolution of concrete technology, leading to the development of high-performance concrete (HPC) [2]. HPC represents a specialized class of concrete engineered to meet stringent performance criteria, including high strength, enhanced durability, and superior workability [3]. Unlike conventional concrete, HPC incorporates optimized mix proportions with advanced materials such as supplementary cementitious materials, high-quality aggregates, and chemical admixtures [4, 5]. These innovations enable HPC to achieve compressive strengths exceeding 60 MPa while demonstrating improved resistance to environmental and mechanical stresses [6].

The significance of HPC lies in its ability to overcome traditional concrete limitations, including low tensile strength, crack susceptibility, and vulnerability to chemical attacks. [7]. Its versatility enables applications across diverse structural systems, from high-rise buildings and long-span bridges to offshore platforms and pavements, where performance and longevity are essential. [8]. The integration of steel, plant-based, and synthetic fibers into HPC has further expanded its capabilities, enhancing properties in both solid and fresh phases, particularly regarding tensile strength, toughness, workability, rheology, and shrinkage control [9, 10].

This chapter comprehensively reviews high-performance concrete technology, encompassing its composition, mechanical properties, durability characteristics, and practical applications. It examines recent advancements in HPC and fiber-reinforced HPC while addressing current challenges and future research directions. Through this analysis of contemporary knowledge and innovations, the chapter establishes a foundation for understanding HPC's potential in modern construction and contextualizes the research presented in this thesis.

1.2. Characteristics of fresh high-performance concrete (HPC)

The fresh-state properties of high-performance concrete (HPC) are critical to its successful placement, consolidation, and long-term performance. Unlike conventional concrete, HPC is designed with a low water-to-binder (w/b) ratio and often incorporates supplementary cementitious materials and chemical admixtures, significantly influencing its behavior in the fresh state. Below are the key characteristics of fresh HPC:

1.2.1. Slump

Workability refers to the ease with which concrete can be mixed, transported, placed, and compacted without segregation or bleeding. In HPC:

1.2.1.1. High Fluidity:

Despite its low w/c ratio, HPC often exhibits high fluidity due to superplasticizers, which disperse cement particles and reduce internal friction.

1.2.1.2. Self-Compacting Properties:

Some HPC mixes are designed to be self-compacting, meaning they can flow and fill formwork under their weight without vibration.

1.2.1.3. Consistency:

The slump of HPC typically ranges from 150 mm to 250 mm, depending on the application and mix design.

The Abrams cone slump test, also known as slump, is performed on fresh, low-fluidity cement concrete to determine its consistency. Standard NF EN 12350-2 describes this test, which is illustrated in Figure 1.1.

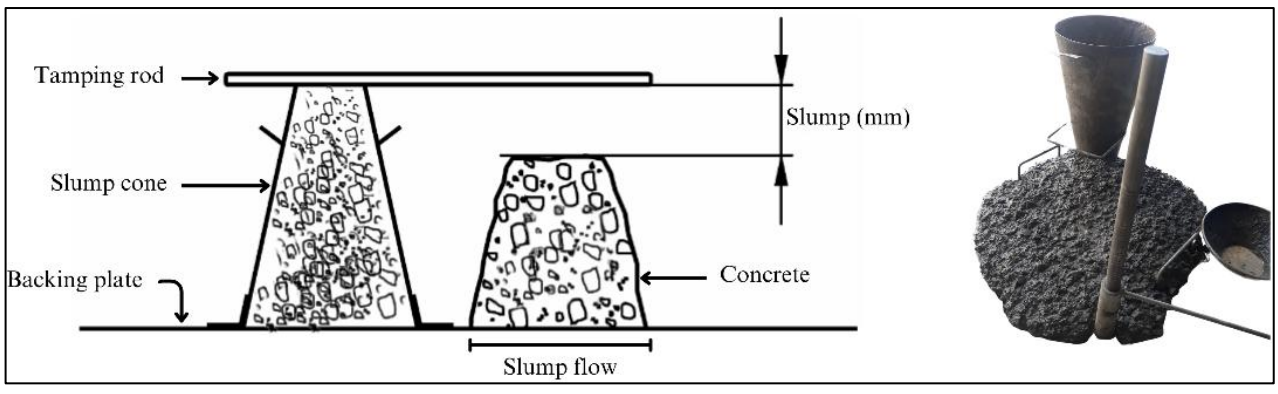

Figure 1.1 Slump test.

1.2.2. Rheometer testing

Rheometers are devices used to determine the rheological behavior of materials. They can be broadly classified into three categories according to their operating regime [11]

- Steady-state rheometers: used to determine the flow characteristics of liquid substances
- Rheometers operating under transient conditions can be used to determine the viscoelastic characteristics of both liquids and solids.
- Rheometers operating in the dynamic (sinusoidal) regime enable comprehensive determination of the rheological characteristics, including flow and viscoelastic properties, of liquid and solid materials.

1.2.2.1. ICAR rheometer

The ICAR rheometer was developed by Eric P. Koehler in 2006 [12] It consists of 3 parts:

- A cylindrical container with a height of H=30cm and a diameter of D=30.5cm.
- A steel blade with a height of h=12.5cm and a diameter of d=12.5cm
- An agitator

The complete setup is illustrated in Figure 1.2.

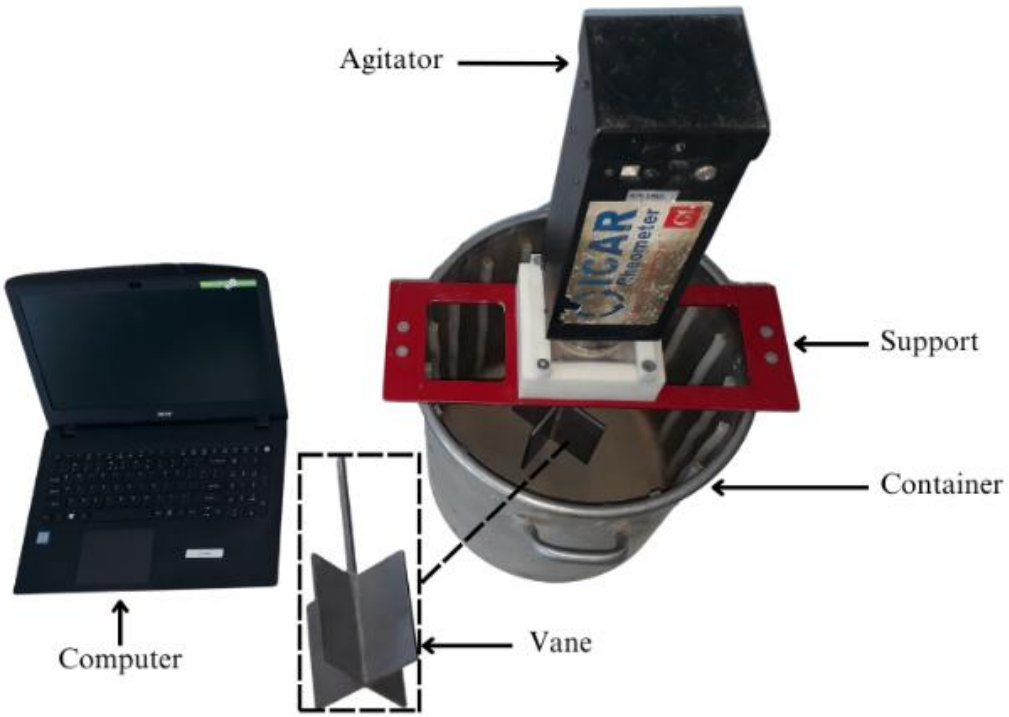

Figure 1.2 ICAR Rheometer.

1.2.2.2. Test procedure:

Once the container is filled with concrete, the blade is immersed in the container, and the concrete is sheared, imposing the velocity profile shown in Figure 1.3 .The test takes less than a minute.

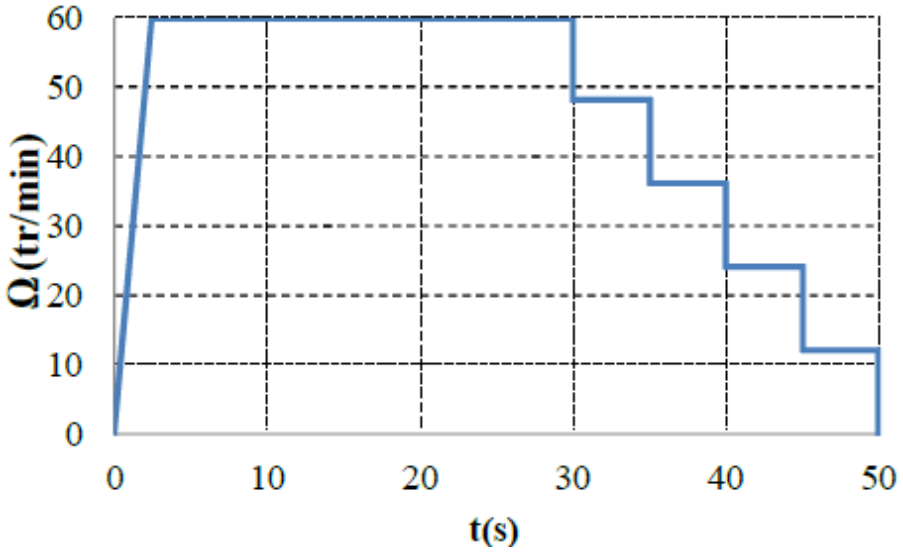

Figure 1.3 Speed profile for ICAR rheometer.

1.3. HPC formulation

High-performance concrete (HPC) is a specialized class of concrete designed to meet stringent performance requirements, such as high strength, durability, and workability. The formulation of HPC involves a meticulous selection and proportioning of materials to achieve these properties. Among the various mix design methods available, the Sherbrooke Method stands out as a scientifically rigorous approach, particularly for designing ultra-high-performance concrete (UHPC). This section provides a detailed analysis of different formulation methods, focusing on the Sherbrooke Method, including its principles, steps, and applications.

1.3.1. Overview of HPC Formulation Methods

The formulation of HPC requires a balance between achieving high performance and ensuring practical workability. Several methods have been developed over the years, each with its strengths and limitations. These methods can be broadly categorized into empirical, particle packing models, and performance-based methods.

These methods can be broadly categorized into empirical, particle packing models, and performance-based methods, as summarized in Table 1.1.

Table 1.1 General comparison formulation methods (empirical, particle packing models, and performance-based methods).

	Examples	**Strengths**	**Limitations**
Empirical Methods	ACI 211.1: The American Concrete Institute's standard method for regular concrete. IS 10262: The Indian Standard guidelines for concrete mix design.	Simple and easy to apply. Well-documented and widely accepted.	- Not tailored for HPC or UHPC. - Limited ability to optimize advanced material combinations.
Particle Packing Models	Andreasen and Andersen Model: A continuous particle size distribution model. Furnas Model: A discrete particle packing model.	-Improved mechanical properties due to dense packing. -Reduced permeability and enhanced durability.	-Requires detailed material data. -May not account for workability and practical placement considerations.
Performance-Based Methods	Dreux-Gorisse Method: A performance-based approach that considers material properties and performance requirements. Sherbrooke Method: A specialized UHPC method developed at the University of Sherbrooke, Canada.	-Tailored to meet specific performance criteria. -Suitable for advanced materials and complex mix designs.	-Requires advanced knowledge and precise control. -More time-consuming and resource-intensive.

– **Empirical methods** are based on trial mixes, historical data, and established guidelines. They are widely used for conventional concrete but are less precise for HPC due to their complex composition and advanced material requirements.

– **Particle packing models** aim to optimize the granular skeleton of concrete by manximizing the density of the solid particles. These methods benefit HPC, reducing voids and enhancing strength and durability.

– **Performance-Based Methods** focus on achieving specific performance targets, such as compressive strength, workability, and durability. These methods are highly adaptable and are often used for HPC and UHPC.

1.3.2. The Sherbrooke formulation method

The Sherbrooke Method, developed by Richard and Cheyrezy (1995), is a performance-based approach designed explicitly for ultra-high-performance concrete (UHPC). As stated in their seminal paper [11]The method emphasizes optimizing particle packing, using advanced materials, and achieving superior mechanical and durability properties.

The formulation method developed at the Université de Sherbrooke can be used to formulate HPC without entrained air: it can also be used to formulate HPC with entrained air entrained air, provided that the reduction in compressive strength due to the air bubbles air bubbles in the concrete.

This simple method follows the same approach as ACI 211-1. It involves a combination of empirical results and calculations based on the absolute volume method method [2]. The quantity contained in the superplasticizer is considered part of the mixing water.

The flow chart for this method is shown in Figure 1.4. The formulation begins with the selection of five specific characteristics of the HPC or materials used:

- the W/B ratio.
- the water content.
- the superplasticizer dosage.
- the coarse aggregate content.

- the entrapped air content (assumed value).

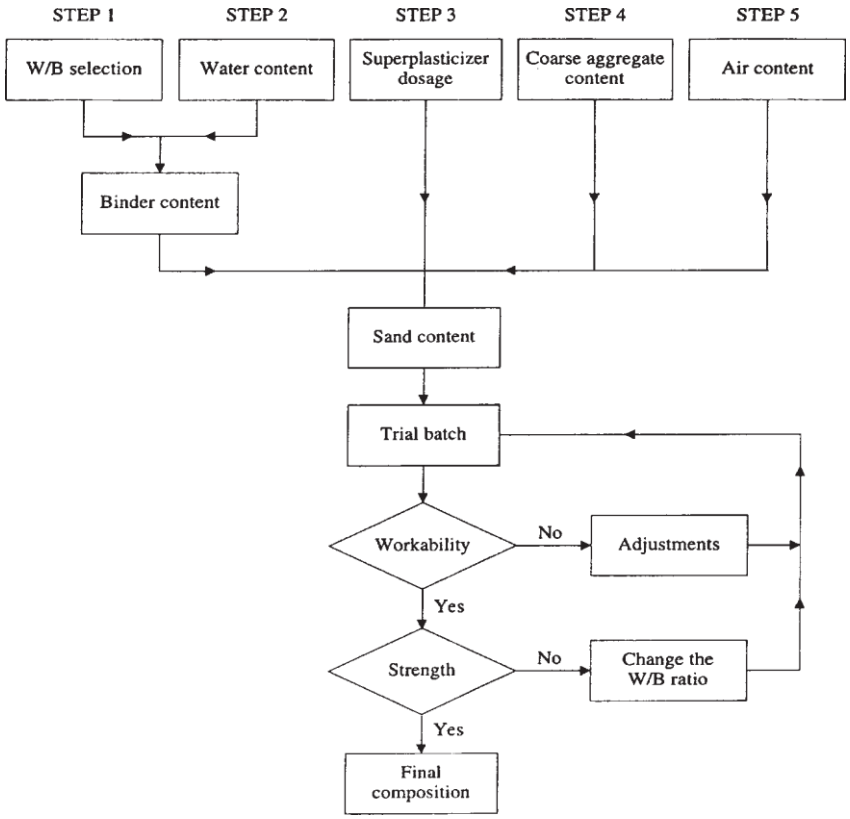

Figure 1.4 Flow chart of the proposed mix design method.

This method's advantages over other approaches are highlighted in Table 1.2.

Table 1.2 Comparison with Other Methods

Method	Strengths	Limitations
Sherbrooke Method	Optimized for UHPC, high packing density, tailored performance	Requires advanced materials and precise control
ACI 211.1	Simple, widely used, suitable for conventional concrete	Less precise for HPC/UHPC
Dreux-Gorisse	Performance-based, considers material properties	Complex calculations, less focus on particle packing
Packing Models	Maximizes density, improves strength and durability	Requires detailed material data, may not account for workability

1.3.2.1. The W/B ratio

Concrete strength increases inversely with the W/B ratio (effective water/cement). The water/cement ratio can be found using Figure 1.5 for a given 28-day compressive strength (compressive strength is measured on 100×200 mm cylinders). The spindle in Figure 1.5 Gives a relatively wide range of water/cement ratios for a given strength.

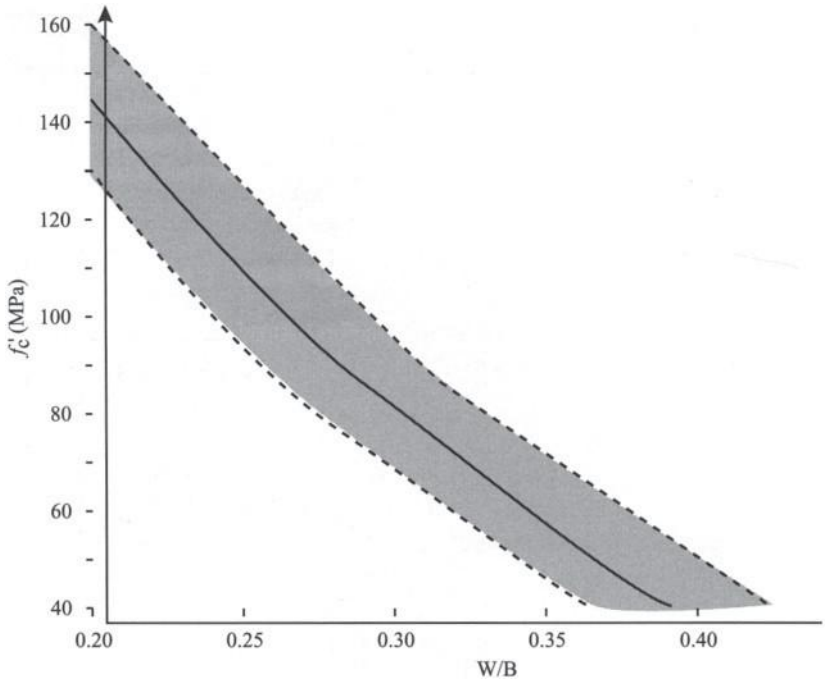

Figure 1.5 Proposed W/B vs compressive strength relationship [2].

1.3.2.2. The water content

Figure 1.6 Shows a simplified approach based on the concept of the saturation point.

The saturation dose corresponds to the quantity of superplasticizer incorporated into the mix, beyond which there will be no additional fluidizing effect. Determining this dose is usually carried out using the Marsh cone grouting method.

5 l/m^3 can be added to all the values shown in Figure 1.6 When the superplasticizer's saturation point is unknown, we suggest starting with 145 l/m3 of mixing water.

Saturation point	0.6	0.8	1.0	1.2	1.4	per cent
Water dosage	120 to 125	125 to 135	135 to 145	145 to 155	155 to 165	l/m

Figure 1.6 Determining water dosage [2].

1.3.2.3. The superplasticizer dosage

For a W/B ratio of less than 0.4, corresponding to the HPC range, the predicted strength exceeds 50 MPa. In practice, however, mixing becomes more difficult as there is no longer enough water to ensure fluidity.

There is no longer enough water to ensure fluidity. The solution is to deflocculate the cement using superplasticizers. The dosage of superplasticizer is deduced from the dosage at the saturation point.

Saturation point. If you don't know the saturation point, you can always begin with a superplasticizer dosage equal to 1%.

1.3.2.4. The coarse aggregate content

The coarse aggregate content can be obtained from Figure 1.7 as a function of typical particle shape. If the shape of the coarse aggregate is doubted or not known, it is recommended that 1000 kg/m3 of coarse aggregate be used as a starting point.

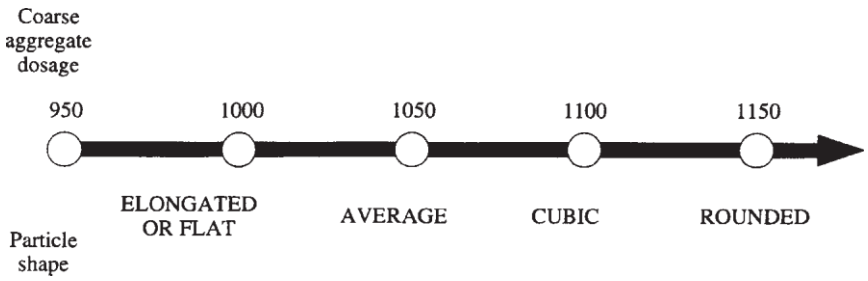

Figure 1.7 Coarse aggregate dosage [2].

1.3.2.5. The entrapped air content (assumed value)

The only quantity of air in HPCs is the volume of trapped air. However, some authors suggest systematically adding minimal entrained air to the HPC to improve HPC handling and setup. Consequently, some authors recommend using 1.5% as an initial value for the amount of trapped air and then adjusting the results according to what is obtained in the batch test batches.

1.4. Characterization of Hardened High-Performance Concrete (HPC)

High-Performance Concrete (HPC) has been a significant advancement in the construction industry since its development in the late 20th century (Mehta and Aïtcin 1990). Over the years, extensive research has been dedicated to studying and evaluating the unique properties of HPC, which distinguish it from conventional concrete. The hardened-state properties of HPC are of paramount importance to concrete formulators and structural designers. Key properties such as

compressive strength, tensile strength, and modulus of elasticity are routinely assessed during mix design studies. Other critical characteristics, including shrinkage, durability, and long-term performance, have often been the focus of more specialized investigations.

In recent decades, numerous international conferences and symposia have been organized specifically to address the advancements and challenges associated with HPC. For instance, the International Congress on the Chemistry of Cement (ICCC) and the International Symposium on High-Performance Concrete have provided platforms for researchers and practitioners to share findings and innovations. As a result, a substantial body of knowledge has been developed regarding the hardened-state properties of HPC, supported by extensive experimental data and case studies.

In the following sections, we will describe the principal properties of HPC in its hardened state, drawing on the latest data and findings from the literature. These properties include mechanical characteristics such as compressive, Flexural, and tensile strength and fracture toughness, as well as durability-related aspects like resistance to fire, Capillary Absorption, porosity, thermal conductivity, and shrinkage and modern imaging techniques such as digital image correlate (DIC). By synthesizing this information, we aim to provide a comprehensive understanding of HPC's behavior and its implications for structural design and construction practices.

1.4.1. Compressive behavior

When concrete of normal strength is compressed, bond cracks between the mortar matrix and the aggregate will propagate around the aggregate. At close to compressive strength, these bond cracks will propagate throughout the mortar matrix, leading to cracks in the mortar. Ultimately, the concrete will fail as a result of a network of uninterrupted cracks in the mortar, while the aggregates remain undamaged Figure 1.8 (a). A better bond between the aggregates and the cement matrix characterizes HPC. In addition, the strength of the matrix will be virtually equal to the strength of the aggregates. As a result, the appearance and development of bond cracks or microcracks will be delayed. By the time failure approaches, cracks will generally have propagated through the aggregates Figure 1.8 (b).

Compressive strength is a benchmark quality for HPC, which is considerably higher than ordinary concrete. The significant advantage of these high-performance concretes is their high strength; concretes with strengths over 60 to 65 MPa and up to 80 MPa have been used on-site [12].

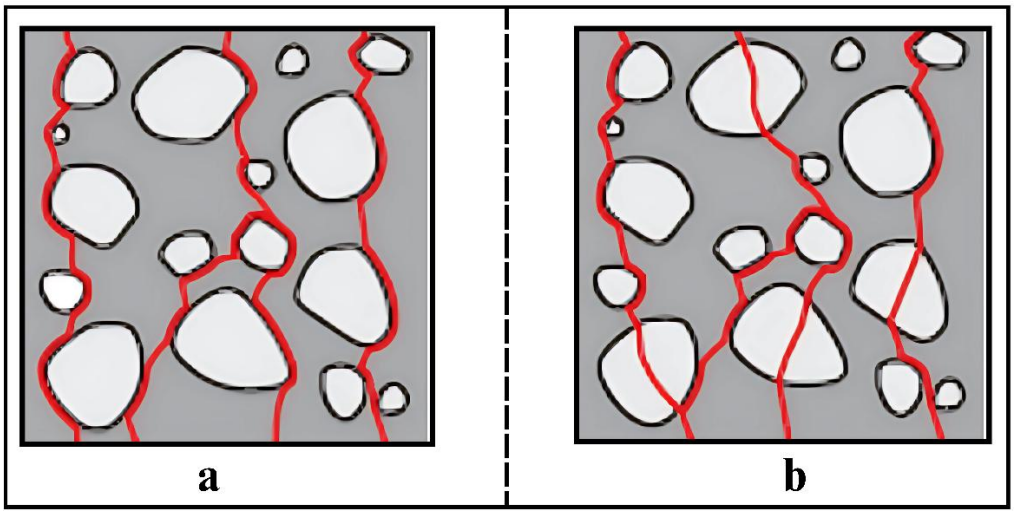

Figure 1.8 a) Ordinary concrete: cracks and mortar cracks b) High-performance concrete: the aggregates are also cracked [13].

In the stress-strain diagram Figure 1.9, this phenomenon is expressed by a slightly more linear behavior than conventional strength concrete. Similarly, high-performance concrete exhibits more marked shrinkage after compressive strength has been reached, i.e., after the concrete has broken down, and the bearing capacity tends very quickly towards zero. In other words, HPC exhibits a more pronounced brittle fracture behavior than conventional strength concrete.

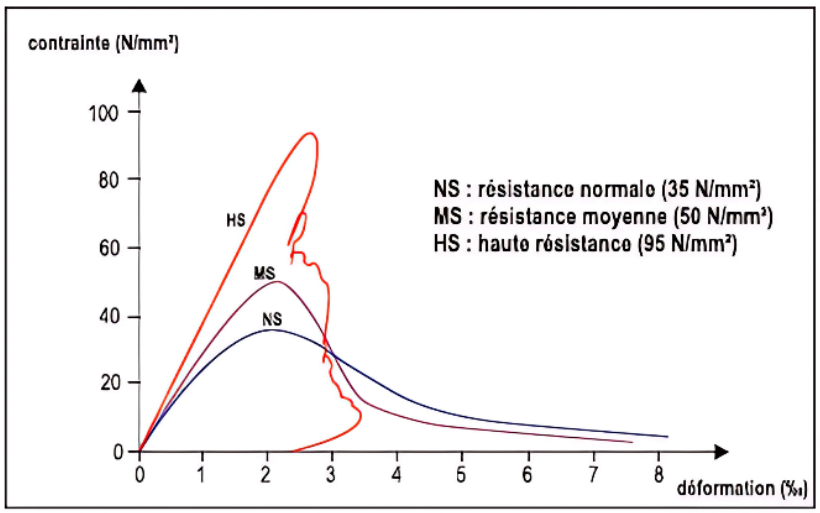

Figure 1.9 Stress-strain diagram [16].

1.4.2. Tensile behavior

Generally speaking, the tensile strength of concrete is related to its compressive strength, and can be obtained in two ways: bending and splitting. Both methods methods measure tensile strength indirectly.

1.4.2.1. Flexural tensile strength

The relationship between compressive strength and tensile strength is of the order of 1/10 to 1/13, or 0.10 to 0.077, but when compressive strength is of the order of 100 MPa, the value of the ratio (ft/fc) is much smaller, of the order of 1/20. The densification of the matrix and the paste-aggregate interface is originally due to the improved tensile strength. In splitting tests, the fracture surface is systematically transgranular (even with siliceous aggregates), demonstrating the material's mechanical homogeneity [14].

1.4.2.2. Splitting tensile strength

Some investigators have studied the relationship between splitting tensile strength and compressive strength of HPCs. They conclude that for low strengths, the tensile splitting strength is 10% of the compressive strength, while for high strengths, it is around 5% [14]. Usually, the tensile strength of concrete is related to compressive strength. Different formulas are applied to ordinary concrete. In EN 1992-1-1:2004, a different formula is proposed for high-strength concrete than for ordinary concrete Table 1.3.

Table 1.3 High-strength concrete versus conventional concrete.

Characteri tics	**Resistance classes**													
f_{ck} characteristic cylinder compressive strength (MPa)	12	16	29	25	30	35	40	45	50	55	60	70	80	90
fck-cube characteristic cube compressive strength (MPa)	15	20	25	30	37	45	50	55	60	67	75	85	95	105
f_{cm} average compressive strength (MPa)	20	24	28	23	33	43	48	53	58	63	68	78	88	98
fctm average direct tensile strength (MPa)	1.6	1.9	2.2	2.6	2.9	3.2	3.5	3.8	4.1	4.2	4.4	4.6	4.8	5.0
E_{cm} secant modulus of elasticity (GPa)	27	29	30	31	33	34	35	36	37	38	39	41	42	44
ε_{c1} deformation at peak stress (‰)	1.8	1.9	2.0	2.1	2.2	2.25	2.3	2.4	2.45	2.5	2.6	2.7	2.8	2.8

1.4.3. Rigidity

The modulus of elasticity of concrete is essentially determined by the properties of the aggregates and the mortar matrix. As the matrix consolidates and stiffens, the concrete will also exhibit increased rigidity. The modulus of elasticity of high-performance concrete is always related to compressive strength, and higher than that of conventional concretes [15].

1.4.4. Shrinkage

By definition, there are two types of shrinkage, depending on how the concrete is stored. Endogenous or self-destructive shrinkage occurs when there is no water exchange with the external environment. These deferred free deformations are then characteristic of the material's behavior at the heart of the structure. When water exchange is permitted, shrinkage is said to be desiccation or drying [16].

The essential difference between traditional concrete and high-performance concrete is that traditional concrete develops little or no endogenous shrinkage, whether or not it has undergone water curing. Table 1.4 shows the essential differences between the shrinkage of ordinary and high-performance concrete [2].

Table 1.4 Differences between shrinkage of ordinary concrete and HPC.

Type of Shrinkage	Ordinary Concrete	High-Performance Concrete (HPC)
Endogenous	Little or none	Very high
Drying	Very high	Low

Le Roy and De Larrard compared the endogenous shrinkage of HPC and ordinary concretes at different W/C ratios with silica fume incorporation for curing ages of 400 days. They concluded that endogenous shrinkage increases with decreasing W/C ratios and for concretes incorporating silica fume [17].

Persson, 1998 [18] shows the relationship between endogenous shrinkage and the relative humidity of concrete between 3 and 4 years. The higher the initial relative humidity of the concrete, the less endogenous shrinkage occurs. This is because concrete shrinks less as a result of lower internal relative humidity during the hydration process Figure 1.10.

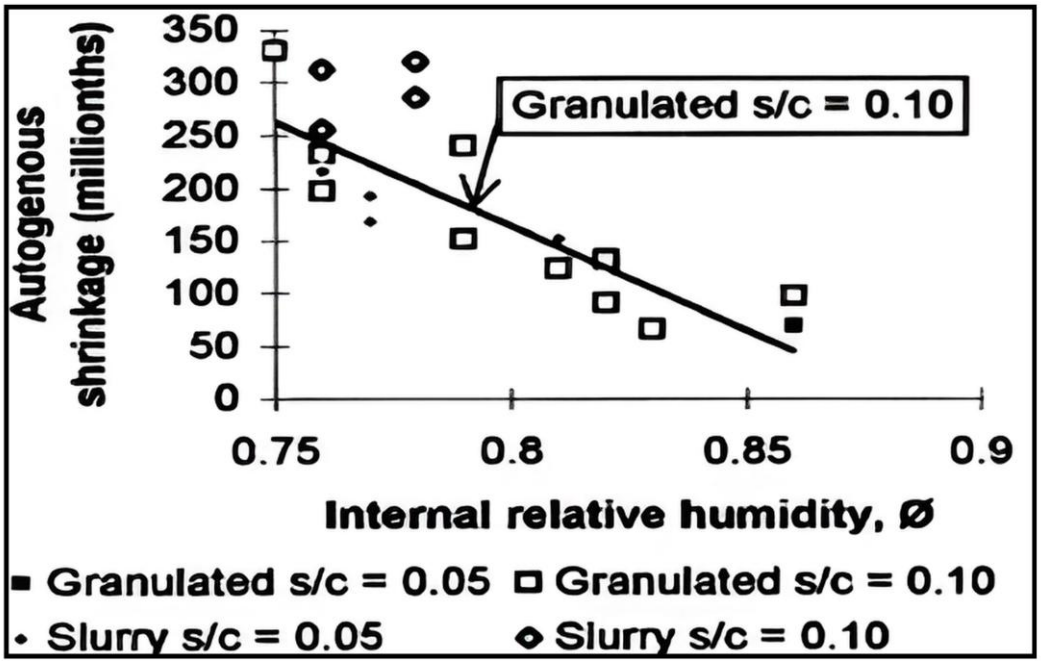

Figure 1.10 Endogenous shrinkage at 3-4 years depending on internal relative humidity[55].

Sicard, 1993 [19] also carried out tests on cylinders 12 cm in diameter and 24 cm in length. For concretes aged 600 days, he showed that endogenous shrinkage increases with decreasing W/B ratios; that it is higher for limestone aggregates than for silico-limestone aggregates; and that it is higher for concretes containing silica fume than for those without, since silica fume generates high self-drying shrinkage linked to hydration and porosity refinement Figure 1.11.

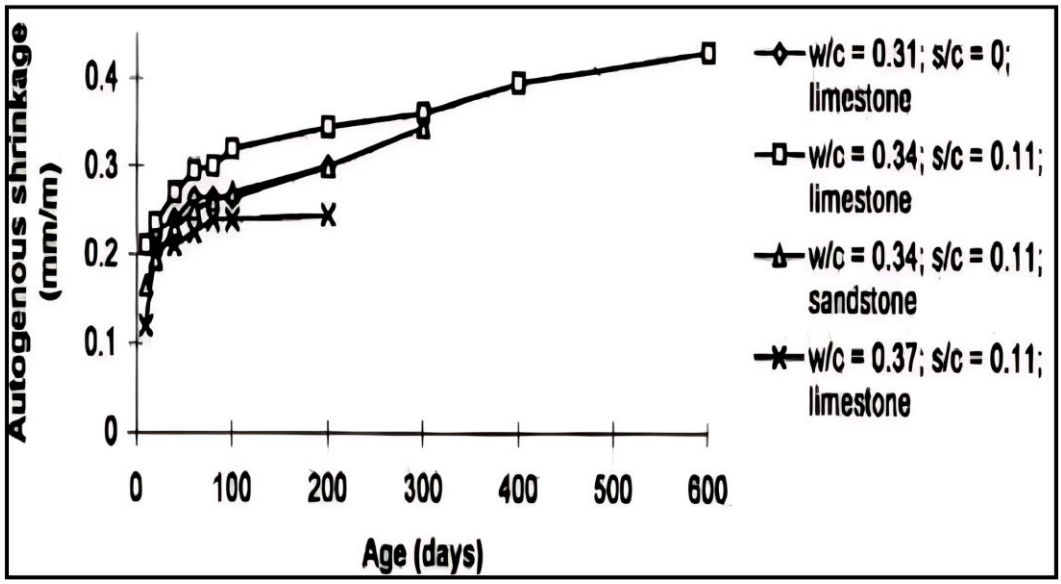

Figure 1.11 Endogenous shrinkage after 600 days for calcareous and silicocalcareous aggregates, c=cement, s=silica fume [55].

1.4.5. Fluage

Creep deformation remains proportional to the applied stress (i.e., initial strain) for loads applied at the same concrete age. For concrete containing silica fume, creep increases rapidly immediately after loading, reaching 25–30% of the total creep within the first day. However, the total creep of silica fume concrete is generally 40–50% lower than that of conventional concrete. The reduction in creep depends on the percentage of silica fume incorporated, with higher percentages (above 6%) resulting in poorer performance compared to lower percentages, where the lowest creep is observed [19, 20].

According to BPEL91, when calculating the creep of high-performance concrete (HPC) with a characteristic strength (f_{c28}) greater than 50 MPa, the creep coefficient (ϕ), defined as the ratio of final creep deformation to instantaneous deformation, can typically be taken as 2. However, a lower value may be used if justified by experimental data. This reflects the fact that creep deformation in HPC is significantly lower than in conventional concrete, where creep deformation is approximately twice the instantaneous deformation [20, 21].

Chaid [22] further supports this by noting that concretes incorporating supplementary cementitious materials (SCMs), such as silica fume, exhibit lower creep and shrinkage deformations compared to reference concrete without SCMs. This behavior is illustrated in Figure 1.12 of Chaid's study, which highlights the beneficial effects of SCMs on reducing long-term déformations.

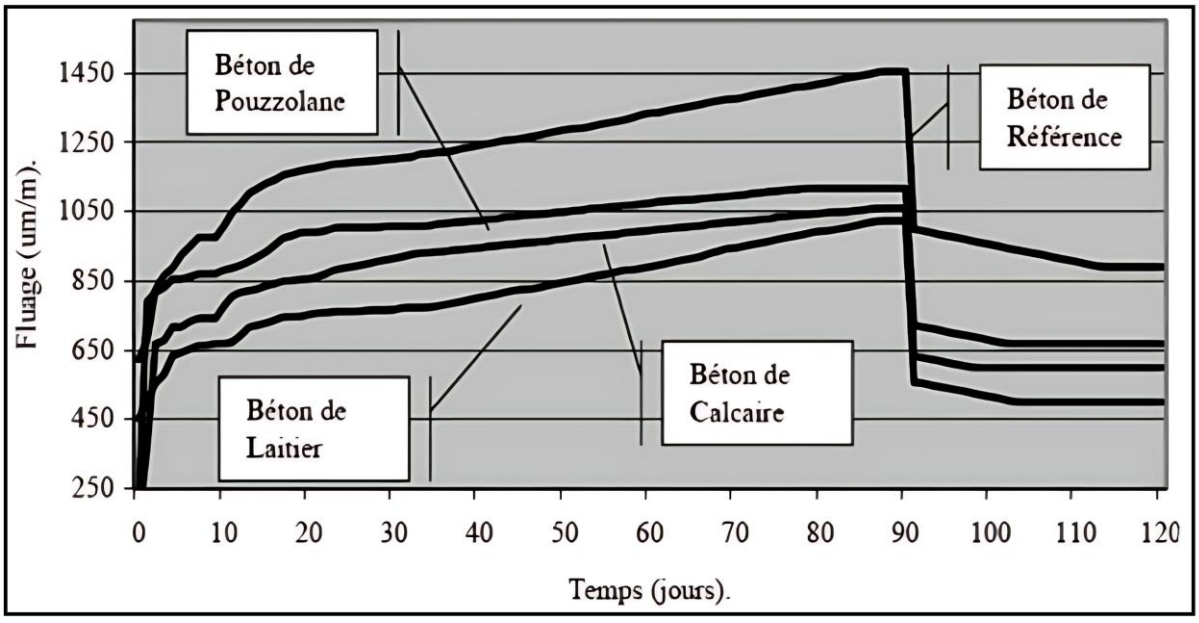

Figure 1.12 Creep behaviour of different concretes[55].

1.4.6. Durability

High-Performance Concrete (HPC) exhibits superior durability due to its reduced porosity and permeability, which collectively inhibit the ingress of deleterious substances [1]. This denser microstructure significantly slows carbonation progression at greater depths, thereby enhancing the long-term protection of embedded reinforcement against corrosion a critical advantage in aggressive environments [7]. Furthermore, HPC demonstrates exceptional resistance to chemical degradation, a property that renders it highly effective in marine settings or regions exposed to corrosive agents such as chlorides and sulfates [23].

Research underscores that HPC possesses intrinsic "potential" durability, particularly due to its capacity to restrict external aggressive processes (e.g., chloride ion penetration and carbonation) to superficial layers, while simultaneously mitigating internal degradation mechanisms such as alkali-silica reaction and leaching [24]. These attributes are supported by empirical studies, which highlight HPC's ability to extend the service life of reinforced or prestressed concrete structures by decades compared to conventional concrete [25]. The material's enhanced performance provides a compelling rationale for its specification in projects demanding resilience against environmental and chemical stressors, ultimately reducing the incidence of structural pathologies and lifecycle maintenance costs [26].

1.5. HPC microstructure

High-Performance Concrete (HPC), like conventional concrete, is inherently heterogeneous due to its complex composition. This heterogeneity arises not only from the broad granulometric distribution of aggregates but also from the varied hydration products formed during curing, which are influenced by environmental factors such as temperature and relative humidity during hydration and storage [1]. Structurally, HPC comprises two primary phases: a binder phase (hardened cement paste or matrix) and a granular phase (aggregates), interconnected by the interfacial transition zone (ITZ), a critical region at the paste-aggregate boundary known for its microstructural vulnerabilities [15].

At the microscale, the cement paste matrix consists of hydration products such as calcium silicate hydrate (C-S-H gel), calcium hydroxide ($Ca(OH)_2$), and sulfoaluminates, alongside unhydrated clinker remnants (e.g., calcium silicates and aluminates) and inert fillers [26]. However, the microstructure is also marked by textural discontinuities, including microcracks and crystallographic orientations (e.g., $Ca(OH)_2$ deposits in the ITZ). These features can evolve under

aggressive environmental conditions, leading to secondary formations such as ettringite, thaumasite, or alkali-silica reaction (ASR) gels, which compromise durability over time [27].

The ITZ, in particular, represents a zone of heightened porosity and weaker mechanical performance compared to the bulk paste, making it a focal point for degradation mechanisms in HPC. Understanding these microstructural complexities is essential for optimizing HPC's resistance to chemical and physical stressors, particularly in applications demanding long-term structural integrity [28].

1.5.1. Concrete skin

The The near-surface layer of hardened concrete, often termed the "concrete skin," retains a thin, porous microstructure post-curing, analogous to its initial state during placement. In High-Performance Concrete (HPC, this region is characterized by sparse calcium hydroxide ($Ca(OH)_2$) crystals of reduced size compared to conventional concrete, alongside sub-micron-scale microcracks (<1 μm) and a predominance of calcium silicate hydrate (C-S-H) gel, a hallmark of HPC's dense matrix [1].

Microstructural analyses further reveal a honeycomb-like morphology within the skin, hypothesized to result from the imprints of cement grains during sample fracturing. This texture suggests the presence of a water-to-cement (W/B) ratio gradient across the material, reflecting localized variations in hydration efficiency and pore structure [24].

Recent studies have underscored the critical role of the concrete skin—specifically the outermost 20-30 mm in governing long-term durability. Historically, the skin has been recognized to exhibit distinct compositional and microstructural properties relative to the bulk material, a phenomenon attributed to the wall effect. This interfacial disparity arises from particle segregation and differential hydration near formwork or exposure surfaces, leading to increased porosity, altered hydrate distribution, and weakened mechanical performance in the skin region [15]. Such heterogeneities render the skin more susceptible to ingress of aggressive agents (e.g., chlorides, CO_2), accelerating degradation processes like carbonation and corrosion initiation [26]. Consequently, optimizing the skin's microstructure through mix design and curing practices is pivotal for enhancing HPC's resilience in harsh environments.

1.5.2. Internal microstructure

The internal microstructure of the material mirrors the morphological features of the surface layer ("skin") but exhibits a more advanced state of hydration. Microstructural analysis reveals a

complete absence of ettringite ($Ca_6Al_2(SO_4)_3(OH)_{12}\cdot 26H_2O$) crystallization, a phase typically associated with early-stage cement hydration [26]. Portlandite ($Ca(OH)_2$), a secondary hydration product, is also scarcely observed, suggesting limited calcium hydroxide formation under the prevailing conditions. Energy-dispersive X-ray spectroscopy (EDS) of belite (β-C_2S) lamellae confirms negligible hydration activity, aligning with delayed reactivity of silicate phases in low-water environments [29]. Notably, the honeycomb-like calcium silicate hydrate (C-S-H) gel structure, a defining feature of the surface layer, is ubiquitously distributed throughout the internal matrix. This pervasive C-S-H morphology, characterized by its nanoporous architecture, indicates uniform gel nucleation kinetics across both interfacial and bulk regions [30]. Such structural consistency challenges traditional assumptions of hydration heterogeneity in cementitious systems, implying comparable reaction mechanisms at macro- and microstructural scales.

1.5.3. Paste-aggregate interface

The physical-mechanical properties and durability of cementitious materials depend not only on the quality of the cement paste (type of cement used, W/B ratio, admixtures, etc.), the type and grain size of the aggregates and the proportion of each, but also on the quality of the bond established during hydration between the cement paste and the granular particles [31]. This bond gives rise to a zone known as the “transition halo” or “interfacial transition zone”.

For high-performance concretes, modified by the addition of silica fume, we can obtain a reduction in the porosity and thickness of this zone. Compared with ordinary concrete, where the transition aureole is around 50 μm, its thickness for high-performance concretes is limited to 12 μm. Some sources [32], report the absence of the contact zone in high-performance concretes containing silica fume, which creates a more homogenous and dense microstructure at the paste-aggregate interface, as illustrated in Figure 1.13

The quality of the transition zone also depends on the water/cement ratio. As W/C increases, this zone becomes thicker, more porous and consequently less resistant [33].

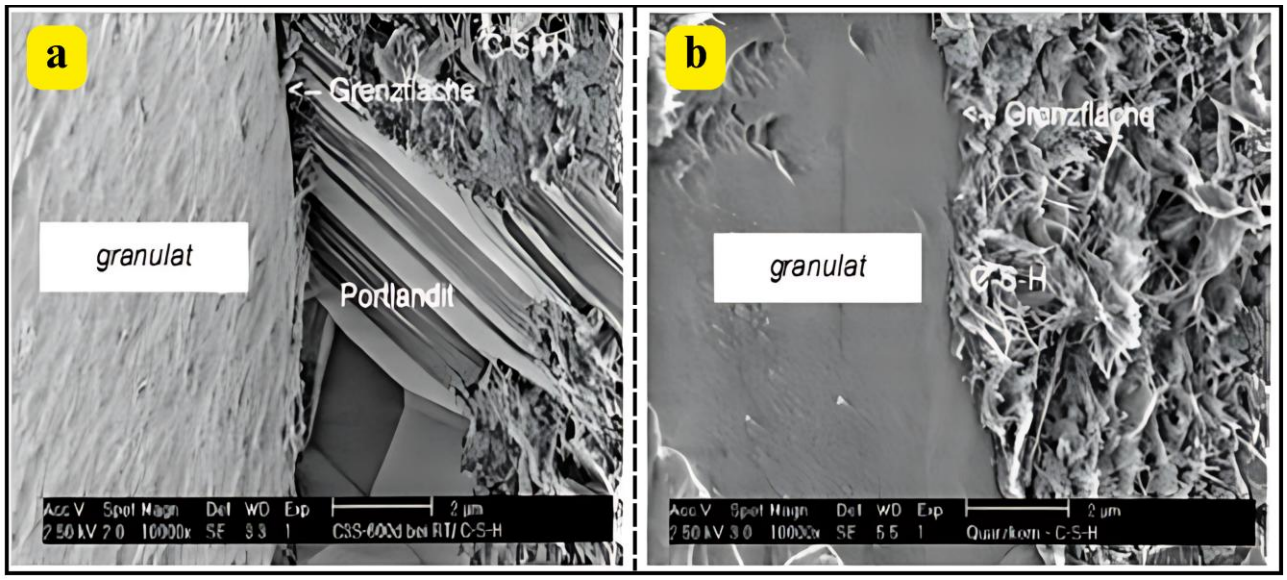

Figure 1.13 Microstructure of the contact zone between paste and aggregate: a) concrete without silica fume; portlandite crystals in the transition zone are oriented perpendicular to the aggregate, b) concrete with silica fume, transition zone absent, CSH gel homogeneous [37].

1.6. Classification and application of HPC

High-performance concrete (HPC) is classified into three categories based on its characteristic strength: conventional concrete, high-strength concrete, and ultra-high-performance concrete (UHPC). Each category exhibits distinct properties and applications, making HPC a versatile material in modern construction.

1.6.1. Classification of HPC

– **High-Strength Concrete**: Ranges from 30 MPa to 70 MPa. It incorporates additives like fly ash and silica fume to enhance strength and durability, making it suitable for high-rise buildings and bridges [34, 35].

– **Ultra-High-Performance Concrete (UHPC)**: Exceeds 70 MPa, often reaching strengths above 150 MPa. UHPC is characterized by its exceptional durability and low permeability, making it ideal for infrastructure projects such as transportation systems [36, 37].

1.6.2. Applications of HPC

– **Civil Engineering**: HPC is crucial in major engineering projects due to its durability and strength, allowing for innovative designs and longer-lasting structures [35].

– **Precast Components**: Used in precast concrete elements, HPC enhances the structural integrity and reduces maintenance needs [34].

– **Transportation Infrastructure**: UHPC is particularly beneficial for applications requiring high durability and resistance to environmental factors, such as bridges and pavements [36].

- Long-span structures (bridges, viaducts, etc.).
- high-rise buildings (IGH), also known as skyscrapers.
- Very short prefabricated parts (voussoirs for bridges, etc.) with very short very short stripping times.
- Structures in marine environments (dikes, oil platforms, etc.).
- Nuclear engineering structures (nuclear power plants).

While HPC offers numerous advantages, challenges such as high production costs and complex mixing processes remain, which may hinder its widespread adoption in some regions.

1.7. Examples of HPC structures

Buildings of Lake Point Tower (fc = 53MPa): a residential skyscraper in Chicago, measuring 197 m built in 1965-1968 [63].Figure 1.14

Figure 1.14 Lake Point Tower.

1.7.1. Tunnels of The Villejust tunnel:

It was built in Paris and located between Massy LNA and Courtalain BIF. (4806 m).Figure 1.15

Figure 1.15 Tunnels de Villejust.

1.7.2. Confederation Bridge, Canada (50–100 MPa)

The Confederation Bridge used high-performance concrete (HPC) in its construction to meet the demanding requirements of a 100-year service life and resistance to harsh marine environments [38]. The typical concrete strengths specified for the bridge were 55 MPa at 28 days and 60 MPa at 91 days [38]. This high-strength concrete was essential to provide durability against corrosion and to withstand the severe environmental conditions, including freeze-thaw cycles, wave action, and ice impacts [39].Figure 1.16

Figure 1.16 Confederation Bridge, Canada.

1.8. Conclusion

In this chapter of the literature review, we have presented a general overview that has enabled us to better understanding of this new technology, then the main properties and constituents of constituents of HPC, as well as its formulation and worldwide use. We highlighted the difference between high-performance concretes (HPC) and ordinary concretes (BO). High-performance concretes contain supplementary cementitious materials (fines), in particular silica fume. silica fume, to improve mechanical strength. They are characterized by low permeability, high density and enhanced durability to develop certain characteristics mechanical strength and rheological properties. New-performance concretes, with their multiple performance features, can be adapted to a wide range of to the various constraints and requirements of structures. They open up great prospects applications for structures requiring high strength, durability and aesthetic appeal. Their exceptional performance opens up new fields of application and new building structures.

Chapter 02

Effect of different fiber types on the behavior of high-performance concrete (HPC)

Chapter 02

EFFECT OF DIFFERENT FIBER TYPES ON THE BEHAVIOR OF HIGH-PERFORMANCE CONCRETE (HPC)

2.1. Introduction

High-performance fiber-reinforced concrete (HPFRC) has emerged as a revolutionary material in civil engineering, offering enhanced mechanical properties and durability compared to conventional concrete. The incorporation of fibers into the concrete matrix significantly improves its tensile strength, crack resistance, and energy absorption capacity. Various types of fibers, including steel, glass, synthetic, and natural fibers, are utilized to achieve specific performance characteristics. Steel fibers, for instance, are widely used for their high tensile strength and ability to control cracking, while synthetic fibers such as polypropylene and polyethylene enhance durability and reduce plastic shrinkage cracks. Glass fibers contribute to improved flexural strength and impact resistance, and natural fibers, though less common, offer eco-friendly alternatives with moderate performance benefits. The selection of fiber type, aspect ratio, and dosage is critical to optimizing the performance of HPFRC for specific applications, such as seismic-resistant structures, industrial floors, and thin-shell elements. This introduction highlights the importance of fibers in modern concrete technology and underscores the need for further research to explore their full potential in advancing sustainable and resilient infrastructure [9, 40, 41].

2.2. General Overview of Fibers

Fibers are discrete, discontinuous materials added to concrete to improve its mechanical properties and durability [42]. They act as a secondary reinforcement system, enhancing the tensile strength, crack resistance, and toughness of concrete. While the use of fibers in construction materials dates back to ancient civilizations, with evidence of straw and horsehair being mixed with mud or lime [9], in modern civil engineering, fibers have become an essential component of high-performance concrete, particularly in applications requiring enhanced durability, impact resistance, and structural integrity [43].

The fundamental mechanism of fiber reinforcement involves bridging microcracks that form in the concrete matrix, preventing their propagation and subsequent failure [44]. This mechanism significantly improves the post-cracking behavior of concrete, making it more ductile and capable of absorbing energy. Research has shown that the effectiveness of fibers depends on multiple factors, including their type, aspect ratio (length-to-diameter ratio), volume fraction, and bonding characteristics with the concrete matrix [45]. According to international standards and research literature, fibers are broadly classified into four categories: steel fibers, glass fibers, synthetic fibers, and natural fibers, each offering unique properties and benefits [1].A detailed flowchart illustrating this classification is shown in Figure 2.1.

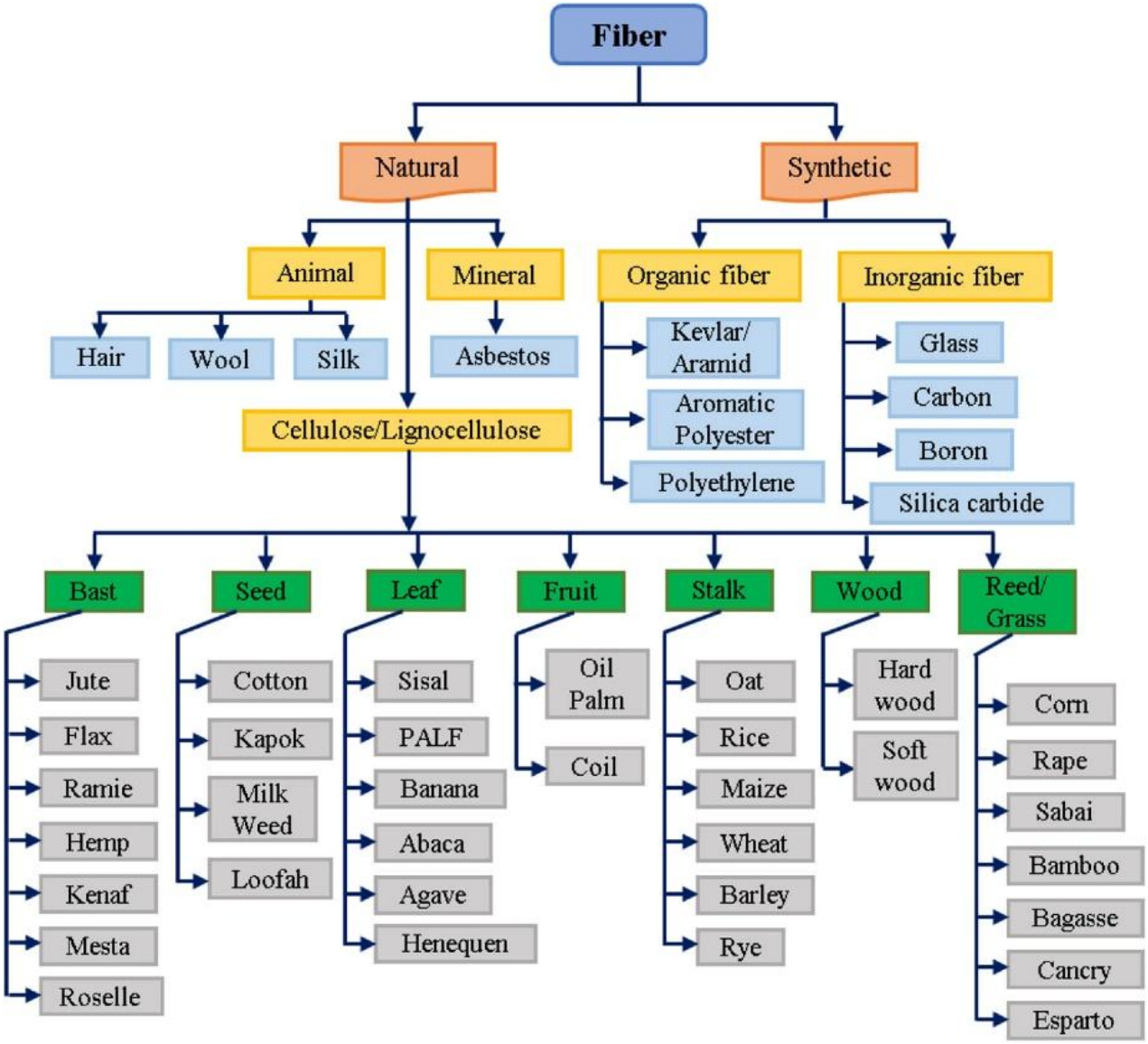

Figure 2.1 Different fibers used in concrete.

2.3. Different Types of Fibers Used for Reinforcing Concrete

2.3.1. Steel Fibers

Steel fibers, predominantly manufactured from carbon steel or stainless steel, are the most widely used type of fibers in concrete applications [46] Figure 2.2. Available in various geometries including hooked, straight, crimped, or deformed shapes, these fibers have demonstrated significant improvements in flexural strength, impact resistance, and fatigue performance of concrete [47]. Research by Vandewalle (2000) has shown their particular effectiveness in industrial floors, pavements, tunnel linings, and seismic-resistant structures.

Figure 2.2 Steel Fibers.

2.3.2. Glass Fibers

Glass fibers, composed of fine strands of glass, are frequently utilized in combination with polymer matrices to form glass fiber-reinforced concrete (GFRC) [48] Figure 2.3. Studies have demonstrated their excellent resistance to cracking and enhancement of concrete's tensile strength [49]. Their lightweight properties and aesthetic appeal make them particularly suitable for thin-shell elements, façade panels, and decorative applications [50].

Figure 2.3 Glass Fibers.

2.3.3. Synthetic Fibers

Synthetic fibers, including polypropylene, polyethylene, nylon, and polyester variants Figure 2.4, have gained increasing popularity due to their versatility, chemical resistance, and cost-effectiveness [51]. Research has shown that polypropylene fibers effectively reduce plastic shrinkage cracks in fresh concrete and improve impact resistance in hardened concrete [52]. These fibers have proven particularly effective in shotcrete applications and for enhancing concrete durability in harsh environments [53].

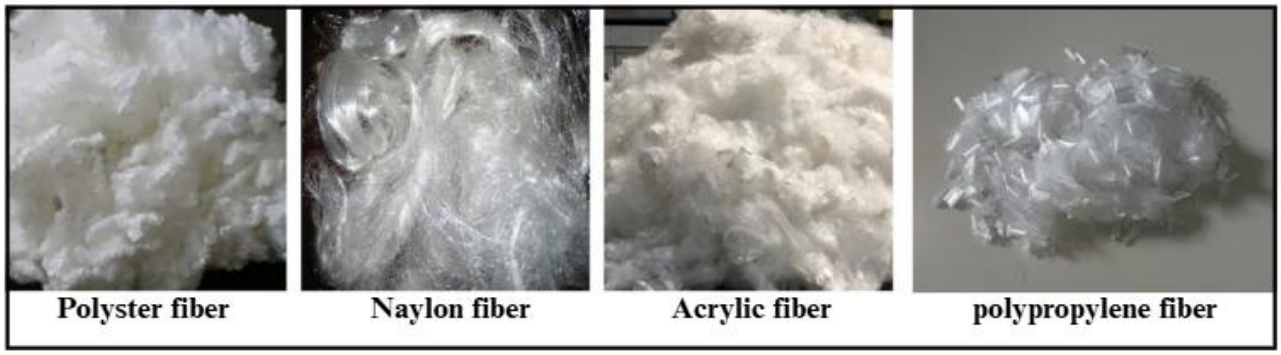

Figure 2.4 Synthetic **Fibers**.

2.3.4. Natural Fibers

Natural fibers, derived from sources such as sisal, coconut, bamboo, jute and flax Figure 2.5, represent eco-friendly alternatives to synthetic and steel fibers [54]. Their renewable source origin and biodegradability align with sustainable construction practices [55]. While research indicates that natural fibers improve concrete's toughness and crack resistance, their performance generally does not match that of synthetic or steel fibers [56].

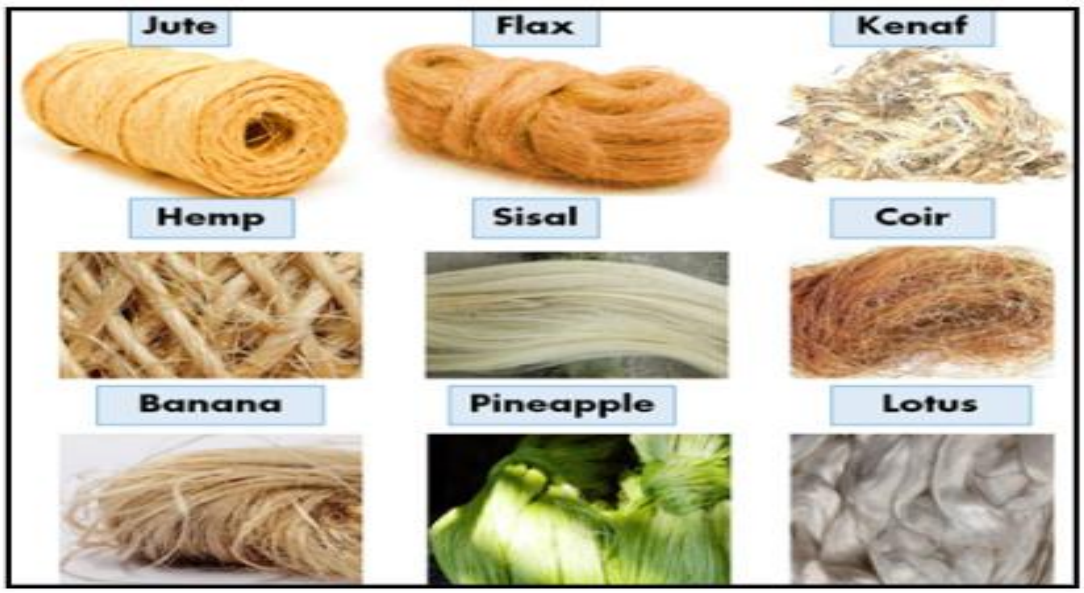

Figure 2.5 Natural Fibers.

A summary of the main advantages and limitations for each of these fiber categories is provided in Table 2.1.

Table 2.1 Advantages and Limitations of Fiber Types.

Fiber Type	Advantages	Limitations
Steel Fibers	- High tensile and flexural strength. - Excellent crack control and energy absorption. - Suitable for heavy-duty applications.	- Susceptible to corrosion in aggressive environments. - Higher cost compared to synthetic fibers.
Glass Fibers	- High tensile strength and flexibility. - Lightweight and easy to handle. - Resistant to chemical attack.	- Brittle nature and susceptibility to alkali-silica reaction (ASR). - Requires surface treatment for durability.
Synthetic Fibers	- Lightweight and easy to disperse in the mix. - Resistant to corrosion and chemical attack. - Cost-effective and widely available.	- Lower modulus of elasticity compared to steel fibers. - Limited improvement in tensile strength.
Natural Fibers	- Environmentally friendly and sustainable. - Low cost and readily available. - Moderate improvement in mechanical properties.	- Susceptible to degradation in alkaline environments. - Variable quality and performance.

2.4. Fiber Characteristics and Properties in Concrete Reinforcement

2.4.1. Physical Characteristics and Properties

The physical attributes of fibers significantly influence their interaction with concrete matrices. Research indicates that fiber geometry, particularly in deformed fibers such as hooked-end steel variants, demonstrates superior mechanical anchorage within the concrete matrix [50]. The aspect ratio (length-to-diameter ratio) serves as a critical parameter, balancing between optimal fiber dispersion and workability. Surface texturing and modifications play a vital role in enhancing the fiber-matrix interface performance.

2.4.2. Mechanical Performance Characteristics

2.4.2.1. Strength Properties

Mechanical performance varies significantly among fiber types. Steel fibers exhibit exceptional tensile strength ranges (500-2,500 MPa) and high elastic modulus (~200 GPa), making them ideal for structural applications [47]. In contrast, synthetic fibers demonstrate moderate strength properties but offer unique advantages in terms of durability and chemical resistance.

2.4.2.2. Load Transfer Mechanisms

The effectiveness of load transfer between fibers and the concrete matrix depends on multiple bonding mechanisms. According to Mechtcherine and Silva (2010) [57], these include:

- Mechanical interlock through deformed or hooked geometries
- Chemical bonding enhanced by surface treatments
- Frictional resistance from surface texturing

2.4.3. Chemical and Durability Aspects

2.4.3.1. Chemical Resistance

Different fiber types exhibit varying levels of chemical resistance. Synthetic fibers demonstrate superior resistance to chemical attack, while steel fibers may require protective treatments in aggressive environments [41]. Glass fibers present particular challenges regarding alkali resistance in cementitious matrices.

2.4.3.2. Long-term Durability

Durability characteristics vary significantly among fiber types:

- Steel fibers excel in freeze-thaw resistance and abrasion protection [58].
- Synthetic fibers offer superior chemical stability.
- Natural fibers, while environmentally friendly, show limited long-term durability [59].

2.4.4. Implementation Considerations

2.4.4.1. Dispersion and Workability

Uniform fiber distribution remains crucial for optimal performance. Shah and Ribakov (2011) [60] note that synthetic fibers generally achieve better dispersion compared to steel alternatives. Workability considerations often necessitate careful mix design and possibly the use of additives.

2.4.4.2. Environmental Impact Assessment

Environmental considerations vary by fiber type:

- Natural fibers: Highest environmental credentials but limited durability.
- Synthetic fibers: Moderate environmental impact with recyclability benefits.
- Steel fibers: Higher initial environmental impact offset by longevity and recyclability.

The key characteristics and properties of different fiber types commonly used in concrete are summarized in Table 2.2

Table 2.2 Fiber Characteristics and Properties.

Property	Steel Fibers	Glass Fibers	Synthetic Fibers	Natural Fibers
Tensile Strength	Very High (500–2,500 MPa)	High (1,500–3,500 MPa)	Moderate (300–700 MPa)	Low to Moderate (50–500 MPa)
Modulus of Elasticity	High (~200 GPa)	Moderate (~70 GPa)	Low (~3–10 GPa)	Low (~10–50 GPa)
Alkali Resistance	Good (if stainless)	Poor (susceptible to ASR)	Excellent	Poor
Corrosion Resistance	Poor (unless coated)	Excellent	Excellent	Good
Thermal Stability	Excellent	Good	Poor (low melting point)	Moderate
Environmental Impact	High (energy-intensive)	Moderate	Moderate (recyclable)	Low (eco-friendly)

2.5. Applications of Fiber-Reinforced Concrete

Fiber-reinforced concrete can be used for a wide variety of applications in building and civil engineering [61]:

- Industrial and Commercial Flooring (Warehouse floors and heavy-duty pavements, Loading docks and industrial plants, Shopping centers and commercial spaces)
- Transportation Infrastructure (Highway and airport pavements, Bridge decks and overlays, Railway sleepers)
- Underground Construction (Tunnel linings using shotcrete, Mine supports, Underground storage facilities)
- Structural Applications (Seismic-resistant structures, High-rise buildings, shear walls, foundations, Precast elements)
- Specialty Applications (Fire-resistant concrete using polypropylene fibers, Blast-resistant structures, Architectural panels)

2.6. Mechanisms of Fiber Reinforcement in High-Performance Concrete

2.6.1. Crack Control and Bridging

Fibers act as a secondary reinforcement system by bridging micro- and macro-cracks, delaying their propagation and redistributing stress. This mechanism is critical in improving tensile strength and fracture toughness:

– **Composite fibers** (e.g., polyacrylonitrile-based carbon, basalt, and glass fibers) form a **mesh structure** within the concrete, stabilizing cracks and reducing brittleness. This structure enhances toughness by over 30% compared to plain concrete [62].

– **Steel fibers** especially hooked-end types, anchor themselves in the matrix, resisting pull-out forces and maintaining structural integrity even after cracking. Their geometry (e.g., hooked ends) increases adhesion, leading to progressive failure modes rather than sudden collapse [63].

– **Synthetic fibers** (polypropylene, nylon, modified polyvinyl alcohol fibers) play a crucial role in enhancing the performance of concrete. These fibers bridge macro-cracks in hardened concrete, thereby delaying failure under cyclic loads [41]. They also inhibit explosive spalling in fire-resistant high-performance concrete (HPC) by melting and creating pathways for steam escape [64]. Moreover, in ultra-high-performance concrete (UHPC), synthetic fibers improve crack resistance by reducing shrinkage-induced cracks and enhancing energy absorption through

interfacial bonding [65]. As a result, these fibers significantly contribute to the durability and resilience of advanced concrete materials

– **Natural fibers** (jute, sisal, coconut, flax) serve as micro-reinforcement during early curing, effectively reducing plastic shrinkage cracks by up to 40% in lightweight concrete [66]. They also enhance toughness by 15–20% in non-structural applications. However, these fibers tend to degrade in alkaline environments if not treated with surface treatments like alkali or acrylic coatings [67]. Despite this limitation, natural fibers offer a sustainable option for improving concrete performance in specific applications.

2.6.2. Energy Dissipation and Ductility Enhancement

Fibers improve energy absorption capacity by dissipating energy through elastic and plastic deformation:

– **Steel fibers** in UHPC contribute to **strain hardening** and **phase transformations** (e.g., austenitic to martensitic transitions), which absorb impact energy and reduce post-impact velocities by up to 31.5 m/s [68].

– **Hybrid fiber systems** (e.g., combining steel and polypropylene fibers) optimize energy dissipation by leveraging the ductility of synthetic fibers and the strength of steel fibers. For example, hybrid fibers in UHPC increase flexural strength by 33% compared to single-fiber systems [68, 69].

– **Synthetic fibers** such as polyester and nylon improve post-crack ductility by absorbing energy through elastic deformation [41]. In ultra-high-performance concrete (UHPC), polyvinyl alcohol (PVA) fibers significantly increase strain capacity by 50% due to their strong interfacial bonding [70]. Moreover, modified PVA fibers enhance ductility in UHPC by improving the interfacial transition zone (ITZ) bonding, allowing for better load distribution across microcracks [65]. These fibers play a crucial role in increasing the resilience and mechanical performance of advanced concrete materials.

– **Natural fibers** enhance energy dissipation in concrete through pull-out mechanisms, with sisal fibers notably improving impact resistance by 25% in eco-friendly concrete [71]. However, their application is limited to low-durability environments due to their biodegradability [67]. Without appropriate surface treatments, these fibers can degrade, particularly in alkaline conditions. Despite these challenges, natural fibers offer sustainable benefits in specific contexts.

2.6.3. Fiber-Matrix Interaction

The effectiveness of fibers depends on their geometry, distribution, and adhesion to the matrix:

– **Aspect ratio and orientation**: Longer and slender fibers (slenderness ratio >80) improve crack resistance but may reduce workability. Proper alignment during mixing ensures optimal load transfer [63, 72].

– **Surface treatments**: Modified PVA fibers with silane coupling agents enhance bonding with the cement matrix, reducing interfacial porosity and improving tensile strength by 15–20% [65].

– **Fiber dispersion**: Poor dispersion leads to clustering, which weakens the matrix. Techniques like 3D printing optimize fiber orientation, enhancing anisotropic mechanical properties in structural elements [72].

– **Natural fibers** require surface treatments, such as silane coupling agents, to improve adhesion and resist alkaline degradation [67]. Treated hemp fibers, for instance, can increase flexural strength by 12% in green concrete [73]. These fibers, when properly treated, offer sustainable advantages and enhance the mechanical properties of eco-friendly concrete mixtures.

2.6.4. Impact on Mechanical Properties

– **Compressive strength**: Fibers generally do not significantly increase compressive strength but improve post-cracking residual strength. For example, UHPC with 1.5% micro steel fibers achieves compressive strengths exceeding 150 MPa [69, 74]. But Natural fibers lower compressive strength [75].

– **Flexural and tensile strength**: fibers in UHPC increase flexural strength by up to 42.5 MPa, while hybrid fibers (steel + polypropylene) mitigate strength loss caused by additives like phase-change materials [68, 74].

– **Fatigue resistance**: Steel fibers extend the fatigue life of concrete by reducing crack growth rates, making them ideal for applications like wind turbine foundations [63].

2.6.5. Durability and Functional Benefits

– **Shrinkage and creep**: Fibers reduce drying shrinkage by up to 50% in HPC by restraining matrix deformation [76].

– **Thermal performance**: Microencapsulated phase-change materials (MPCMs) combined with fibers in UHPC improve thermal energy storage without compromising mechanical properties [74]. Natural fibers Improve thermal insulation (e.g., coconut fiber composites reduce thermal conductivity by 30%) [75].

– **Corrosion resistance**: Non-metallic fibers (e.g., carbon, glass) in FRP-concrete composites prevent corrosion in aggressive environments like marine structures .

2.6.6. Challenges and Limitations

– **Workability reduction**: High fiber content (>2% by volume) decreases flowability, requiring superplasticizers to maintain consistency [63, 76].

– **Cost and standardization**: UHPFRC's high material costs and lack of universal design codes limit widespread adoption [69].

– **Electrical conductivity**: Steel fibers reduce electrical resistivity, which may compromise concrete in sensitive applications [76].

2.7. Influence of fibers on fresh high-performance concrete

The incorporation of fibers into high-performance concrete (HPC) matrices induces significant alterations in their rheological behavior and fresh-state properties. The introduction of fibrous reinforcement, irrespective of their compositional nature (metallic, polymeric, or natural), engenders a marked reduction in flowability coupled with an augmentation in viscosity of the cementitious composite. This phenomenon is predominantly attributed to the enhanced internal friction between constituent materials and the formation of a complex three-dimensional fiber network within the matrix [9].

The geometric characteristics of fibers, particularly their aspect ratio (length-to-diameter ratio), exert a profound influence on the fresh-state properties. Experimental investigations by Grünewald and Walraven (2001) [77] have elucidated that elevated aspect ratios correlate with diminished workability, becoming particularly pronounced at fiber volume fractions exceeding 1%. This relationship can be attributed to the increased specific surface area of the fibers, necessitating additional cement paste for adequate fiber coating and workability maintenance.

The spatial distribution and orientational characteristics of fibers within the fresh concrete matrix fundamentally influence its rheological behavior. Khayat and Roussel's (2000) [78] research demonstrates that fibers of greater length exhibit enhanced flow resistance and increased susceptibility to agglomeration, particularly at elevated dosage rates. The mitigation of these effects

typically necessitates compositional modifications, including increased paste volume or the incorporation of high-performance chemical admixtures.

The temporal aspects of fiber incorporation during the mixing process represent a critical parameter affecting the fresh-state properties. Research conducted by Martinie et al. (2010) [79] indicates that delayed fiber addition in the mixing sequence facilitates superior fiber distribution and minimizes adverse effects on workability. This observation carries significant implications for optimizing production protocols and quality assurance procedures.

Furthermore, the water demand characteristics of fiber-reinforced HPC systems, as documented by Markovic (2006) [80], exhibit notable increases with fiber incorporation. This necessitates careful water management to maintain the requisite low water-to-cement ratios while ensuring adequate workability. Contemporary mix design methodologies frequently employ advanced chemical admixtures, including high-range water reducers and viscosity modifiers, to optimize the fresh-state properties of fiber-reinforced HPC systems.

The influence of fiber type on fresh concrete properties varies significantly, with research by Swamy (1974) [81] demonstrating that polymeric fibers, particularly polypropylene, generally exhibit reduced impact on workability compared to their metallic counterparts at equivalent volume fractions, primarily due to differences in specific gravity and surface characteristics.

2.8. Influence of fibers on the behavior of high-performance concrete in the hardened state

2.8.1. Mechanical Performance

The incorporation of fibers into high-performance concrete (HPC) fundamentally transforms its mechanical behavior through multiple interrelated mechanisms. The most significant enhancement occurs in the post-cracking response, where fibers act as bridges across developing cracks, providing resistance to crack propagation [82].This mechanism is particularly crucial in HPC, where the inherently high matrix strength would typically result in brittle behavior without fiber reinforcement.

The tensile behavior of fiber-reinforced HPC exhibits a marked transformation from brittle to pseudo-ductile response. As microcracks develop, fibers engage progressively, transferring stresses across these cracks through fiber bridging action. This effectiveness is enhanced in HPC due to its dense microstructure and improved interfacial transition zone. Research by Li and Wu

(2018) [83] has demonstrated that this fiber bridging mechanism can lead to multiple cracking behavior, significantly improving the material's strain capacity before failure.

In terms of flexural performance, fiber-reinforced HPC demonstrates substantial improvements compared to plain HPC. While plain HPC fails abruptly after crack initiation, fiber-reinforced variants maintain load-carrying capacity post-cracking. Experimental studies by Yoo et al. (2015) [84] have shown that this behavior is characterized by multiple cracking patterns, where numerous small cracks develop instead of a single large crack. The energy absorption capacity, measured through the area under the load-deflection curve, shows remarkable enhancement, often increasing by several orders of magnitude.

The compressive behavior of fiber-reinforced HPC shows improvements primarily in the post-peak region. While the peak compressive strength might only see modest increases of 5-15% [85]. The post-peak descent becomes more gradual, indicating enhanced energy absorption capacity. This characteristic is particularly valuable in high-strength applications where explosive failure modes can pose safety concerns.

Impact and fatigue resistance show significant enhancement with fiber incorporation. The three-dimensional fiber network provides multiple energy dissipation mechanisms, including fiber pullout, fiber stretching, and crack bridging. Research by Abbas and Khan (2016) [86] has demonstrated that these mechanisms are especially effective in HPC due to the superior fiber-matrix bond, leading to improved resistance against repeated loading and sudden impact forces. A summary of key research studies investigating the effects of various fibers on the mechanical properties of concrete is presented in Table 2.3.

Table 2.3 summary of key research studies investigating the effects of various fibers on concrete properties

Study	Fiber Type and Fiber Content	Research Focus	Key Findings
Song et al. (2005) [87]	Nylon/PP 0.1-0.5% by volume	Compressive and flexural strength	Minimal compressive effect; 20-30% flexural improvement
Qian & Stroeven (2000) [88]	PP/Steel hybrid (0.1-0.3% each type)	Hybrid fiber systems	Synergistic effects in hybrid systems
Zollo (1997) [45]	Polypropylene (0.1-0.2% by volume)	30-year development review	20-30% first-crack strength; 50-100% ultimate flexural
Johnston (2001) [46]	Various synthetic (0.1-0.3% by volume)	General FRC performance	10-25% split tensile improvement; uniform crack distribution
Silva et al. (2010) [89]	Plant fibers (0.5-1.0% by volume)	Flexural performance of natural FRC	25-40% flexural strength increase with optimal fiber length
Bos et al. (2006) [90]	Flax(0.6-0.8% by volume)	Tensile properties of flax FRC	30-50% direct tensile strength improvement with treatment
Yan et al. (2016) [91]	Flax (0.5-1.0% by volume)	Four-point bending behavior	3-5 fold toughness increase; pseudo- ductile behavior

2.8.2. Deferred Deformation (Shrinkage and Creep)

The influence of fibers on time-dependent deformations in HPC manifests through various mechanisms affecting both shrinkage and creep behavior. Shrinkage control is particularly significant in HPC, where higher cement content and lower water-to-cement ratios can lead to increased shrinkage potential. Fibers act as internal restraints, reducing both plastic shrinkage cracking in early ages and drying shrinkage in the long term [92].

Plastic shrinkage, occurring in the first few hours after casting, sees substantial reduction with fiber incorporation. Research by Wongtanakitcharoen and Naaman (2007) [93] has shown that fibers can reduce plastic shrinkage crack widths by up to 50% and total crack area by up to 85%. This improvement is attributed to the fibers' ability to bridge developing cracks and provide internal restraint against volume changes.

Drying shrinkage, a long-term phenomenon, also shows improvement with fiber reinforcement. Studies by Zhang and Li (2002) [94] have demonstrated that fiber-reinforced HPC exhibits reduced drying shrinkage strain compared to plain HPC, with reductions typically ranging from 10% to 30% depending on fiber type and content. This reduction is particularly beneficial in large-scale applications where shrinkage-induced cracking can compromise structural integrity.

Regarding creep behavior, fibers provide a restraining effect against long-term deformation under sustained loading. Research by Neville and Brooks (2010) [95] indicates that the creep coefficient can be reduced by up to 20% with optimal fiber reinforcement. This improvement is attributed to the fibers' ability to transfer stresses more uniformly through the matrix and their role in preventing the progression of internal microcracking under sustained load.

The type and volume fraction of fibers significantly influence their effectiveness in controlling deferred deformations. Steel fibers typically provide better restraint against both shrinkage and creep compared to synthetic fibers, primarily due to their higher elastic modulus. However, hybrid fiber systems, combining different fiber types, have shown promising results in optimizing both early-age and long-term deformation control (Shen et al., 2019) [96].

2.9. Durability Of Fiber-Reinforced High-Performance Concrete

The durability of fiber-reinforced high-performance concrete (FR-HPC) encompasses its ability to maintain serviceability and mechanical properties throughout its service life under various environmental exposures and loading conditions [10]. Understanding the durability mechanisms

requires examining several interconnected factors that contribute to the material's long-term performance.

2.9.1. Crack Control and Permeability

The primary enhancement to durability comes through crack control mechanisms, where fibers effectively bridge microcracks as they develop from mechanical or environmental stresses. This crack-bridging action significantly reduces concrete permeability, providing enhanced protection against aggressive agents such as chlorides and sulfates [97]. Research by Li and Kanda (1998) [98] has demonstrated that this crack control mechanism can reduce the average crack width by up to 60% compared to plain HPC.

2.9.2. Environmental Resistance

2.9.2.1. Freeze-Thaw Resistance

Freeze-thaw resistance in FR-HPC shows marked improvement through multiple mechanisms. The fiber network creates pressure relief points that help mitigate internal stresses during freezing cycles. Studies by Zhang et al. (2011) [99] have documented that properly designed FR-HPC can maintain up to 95% of its original strength after extensive freeze-thaw cycling, significantly outperforming conventional concrete systems.

2.9.2.2. Chemical Resistance

Chemical resistance benefits from the synergistic effect of HPC's dense microstructure and fiber reinforcement. According to Mehta and Monteiro (2017) [1], the fiber network helps maintain matrix integrity even under chemical attack, though fiber selection must align with exposure conditions. Their research indicates that synthetic fibers often demonstrate superior performance in highly acidic environments compared to steel fibers.

2.9.3. Long-Term Performance

2.9.3.1. Fatigue Behavior

The fatigue performance of FR-HPC shows significant enhancement through improved stress distribution mechanisms. Ganesan et al. (2015) [100] documented that fiber reinforcement can increase fatigue life by up to 200% compared to plain HPC, particularly under flexural loading

conditions. This improvement is attributed to the fibers' ability to arrest microcrack propagation and redistribute stresses more uniformly throughout the matrix.

2.9.3.2. Corrosion Resistance

Corrosion resistance, particularly relevant for steel fiber systems, depends heavily on the matrix density and exposure conditions. Research by Meson (2019) [101] demonstrates that while HPC's dense matrix provides good initial protection, surface fibers may require additional protective measures. Their studies suggest that hybrid systems combining different fiber types can optimize both mechanical performance and durability characteristics.

2.9.4. Surface Durability and Environmental Aging

2.9.4.1. Impact and Abrasion Resistance

Impact and abrasion resistance show marked improvement with fiber incorporation. Studies by Wang et al. [102] indicate that FR-HPC can exhibit up to 50% higher abrasion resistance compared to conventional HPC. This enhancement is particularly beneficial in applications such as industrial floors and pavements where surface degradation is a primary concern.

2.9.4.2. Environmental Aging Effects

Environmental aging effects on FR-HPC vary significantly based on fiber type and exposure conditions. Long-term studies by Wang and Xu (2023) [103] highlight the importance of understanding degradation mechanisms for different fiber types, particularly the effects of UV radiation on synthetic fibers and moisture fluctuations on fiber-matrix bond strength.

2.10. High-Performance Concrete Reinforced with Vegetable Fibers

The construction industry is increasingly turning to sustainable alternatives to conventional materials, driven by environmental concerns and the pursuit of enhanced performance. High-performance concrete (HPC) represents a paradigm shift in this context, combining superior mechanical properties, durability, and workability. However, its reliance on synthetic fibers (e.g., polypropylene, steel) and cementitious binders raises ecological and economic challenges. This review explores the potential of vegetable fibers as eco-friendly reinforcements in HPC, addressing their impact on fresh and hardened properties, durability, and long-term sustainability.

2.10.1. Types of Vegetable Fibers

Vegetable fibers derive from diverse plant sources, including leaves, stems, seeds, and fruits. Key examples relevant to HPC applications include:

– **Hemp (Cannabis sativa)**: Known for high tensile strength (600–1,100 MPa) and compatibility with cementitious matrices, hemp fibers are widely studied for improving flexural toughness and reducing shrinkage in HPC [104].

– **Date Palm (Phoenix dactylifera)**: Abundant in arid regions, date palm fibers exhibit moderate tensile strength and thermal stability, making them suitable for high-temperature environments [105].

– **Sisal (Agave sisalana)**: With high cellulose content, sisal fibers enhance energy absorption but require surface treatments to mitigate alkaline degradation [106].

– **Coir (Cocos nucifera)**: Derived from coconut husks, coir fibers improve water retention and crack resistance in HPC, though their hydrophilicity demands careful integration [107].

– **Flax (Linum usitatissimum)**: Lightweight and flexible, flax fibers contribute to enhanced ductility but face challenges related to moisture absorption [Ahmed, 2013].

2.10.2. Impact of Vegetable Fibers on HPC Properties

2.10.2.1. Fresh State Behavior:

Vegetable fibers often reduce workability due to their hydrophilic nature, increasing water demand and affecting flowability. However, studies suggest that optimized fiber dosage (e.g., 0.5–2 kg/m³) and surface treatments (e.g., silane coatings) can mitigate these issues while preserving self-compacting properties [108, 109].

2.10.2.2. Mechanical Performance:

– **Flexural Strength**: Incorporation of hemp or flax fibers enhances fracture toughness by 15–30%, attributed to fiber-matrix interfacial bonding [110].

– **Compressive Strength**: Moderate reductions (5–20%) in compressive strength are observed at higher fiber dosages (>1%), but these are offset by improved post-cracking resistance [111].

– **Tensile Strength**: Date palm fibers increase splitting tensile strength by 10–15%, leveraging their natural roughness for improved anchorage [112].

2.10.3. Durability:

– **Alkaline Degradation:** The high pH of cementitious environments degrades lignin and hemicellulose in vegetable fibers, reducing tensile strength by up to 70% after prolonged exposure [113].

– **Chloride Penetration:** Coir fibers reduce chloride ingress by 30–40% in marine-exposed HPC, enhancing corrosion resistance [114].

– **Carbonation Resistance:** Partial cement replacement with pozzolanic materials (e.g., metakaolin) lowers matrix alkalinity, protecting fibers from degradation and improving carbonation resistance [115].

2.10.4. Strategies to Enhance Fiber-Matrix Compatibility

2.10.4.1. Matrix Modification:

– Substituting 30–50% of cement with silica fume or metakaolin reduces OH^- ion concentration, slowing fiber degradation [116].

– Rapid carbonation techniques further lower pH, enhancing fiber longevity [117].

2.10.4.2. Fiber Surface Treatment:

– Hydrophobic coatings (e.g., silane, wax) reduce water absorption by 30–50%, improving workability [118].

– Alkaline treatment (e.g., NaOH) increases fiber tensile strength and matrix adhesion, the alkaline treatment acts as a refining process. It strips away the fiber's weak outer layers to create a rougher, stronger surface for better adhesion, while also improving the internal structural integrity of the fiber itself [119].

2.11. Conclusion

The incorporation of various fiber types in high-performance concrete (HPC) significantly enhances its mechanical properties, durability, and functional benefits. Steel fibers, glass fibers, synthetic fibers, and natural fibers each offer unique advantages and limitations, making them suitable for specific applications. The selection of fiber type, aspect ratio, dosage, and surface treatment is critical to optimizing the performance of fiber-reinforced HPC.

The mechanisms of fiber reinforcement, including crack control, energy dissipation, and load transfer, play a crucial role in improving the post-cracking behavior, impact resistance, and fatigue performance of HPC. However, challenges such as workability reduction, cost, and environmental impact must be carefully addressed through advanced mix design, chemical admixtures, and sustainable practices.

The use of vegetable fibers in HPC emerges as a promising avenue for sustainable construction, offering eco-friendly alternatives with moderate performance benefits. However, further research is needed to address issues related to alkaline degradation, moisture absorption, and long-term durability of vegetable fibers in cementitious matrices.

Overall, fiber-reinforced HPC represents a significant advancement in civil engineering materials, contributing to the development of sustainable and resilient infrastructure.

Chapter 03

Materials and tests methods

Chapter 03

MATERIALS AND TESTS METHODS

3.1. Introduction

This chapter provides a comprehensive overview of the materials and experimental protocols central to our research program, structured into three interconnected sections. First, we systematically present the tests and methodological procedures implemented to ensure rigorous data collection. Second, we detail the rationale behind the selection of base materials, emphasizing locally sourced, widely available constituents that align with sustainable and cost-effective practices. Third, we characterize the engineered materials, focusing on their mechanical performance, durability, and environmental impact. The formulations explored integrate a curated range of materials, including CEM I 52.5 Portland cement as the primary binder, natural aggregates (sand and gravel) from the BENI FOUDA quarry to ensure regional resource efficiency, and the third-generation polycarboxylate ether-based superplasticizer medaflow 30 to enhance workability. Potable tap water from urban networks is used for mixing, while natural flax fibers and synthetic polypropylene fibers are incorporated to improve tensile strength and crack resistance. Granulated blast-furnace slag from El Hadjar (Annaba) serves as a supplementary cementitious material, reducing the carbon footprint while enhancing durability. These materials collectively optimize mechanical properties and sustainability, aligning with the development of high-performance concretes.

3.2. Cement

The cement used are of the CEMI 52 N-LH/SR5 type in accordance with Algerian standard NA 442. The various chemical, physical and mechanical characteristics of the cement used are set out in data sheets supplied by the cement manufacturer. The results of the chemical composition and Physical properties of the clinker of the cement are shown in Table 3.1.

Figure 3.1 a) Cement CEMI 52 and b) Blast furnace slag used.

Table 3.1 The chemical composition and Physical properties of the clinker of the cement.

Chemical composition (%)	
SiO_2	20.75
$Al2O_3$	4.52
Fe_2O_3	5.22
CaO	63.54
MgO	1.27
SO_3	2.44
K_2O	0.22
Na_2O	0.18
CL	0.0001
LOI	0.72
Physical properties	
Specific Gravity	3.23
Blaine (cm^2/g)	3418
Passing 45 µm (%)	13.64

3.3. Aggregates

The standard (NF P18-541) shows that aggregates have certain characteristics that make them suitable for use in making concrete. Aggregates used in building and civil engineering works must meet quality requirements and characteristics specific to each use. These characteristics must be established by means of various laboratory tests.

The gravel and sand used comes from a calcareous rock from the beni fouda setif region. Two fractions for gravel, G4/8 mm and G8/16 mm, and quarry sand, size 0/1 and 0/4 mm.were chosen for our concrete formulation. Aggregates is the most important constituent of concrete, and its quality is therefore a determining factor in the quality of the resulting concrete.

Figure 3.2 aggregates used.

3.3.1. Granulometric analysis

Aggregates are of natural origin, crushed limestone from the BENI FOUDA quarry in Setif (eastern Algeria). From this quarry, we were able to obtain three granular classes delivered under the following trade names: Sand 0/4, Gravel 4/8, 8/16. And dune sand of ADRAR class 0/1 Granulometric analysis enables us to determine the size and respective weight percentages of the different families of grains making up the sample. The test results for the aggregates used are shown in Figure 3.3.

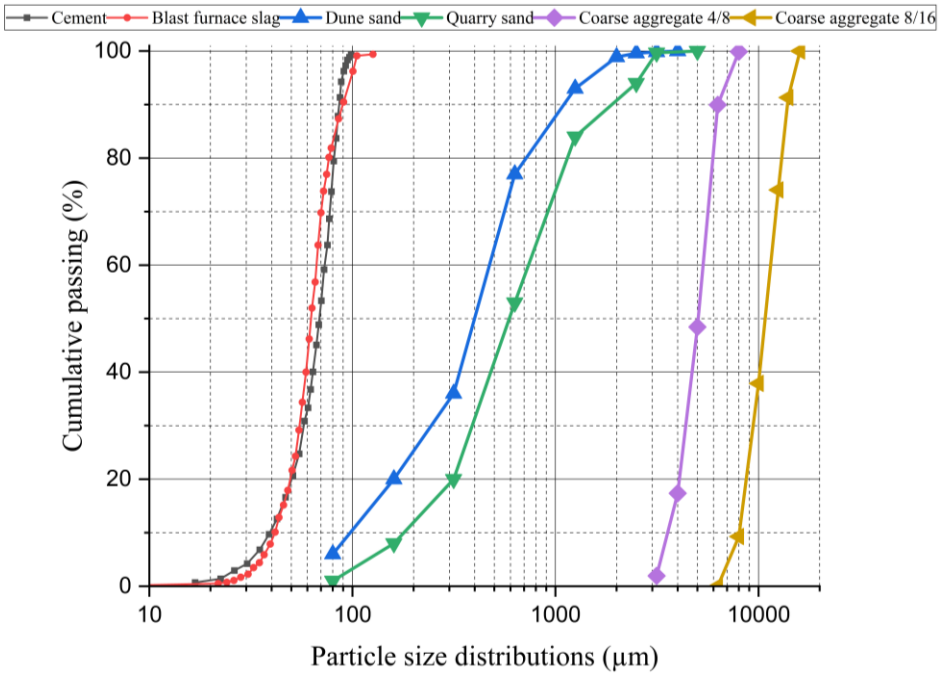

Figure 3.3 Granulometric analysis of aggregates.

3.3.2. Flattening coefficient (NF EN 933-3)

The flattening coefficient test is one of the tests used to characterize the shape of aggregates. The sample must be prepared in accordance with the standard (NF EP 18-553).

- Results should be recorded on test sheets see $\boldsymbol{R_i}$ est la masse de chaque granulat élémentaire *di* /*Di*, exprimée en grammes ;
- $\boldsymbol{m_i}$ est la masse du matériau de chaque granulat élémentaire *di* /*Di* passant à travers la grille à fentes correspondante, d'écartement *Di*/2, en grammes.

Table 3.2). Calculate the sum of masses of the elementary aggregates di /Di, or M_1.

Calculate the sum of the masses of the grains of each elementary aggregate di/Di passing through a corresponding corresponding slotted grid, spaced Di /2, or M_2.

The overall flattening coefficient A is calculated from the following equation:

$$\mathbf{A} = \sum \frac{\mathbf{M_2}}{\mathbf{M_1}} \times \mathbf{100} \qquad \textbf{(3.1)}$$

Where :

- $\mathbf{M_1}$ is the sum of the masses of the elementary aggregates di /Di, in grams.
- $\mathbf{M_2}$ is the sum of the masses of passers-by on the corresponding slotted grids of spacing Di /2, in grams.

The flattening coefficient for each elementary aggregate Ai should be calculated, if necessary, from the following equation:

The flattening coefficient of each elementary aggregate Ai should be calculated, if necessary, from the following equation:

$$A_i = \sum \frac{m_i}{R_i} \times 100 \quad \textbf{(3.2)}$$

- R_i est la masse de chaque granulat élémentaire *di* /*Di*, exprimée en grammes ;
- m_i est la masse du matériau de chaque granulat élémentaire *di* /*Di* passant à travers la grille à fentes correspondante, d'écartement *Di*/2, en grammes.

Table 3.2 Flattening coefficient.

Tamisage sur tamis		**Tamisage sur grilles**	
Classe granulaire en (mm)	**M (gr)**	**Ecartement des grilles**	**Passant M**
50		31,5	
40-50		25	
31.5 – 40		20	
25 – 31.5		16	
20 – 25		12,5	
16 – 20	201.1	10	25.1
12.5 – 16	1564.4	8	233.8
10 – 12.5	967.9	6,3	151.89
8 – 10	334.7	5	54.1
6.3 – 8	92.1	4	16.8
5 – 6.3	9.9	3.15	1.8
4 – 5	1	2.5	
$M_1 = \sum = 3171.1$ gr		$M_2 = \sum = 483.5$ gr	
The flattening coefficient (A) is given by Equation (3.2) = 15 %			

Figure 3.4 a) series of sieves used. b) flattening window grid.

3.3.3. Absolute and apparent density of aggregates

Density is one of the most important physical characteristics of aggregates, influencing the behavior of fresh concrete and consequently its performance after hardening. Different densities can be defined for aggregates: apparent and absolute densities (NF EN 1097-3). Figure 3.5 shows the different aggregates used.

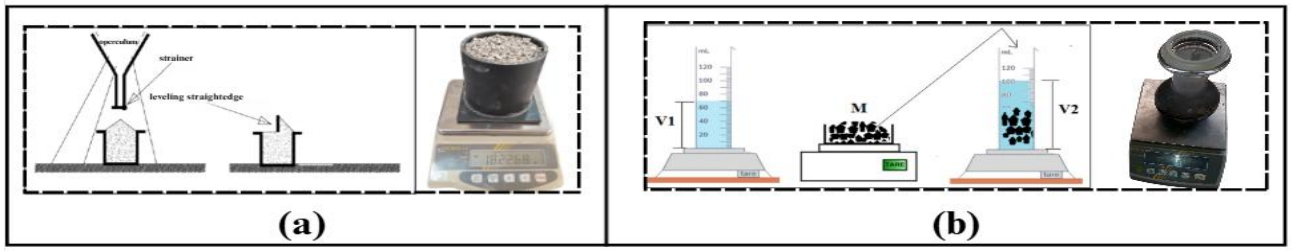

Figure 3.5 Density determination procedure: a) Apparent density. b) Absolute density.

Table 3.3 Density values of aggregates used.

	Absolut (g/mm³)	**Apparent (g/mm³)**
Sand	2.66	1.55
Goarse aggregats (4/8)	2.70	1.41
Goarse aggregats (8/16)	2.73	1.58

3.3.4. Methylene blue and sand equivalent test

The methylene blue test, also known as the "blue test", is a test used to determine the cleanliness of a sand and the different types of clays it contains. Sand equivalent is an indicator of sand cleanliness. It indicates the content of fine elements of essentially clay, plant or organic origin on the surface of the grains. Table 3.4 shows the values for methylene blue (NF EN 933-9+A1) and sand equivalent (NF EN 933-8+A1).

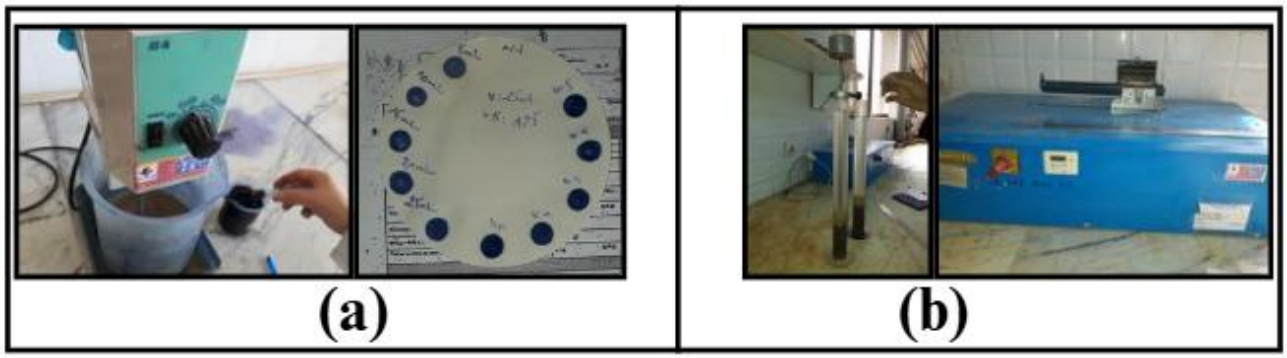

Figure 3.6 Tests for: a) Methylene blue. b) sand equivalent.

Table 3.4 Values for methylene blue and sand equivalent.

	SET	Methylene blue
Sand	67	1.25

3.3.5. Aggregate strength

When making concrete, mixing is the source of intense friction between the grains. If the aggregates are not strong enough, they can break, producing sand or fine particles. The tests carried out are:

3.3.5.1. Impact resistance Los Angeles (NF EN 1097-2):

The test consists in measuring the mass of elements smaller than 1.6 mm. Produced by the fragmentation of the aggregate tested, which is subjected to the impact of standardized balls in the cylinder of the Los Angeles machine over 500 rotations.

3.3.5.2. Wear resistance Micro Deval test (NF EN 1097-1):

The test consists in measuring, under standardized conditions, the wear of aggregates produced by mutual friction, in the presence of water and an abrasive charge, in a rotating cylinder. Table 3.5 shows the mechanical characteristics of 8 /16 gravel.

Table 3.5 Mechanical characteristics of 8/15 chippings.

Micro Deval	Los Angeles	Gravier
14%	17%	(10/14)

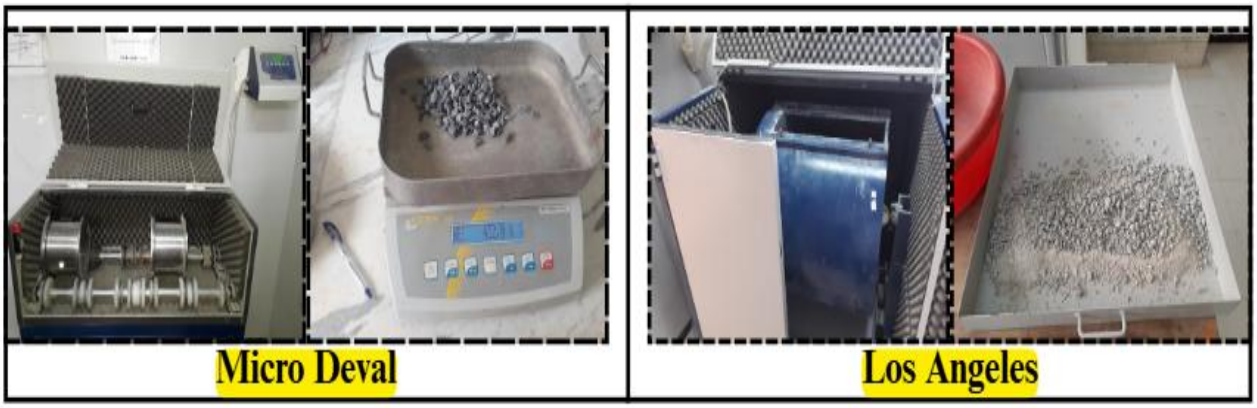

Figure 3.7 Aggregate strength tests.

3.4. Mineral additions

The mineral additions used in our study are characterized by a particle size of less than 80µm, the Figure 3.8 shows the stages of its preparation for use in concrete as a powder that replaces cement by 10%.blast-furnace slag from El Hadjar (Annaba) whose main characteristics are shown in Table 3.6,And its granulometric analysis in Figure 3.3.

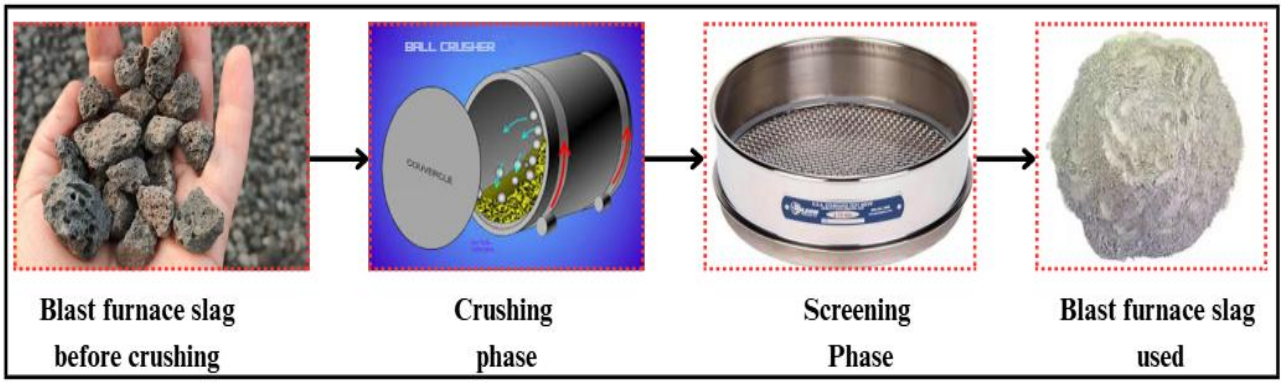

Figure 3.8 Phases of powder blast furnace slag preparation.

Table 3.6 Chemical and physical composition of blast-furnace slag

Chemical composition (%)	
SiO_2	32.84
Al_2O_3	5.09
Fe_2O_3	0.94
CaO	33.55
MgO	4.35
SO_3	1.12
K_2O	0.49
Na_2O	0.33
Physical properties	
Specific Gravity	2.91
Blaine (cm^2/g)	2364

3.5. Additives (superplasticizers)

Admixtures are water-soluble products. They are incorporated into concrete in doses of 2% or less by weight of cement. In our study, we used MEDAFLOW 30 Superplasticizer, a third-generation high water-reducing superplasticizer. It is based on ether polycarboxylates, which considerably improve concrete properties. MEDAFLOW 30 enables the production of high-quality concrete and mortar. In addition to its main function as a superplasticizer, it enables the water content of concrete to be greatly reduced without altering consistency. MEDAFLOW 30 has no retarding effect on setting. Some of MEDAFLOW 30's characteristics are presented in the appendix.

3.6. Mixing water [NA EN 1008]

To mix our concrete, we used the tap water available at our university, whose physicochemical characteristics are as follows:

Table 3.7 Physicochemical characteristics of water.

Parameter	Quantity	Comment
pH	8.12	Acceptable for mixing.
Conductivity	1253 µs/cm	
Rate of (Cl-)	0.23mg/l	0.05 to 0.50
Rate of (NO_2)	0,14mg/l	> max. concentration (0.1)
Rate of (NO_3)	1,9mg/l	< at max. concentration (50)
Turbidity	1,43 NTU	
Total hardness	6,62 °F	15-50
Dry residue	100 mg/l	

Chemical analysis of the mixing water was carried out at the chemistry laboratory of Elbachir El Ibrahimi University, Bordj Bou Arreridj. The results showed that the water tested was suitable for making concrete.

3.7. Fibres

In the study, flax fiber (linen fiber) and polypropylene fiber were used as reinforcement materials in concrete. Flax fiber, known for its high tensile strength, stiffness, and durability, was used in two lengths: 1.5 cm and 3 cm. These lengths were chosen to explore their impact on concrete reinforcement, with longer fibers potentially providing greater tensile strength and shorter fibers offering better dispersion and workability. Polypropylene fiber, a synthetic fiber with high strength, low density, and excellent chemical resistance, was used in a length of 1.2 cm. This

shorter length was selected to ensure good dispersion within the concrete matrix while still providing effective reinforcement. The combination of these fibers in different lengths allows for a comprehensive evaluation of their reinforcement capabilities in concrete applications.

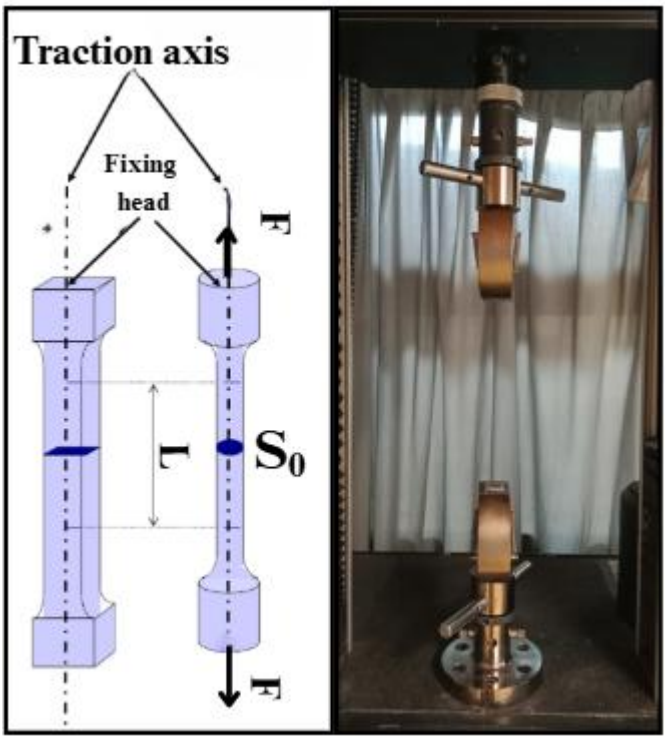

Figure 3.9 Fiber tensile test.

$$\sigma = \frac{F}{S_0} \times 100 \quad (3.3)$$

F: Force (N). **S_0:** Surface (mm). **б:** Tensile stress (MPa).

Table 3.8 Shows the mechanical and physical properties, and Table 3.9 shows the chemical composition of the flax fibers used in our study. of the fibers used in our study. ASTM D8171 was used to determine the density of flax fibers.

Table 3.8 Characteristics of fibers used.

Fiber type	Diameter (mm)	Density (g/cm ^{3})	Water[120] absorption (%)	Tensile stress (MPa)	Lenght (mm)
Flax	0.05	1.42	111	600	15-30
Polypropylene	0.025	0.9	-	450	12

Table 3.9 Chemical composition of flax fiber [121].

Flax	**Cellulose (%)**	**Lignine (%)**	**Cendre (%)**
	43 - 47	21 – 23	5

3.7.1. Alkaline Treatment

The process initiates with an alkaline treatment, where raw flax fibers are submerged in a 5% sodium hydroxide (NaOH) solution for 60 minutes. This concentration was validated via preliminary experiments by Amouri et al., which confirmed its efficacy in optimizing fiber properties. The treatment removes surface impurities and waxes while enhancing fiber roughness, improving adhesion in concrete matrices, as highlighted by Li et al [122].

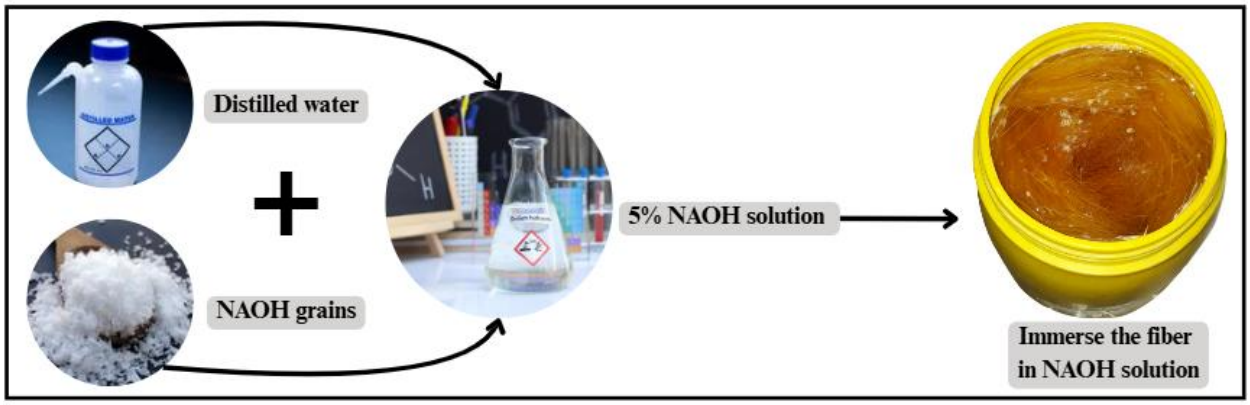

Figure 3.10 Flax fibers alkaline treatment.

3.7.2. Fiber preparation

The fiber preparation process goes through several stages, as follows:

3.7.2.1. Neutralization and Drying

Post-treatment, fibers are rinsed repeatedly with distilled water until the rinse water reaches a neutral pH, ensuring residual NaOH is fully eliminated. The fibers are then air-dried naturally, avoiding external heat sources.

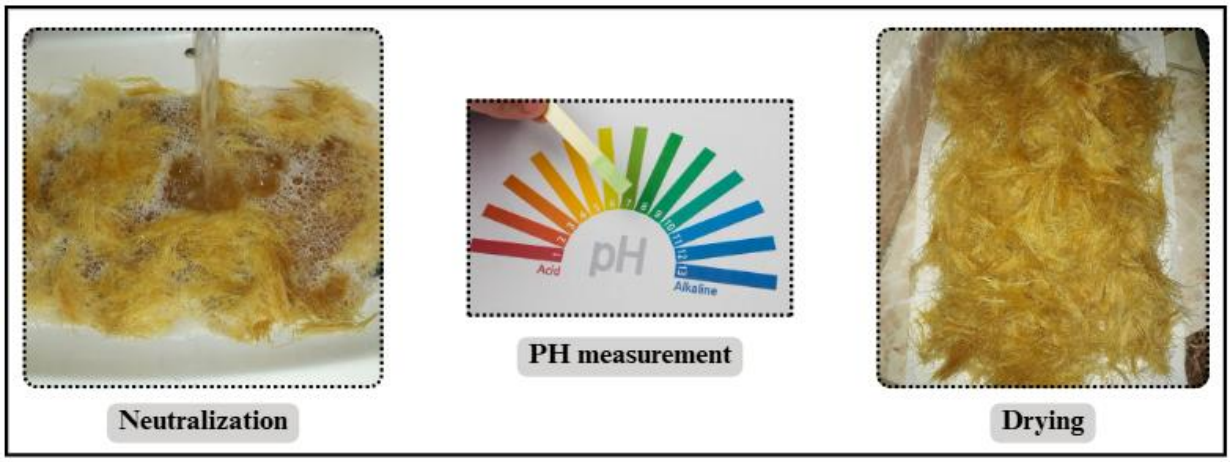

Figure 3.11 Neutralization and drying phase.

3.7.2.2. Bundling and Sorting

Dried fibers are sorted into uniform bundles, each containing fibers of consistent length, weighing ~5 grams, and measuring ~5 mm in diameter. This step standardizes the fibers for precise cutting.

Figure 3.12 Bundling and Sorting phase.

3.7.2.3. Cutting and Storage

Bundled fibers are trimmed to specified lengths using precision tools, with clearly defined cutting zones to maintain uniformity. The resulting segments are stored in sealed containers, ready for integration into high-performance concrete formulations.

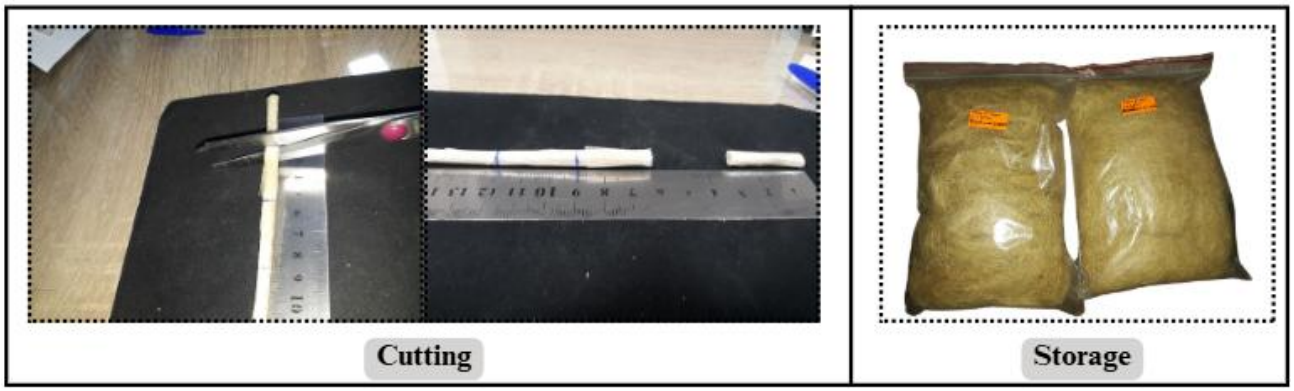

Figure 3.13 Cutting and Storage phase**.**

3.8. Concrete formulation

Nine types of formulations were prepared. Table 3.10 shows the proportions of the mixes used in this study. The preparation of concrete mixes was based on the University of Sharbrook's method

Table 3.10 Composition of different blends (kg/m^3).

	HPC	PP1215	PP1230	FF1515	FF1530	FF1550	FF3015	FF3030	FF3050
w/b	0.30	0.30	0.30	0.30	0.30	0.30	0.30	0.30	0.30
Cement (kg/m^3)	420	420	420	420	420	420	420	420	420
Blast furnace slag(kg/m^3)	47	47	47	47	47	47	47	47	47
Coarse aggregate (kg/m^3)	993	993	993	993	993	993	993	993	993
Fine aggregate (kg/m^3)	836	836	836	836	836	836	836	836	836
Water (kg/m^3)	140	140	140	140	140	140	140	140	140
Superplasticizer (L/m^3)	5	5	5	5	5	5	5	5	5
Polypropylene fiber (kg/m^3)	–	0.76	1.51	–	–	–	–	–	–
Flax fiber length 15 mm (kg/m^3)	–	–	–	0.76	1.51	2.52	–	–	–
Flax fiber length 30 mm (kg/m^3)	–		–	–	–	–	0.76	1.51	2.52

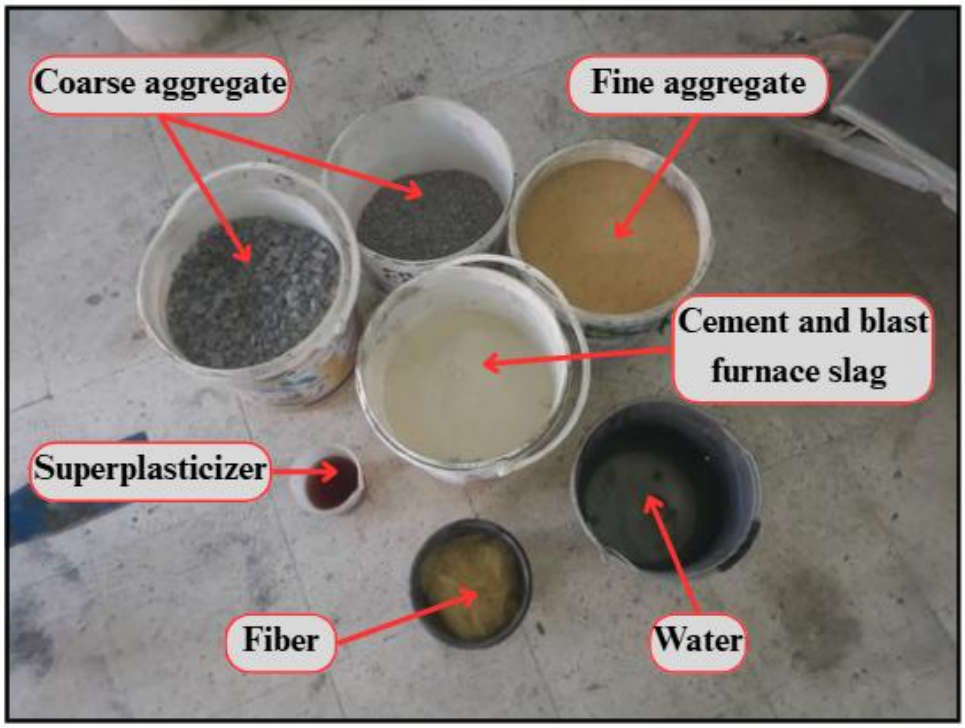

Figure 3.14 Composition of a blends.

3.8.1. Concrete preparation:

All mixes were made in a vertical shaft mixer with a maximum capacity of 70 liters Figure 3.15, mixing as follows:

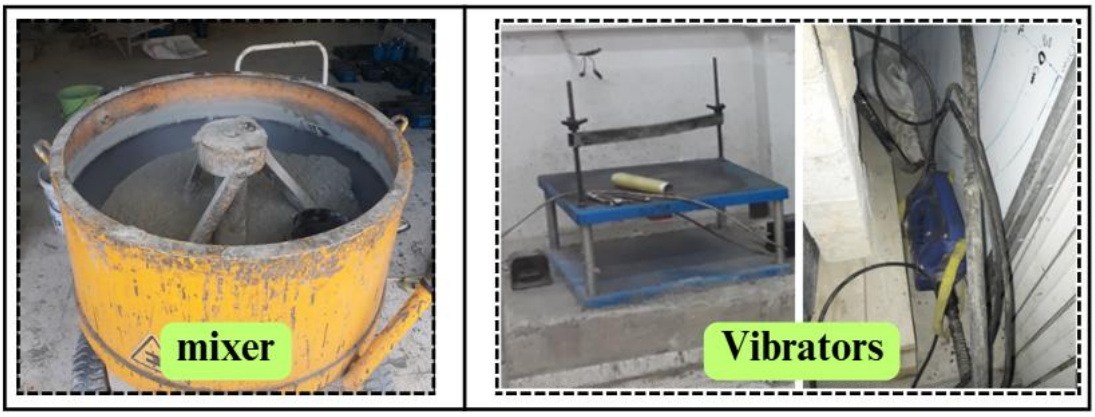

Figure 3.15 Concrete mixer and vibrators used.

The concrete mixing process was executed as follows:

3.8.1.1. Dry Mixing :

- Initially, cement and blast furnace slag were thoroughly combined for 2 minutes until fully homogenized.

- Sand was then added, followed by coarse aggregate.
- Fibers were manually incorporated and evenly dispersed.
- The mixture was subsequently blended for an additional 3 minutes at varying speeds and directions to ensure uniform distribution.

3.8.1.2. Wet Mixing :

- One-third of the water and two-thirds of the superplasticizer were carefully added.
- The remaining two-thirds of water and the remaining one-third of superplasticizer were then incorporated.
- Finally, the concrete was mixed at high speed for 1 minute.

3.8.2. Specimen preparation and storage conditions

After mixing, fill the molds in two layers and vibrate the concrete with a vibrator until a slight bleed appears, then flatten and smooth the concrete surface.

left in the molds for 24 h. Upon demolding, all samples were carefully sealed in transparent plastic to protect them from external influences and retain sufficient internal moisture, ensuring optimal cement hydration. The storage environment, maintained at a constant temperature of 23◦C with controlled relative humidity of 30%, was designed to promote proper cement hydration and minimize environmental variations that could impact material performance.

Figure 3.16 Specimen after demolding and sealed in transparent plastic.

Table 3.11 Tests specific to each type of specimen.

	Specimen types		
	Cubic (100 x 100 x 100 mm³)	**Cylindrical (100 x 200 mm²)**	**Prismatic (70 x 70 x 280 mm³)**
Tests	Compressive test	Split tensile test	fFexural strength test
	Porosity	/	Shrinkage test
	Capillarity absorption	/	/
	Ultrasonic	/	/
	Thermal conductivity	/	/

The test specimens produced after studying the workability of our concrete are as follows: (in accordance with standards ASTM C39,ASTM C496,ASTM C78, ASTM C830, ASTM C1585–20, ASTM C1784,and NF P18–427 [123-129]).

3.9. Characterization tests

Two families of tests are carried out to characterize our mixes:

- Fresh-state tests to select and evaluate concrete workability.
- Tests in the hardened state to determine the concrete's mechanical performance.

3.9.1. Tests carried out in the fresh state

In general, there are several tests available to characterize the rheological properties of high-performance concretes.

In this study, we use the two tests available in the laboratory to optimize and characterize the consistency of our concrete:

- ABRAMS cone slump test.
- Rheology test.
- Measure the density of fresh concrete.

3.9.1.1. ABRAMS cone subsidence test

The slump test is performed to determine the workability of concrete. The test used is that described in ASTM C143 [130]. This test consists of molding concrete cone sections (base diameter 20 cm, top diameter 10 cm) (see Figure 3.17). The cone is filled in 3 layers, each pricked 25 times

with a 16 mm diameter metal rod. The mold is then gently lifted, and the slump (or SLUMP) measured immediately afterwards.

This is still the simplest and most widely used method for characterizing the rheological behavior of site concretes.

Figure 3.17 Subsidence at the ABRAMS cone.

3.9.1.2. Rheology test

To assess the rheological behavior of the concrete, an ICAR concrete rheometer was employed. The ICAR rheometer is a specialized device designed for measuring the fundamental flow properties of fresh concrete, such as yield stress and plastic viscosity, based on the Bingham model. The specific model used in this study was the ICAR Plus, which is a portable and robust instrument suitable for both laboratory and on-site measurements.

The rheometer is equipped with a four-blade vane (RHM-3009), which has an inner radius of 63.5 mm and a height of 127 mm. This vane is inserted into a cylindrical container with dimensions of approximately 30 cm in diameter and height, allowing for the measurement of the concrete's resistance to flow under controlled shear rates. The ICAR rheometer operates by applying a controlled shear rate to the concrete sample and measuring the resulting torque, from which the rheological parameters are determined.

The rheometer is controlled using a dedicated software interface installed on a laptop. This software allows for precise control of the measurement process, including the selection of shear rates, data acquisition, and real-time monitoring of the rheological parameters. The software also

provides tools for data analysis and reporting, enabling a comprehensive evaluation of the concrete's rheological properties.

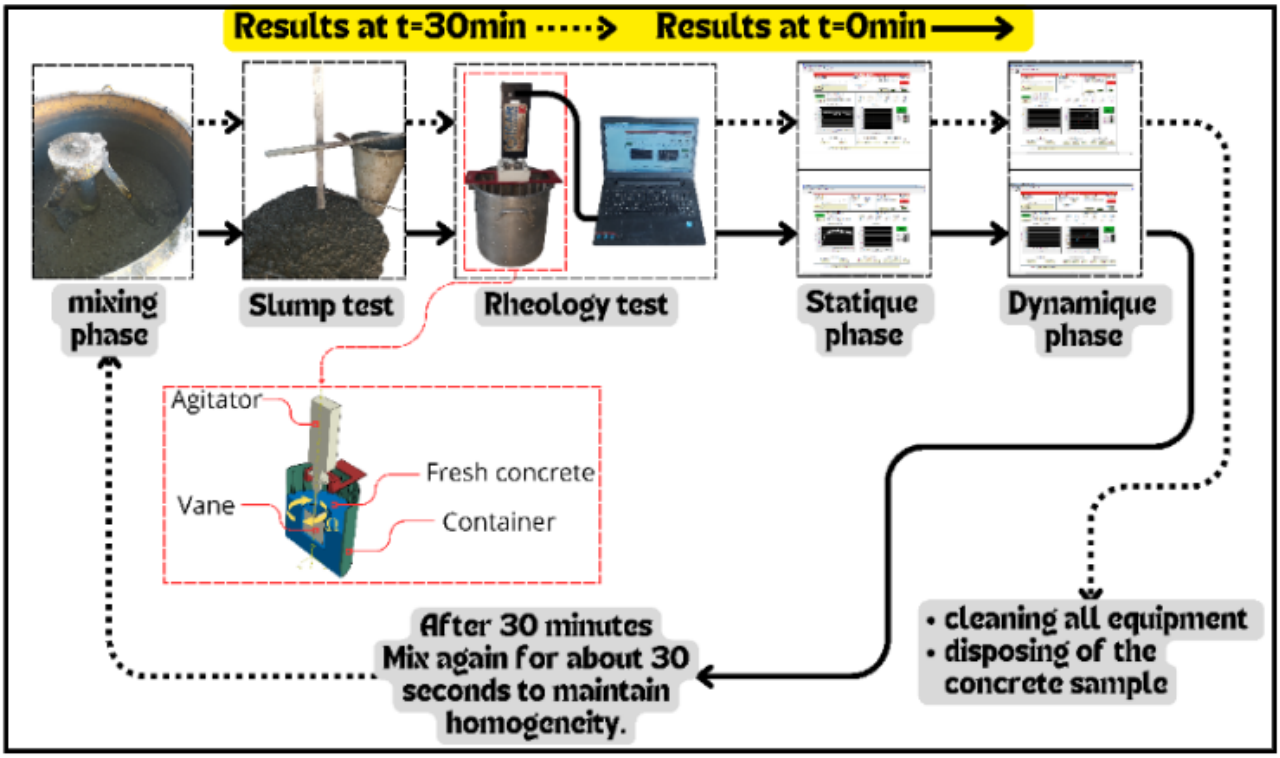

Figure 3.18 Experimental Protocol of Rheology test.

3.9.1.3. Principle of the rheological test

The principle of the rheological test using the ICAR concrete rheometer involves rotating a vane at different speeds within a cylindrical sample of fresh concrete and measuring the applied torque. A vane was chosen over a cylinder because its insertion into the sample causes minimal disturbance compared to a cylinder, which is advantageous for thixotropic materials such as mortar .

The test procedure begins with pouring the prepared fresh concrete (HPC) into the cylindrical container. The vane, which is connected to the rheometer's motor and torque measurement system, is then lowered into the center of the container until it penetrates the concrete. It is crucial to ensure that the upper end of the vane's blades is level with the surface of the concrete. The rotation of the vane is then initiated, following a predefined velocity profile controlled by the software.

The imposed velocity profile is selected based on a series of preliminary tests aimed at finding the profile that provides the most stable measurements while minimizing the phenomenon of segregation. The chosen profile should have a sufficient number of data points to accurately characterize the concrete's behavior. The intervals between the imposed velocity steps should be

spaced appropriately to clearly distinguish the different pairs of angular velocity (Ω) and torque (M).Figure 3.19 illustrates the selected velocity profile for the test procedure.

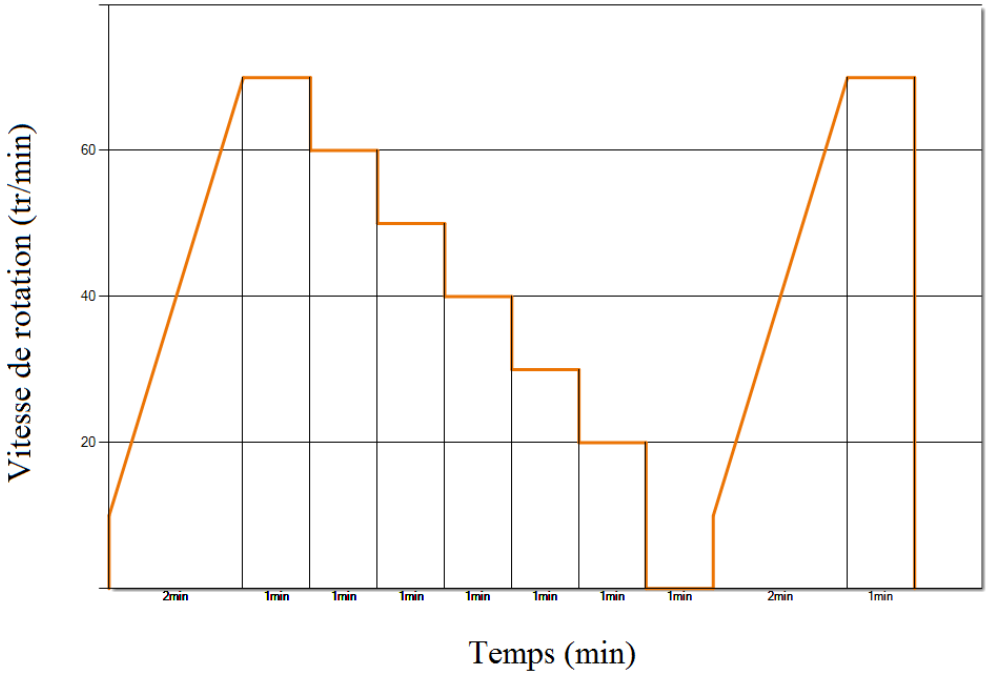

Figure 3.19 Profil de vitesse.

3.9.1.4. Density of HPC in the fresh state

Measuring the density of fresh concrete involves [131]:

- Measuring the density of fresh concrete involves [129] :
- Take the empty container weightM_0 (Kg).
- Fill a container with a sample of volume V (Kg) and weight M_0 (Kg) known by a sample of the fresh concrete, which has undergone vibration.
- Flatten and smooth the surfaces and take the weight of this container of concrete to be M_1 (Kg).

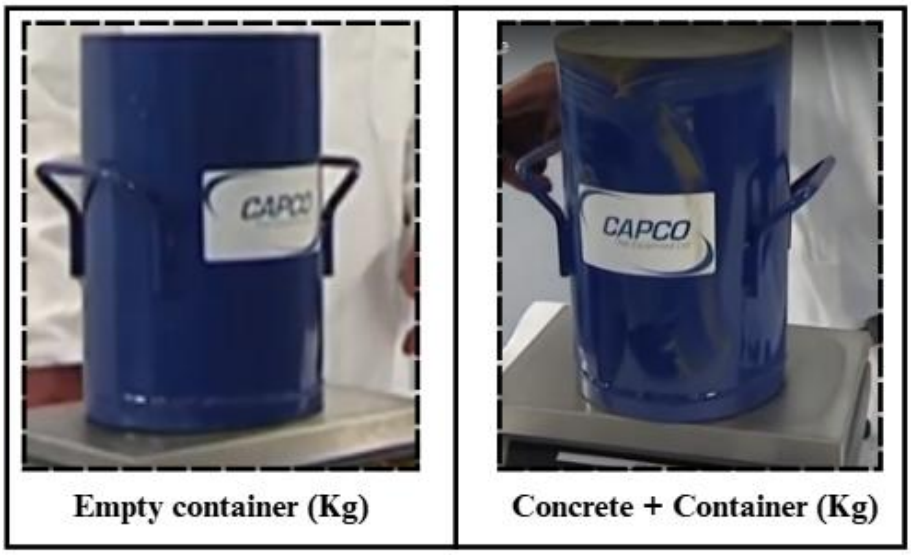

Figure 3.20 Density of HPC in the fresh state.

The density ρ (Kg/m3) of fresh concrete is :

$$\boldsymbol{\rho = \frac{M_1 - M_0}{V}} \tag{3.4}$$

3.9.2. Tests in the hardened state

Tests conducted on hardened concrete evaluate its long-term mechanical properties, durability, and performance after achieving sufficient strength. These tests are critical for assessing structural integrity, safety, and compliance with design specifications. They include both destructive (e.g., compressive strength, tensile strength) and non-destructive methods (e.g., rebound hammer, ultrasonic pulse velocity).

3.9.2.1. Compressive strength

Compressive crushing strength tests were carried out on cubic specimens cubic specimens (100 x 100 x 100) mm3 in accordance with ASTM C39 [123]. The specimens were crushed specimens was carried out on a hydraulic press with a loading speed of 5 ± 0.1 KN/Sec.

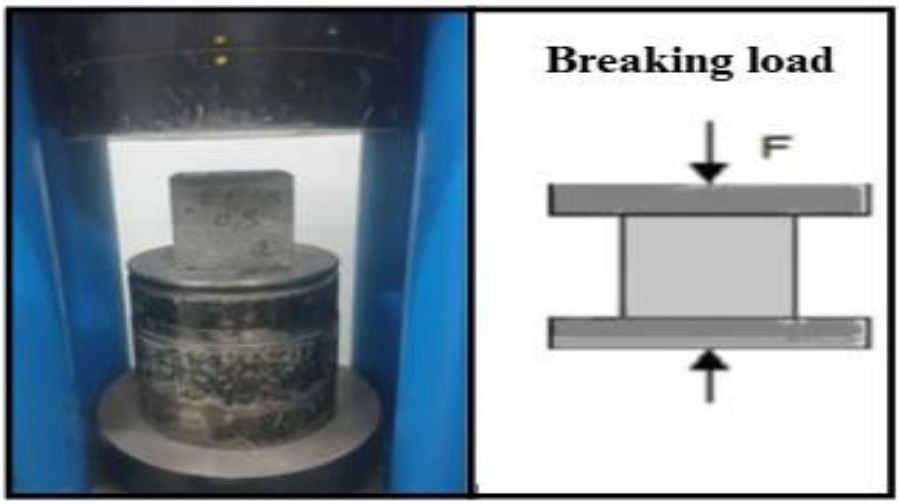

Figure 3.21 Diagram of the compression device.

Compressive strength σ_c is calculated using the following formula:

$$\sigma_c = \frac{F}{S} \tag{3.5}$$

With:

σ_c : Compressive stress (MPa) **F :** Breaking load (in N) **L :** Span length (mm)

S (a^2) : Compression area of specimen (100 x 100 mm2).

3.9.2.2. Flexural tensile strength (3-point bending)

Flexural behavior is the most important aspect for fiber-reinforced concrete, as this composite material is most often subjected to this type of loading in these applications. Fibers are added to the concrete matrix to improve ductility and provide control over the cracking mechanism.

This is the most widely used and best-known material characterization test. The test is carried out on prismatic specimens (70 x 70 x 280 mm³) in accordance with ASTM C78 [125].

The flexural tensile strength (σ) is calculated using the formula:

$$\sigma_f = \frac{F \times L}{2 \times w \times d^2} \tag{3.6}$$

Where :

σ_f : Flexural tensile strength (MPa) **F :** Maximum load at failure (N) **L :** Span length (mm)

w: Width of the specimen (mm) **d :** Depth of the specimen (mm)

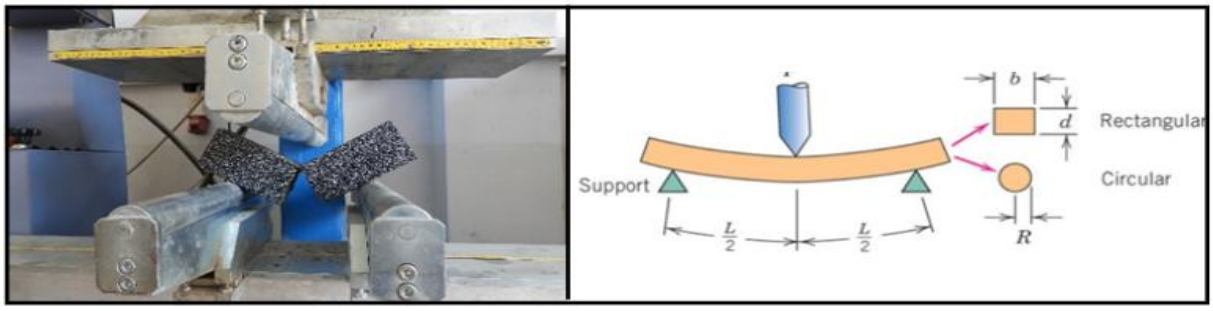

Figure 3.22 Diagram of the 3-point bending device.

3.9.2.3. The split tensile test

The split tensile test, also known as the Brazilian test, is an indirect method used to determine the tensile strength of concrete. It involves applying diametral compressive forces to a cylindrical specimen until it fractures, allowing engineers to calculate the tensile strength. This test is critical for evaluating concrete's ability to resist tension, which is essential for assessing structural integrity and durability in accordance with ASTM C496 [124]

The formula used is:

$$\sigma_t = \frac{2P \times L}{\pi \times L \times D} \quad (3.7)$$

Where:

σ_t : Splitting tensile strength (MPa) **P :** Maximum load at failure (N)

D : Diameter of the specimen (mm) **L :** Length of the specimen (mm)

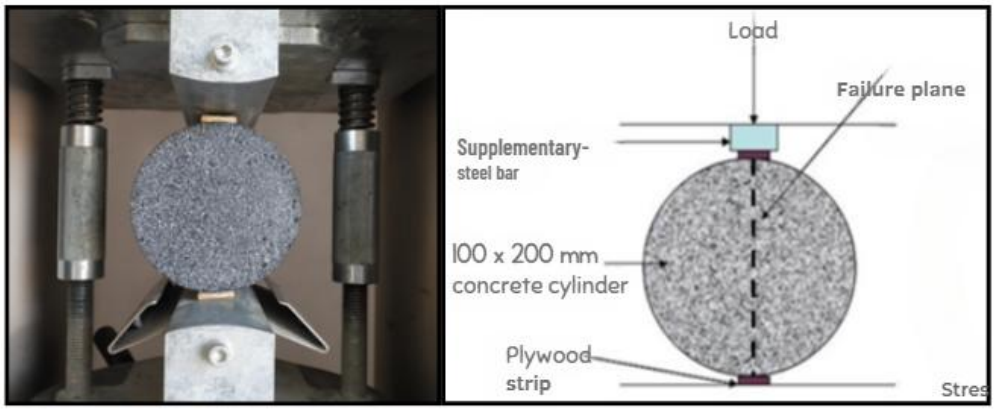

Figure 3.23 Splitting tensile.

3.9.2.4. Porosity Test

A porosity test measures the percentage of voids (pores or air spaces) in concrete relative to its total volume. This property significantly influences concrete's mechanical strength, durability,

permeability, and resistance to environmental degradation. High porosity reduces strength and increases susceptibility to water ingress, freeze-thaw damage, and chemical attack

Physical Measurement Specimens are saturated with water, and the volume of absorbed water (representing pore volume) is measured. Porosity (%) is calculated as:

$$\varphi = \frac{V_v}{V_t} \times 100 \quad (3.8)$$

Where:

Vv : Absorbed water volume (mm^3) **Vt :** Specimen volume (mm^3) **φ :** Porosity (%)

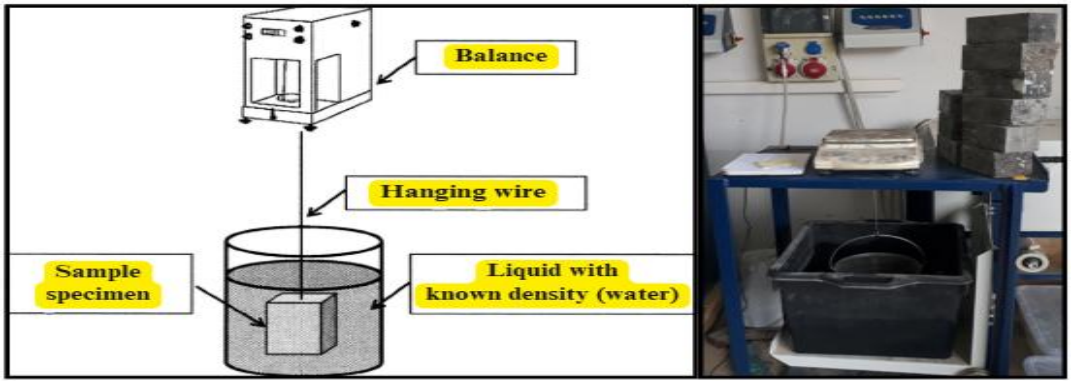

Figure 3.24 porosity test.

3.9.2.5. The capillary absorption test

The capillary absorption test evaluates the rate and extent of water uptake in concrete through capillary pores. This test measures how water migrates into unsaturated concrete via capillary action, which is critical for assessing durability, permeability, and resistance to chloride ingress, carbonation, and freeze-thaw damage

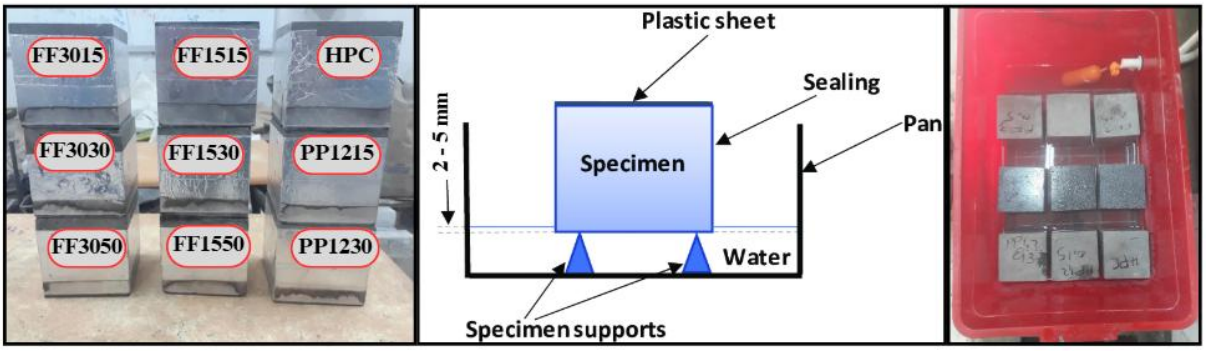

Figure 3.25 The schematic diagram of the capillary absorption test.

Specimen Preparation cubics (100 mm × 100 mm × 100 mm) for 28 days.The bottom surface is sealed with waterproof material (e.g., wax or aluminum), and the sides are coated to prevent lateral water flow.

The specimen is placed vertically in a water through with the bottom end submerged in water (depth: 2–5 mm). The height of the wetting front (water penetration) is recorded at intervals (10 min, 30 min, 1 h, 2 h, 4 h, 24 h), and cumulative water absorption is calculated using the formula:

$$\mathbf{A} = \frac{\mathbf{m}_t - \mathbf{m}_0}{\mathbf{A}_s} \times \mathbf{100} \quad \textbf{(3.9)}$$

Where :

A: Capillary absorption coefficient (g/mm2). **m_t:** Mass of specimen at time (t).

m_0: initial mass (g). **A_s:** Submerged surface area mm2.

3.9.2.6. Ultrasonic tests

The principle of the ultrasonic method is to measure the propagation time of ultrasonic pulses passing through concrete. The main features of all commercially available devices include a pulse generator and a pulse receiver, as shown in Figure 3.26.

Figure 3.26 Ultrasonic tests

This test is carried out in accordance with [132]. It is performed on cubic test specimens (10x10x10) cm3.

After activating the device, the propagation time is read off in microseconds (µsec). The distance between the heads must be known to an accuracy of 1% in order to calculate the propagation velocity using the following expression:

$$\mathbf{V} = \frac{\mathbf{s}}{\boldsymbol{t}} \cdot \mathbf{10^6} \qquad \textbf{(3.10)}$$

With:

V: The propagation speed of ultrasonic waves in concrete in (m/s).

s: The distance between the heads in (m). **t:** The propagation time in (µs).

Table 3.12 Concrete quality as a function of pulse propagation speed.

Propagation speed (m/s)	**Concrete quality**
Above 4575	Excellent
3660 to 4575	Good
3050 to 3660	Poor
2135 to 3600	Poor
Below 2135 Very	Very poor

3.9.2.7. Shrinkages endogenous

For each concrete, shrinkage measurements were carried out longitudinally on 7 x 7 x 28 cm^3 prismatic specimens, tightly wrapped in aluminum foil to prevent external reaction and preservation. These measurements were carried out using a refractometer (accuracy ± 0.001 mm),

see Figure 3.27. The test tubes were stored in the open air at a temperature of 32 ± 2°C and a relative humidity of 50% ± 5%.

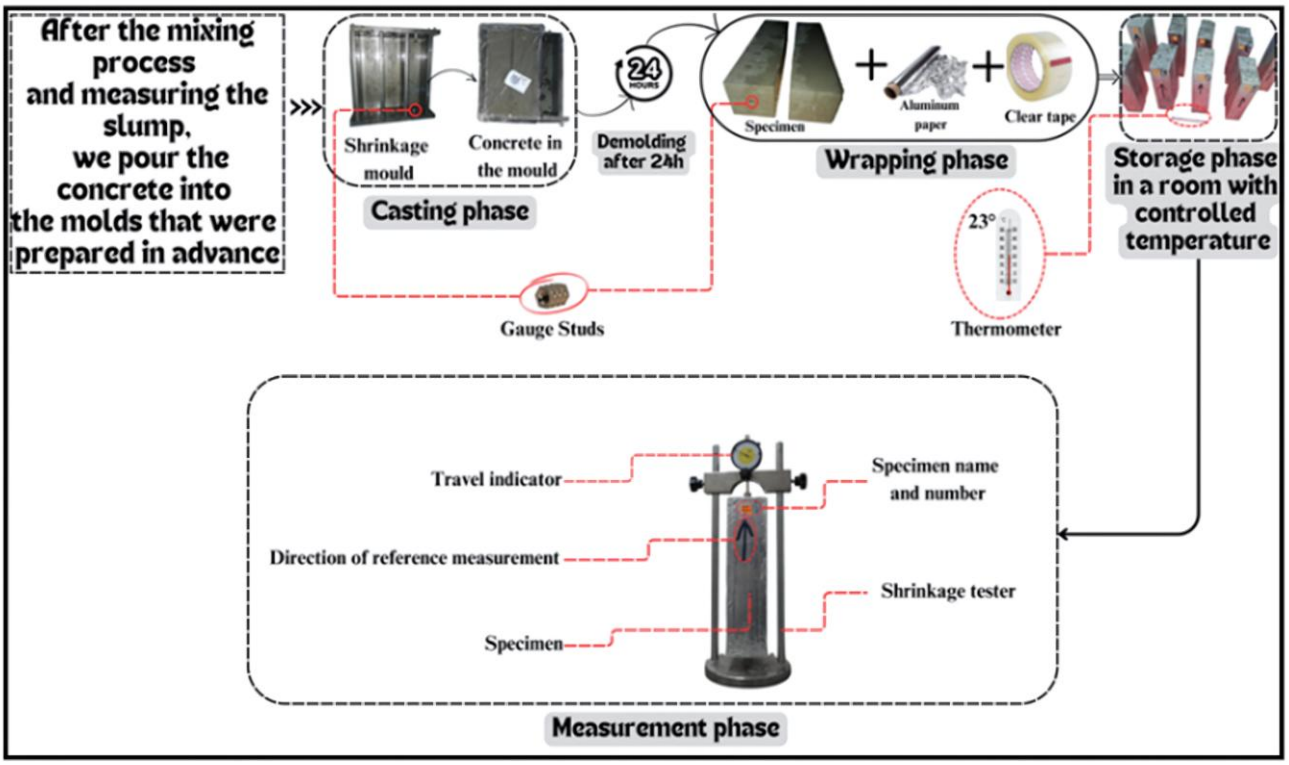

Figure 3.27 Experimental Protocol of shrinkage test.

Figure 3.28 Samples for Shrinkage Experiment.

3.9.2.8. Thermal conductivity

The thermal conductivity of the various mortars was measured using a HOT DISK TPS 1500 conductivity meter [133].

Tests were carried out at a room temperature of 20±2°C and a relative humidity of 50±5%. The thermal probe was inserted between two cubic test specimens (100x100x100 mm3) (Figure 3.29). Measurements were taken at 28 days of age.

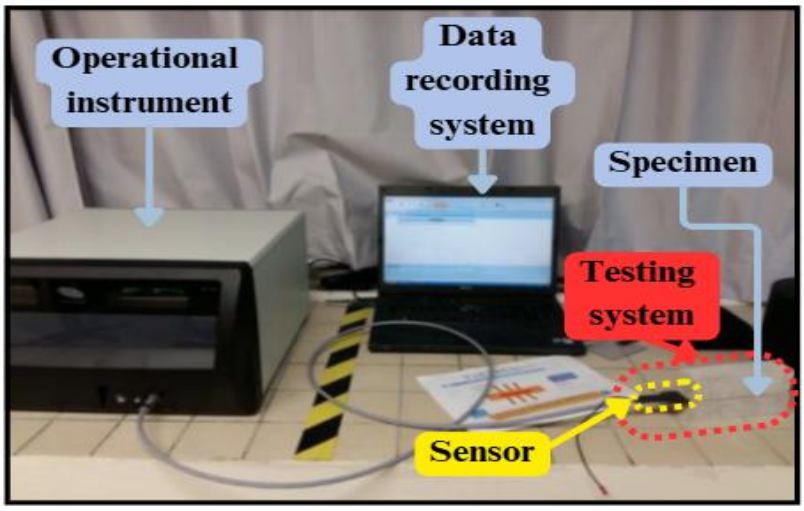

Figure 3.29 Thermal conductivity [133]

3.9.2.9. Digital Image Correlation (DIC)

Digital Image Correlation (DIC) is a non-contact optical measurement technique used to analyze the deformation, strain, and motion of objects by comparing digital images taken before and after loading or deformation. GOM Correlate is a software package developed by GOM (now part of Zeiss) that implements DIC and 3D motion tracking. It is widely used in materials research, engineering, and quality control to study deformation, strain, and motion with subpixel precision.

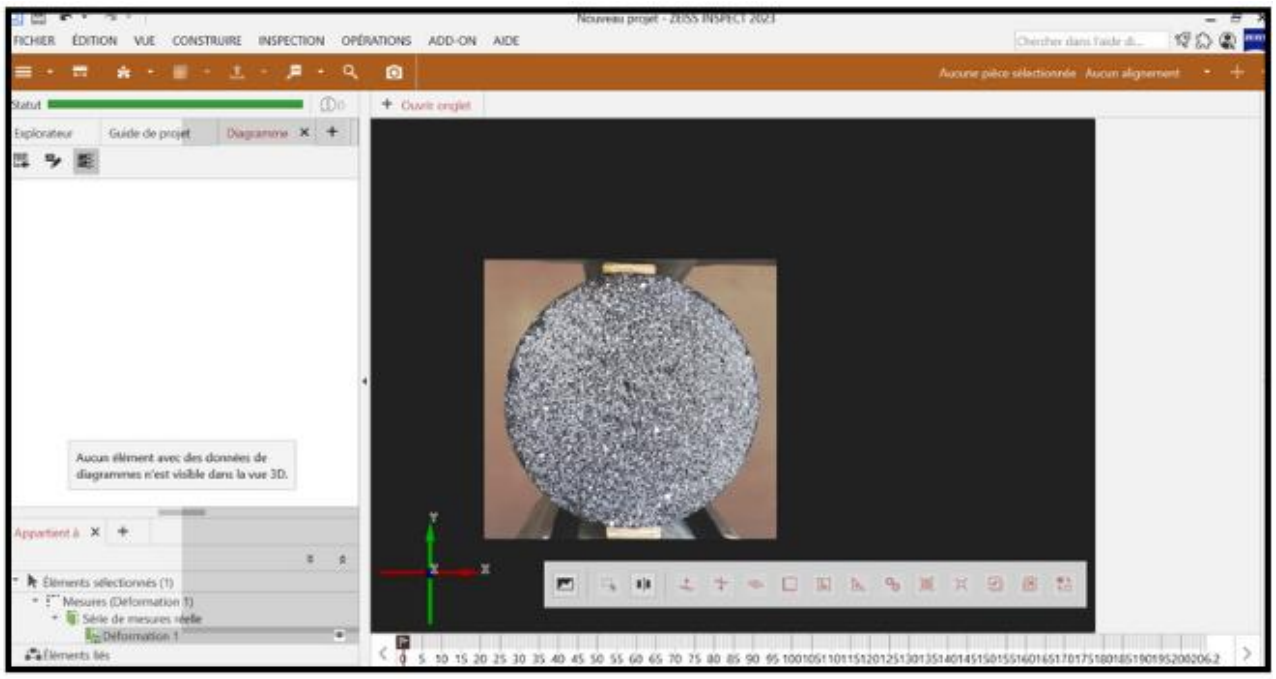

Figure 3.30 GOM Program Interface.

a. Specimen Preparation for (DIC)

Specimen preparation for Digital Image Correlation (DIC) in concrete involves applying high-contrast, isotropic speckle patterns (e.g., spray paint or QR codes) to the surface to ensure DIC algorithms can track deformation accurately; these patterns must be random and consistent in size (~10–20 pixels) show Figure 3.31. Specimens are also sealed to prevent moisture ingress, which could distort measurements. Experimentally, 3D-DIC setups use synchronized camera systems to capture stereoscopic images for full-field 3D deformation analysis, with camera calibrated to mitigate environmental factors like lighting or vibrations. During testing, specimens are subjected to controlled loads (compressive, tensil,fluxural) to induce deformation or cracking, while DIC captures images at incremental load stages for detailed analysis.

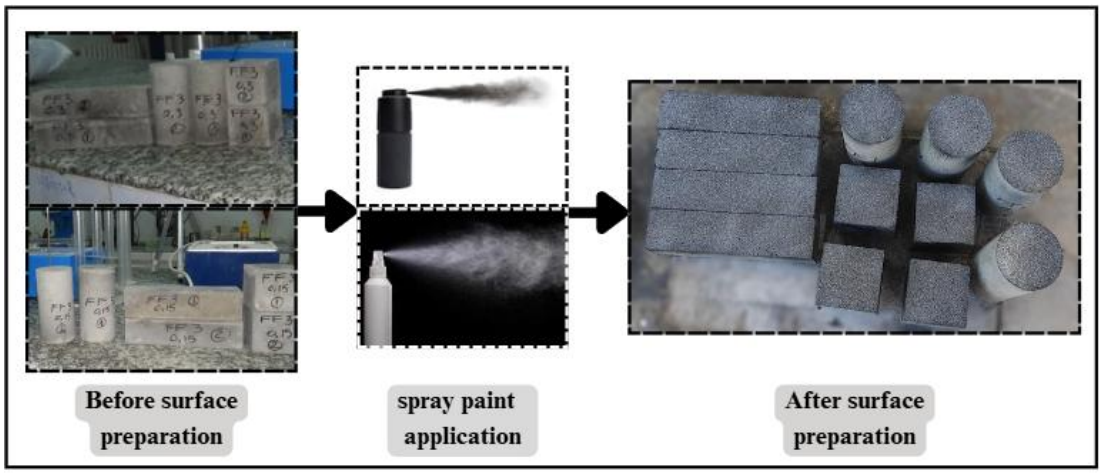

Figure 3.31 Specimens Preparation for (DIC)

b. During testing

The prepared specimen is placed in a compression testing machine, and a high-resolution 4K camera (such as a Nikon Coolpix P1000 with 3840x2160 pixel resolution and an f/2.8 aperture), meticulously mounted on a specialized tripod and precisely aligned perpendicular to the specimen surface, captures a series of images (or video) documenting the deformation. These photos, collected at regular intervals, establish a thorough record of the material's reaction to applied stresses. Utilizing digital image and video processing software (such as GOM Correlate), the essence of DIC rests inside a sophisticated image correlation technique. This method analyzes the collected pictures to monitor exact point motions, local strain distributions, and possible micro-cracking spots. By establishing the first picture as a reference state (undeformed configuration), subsequent images are tested against this baseline. The program then separates each picture into tiny subsets or facets (usually 20-50 pixels square) and records the movement and distortion of each subset across subsequent photos.

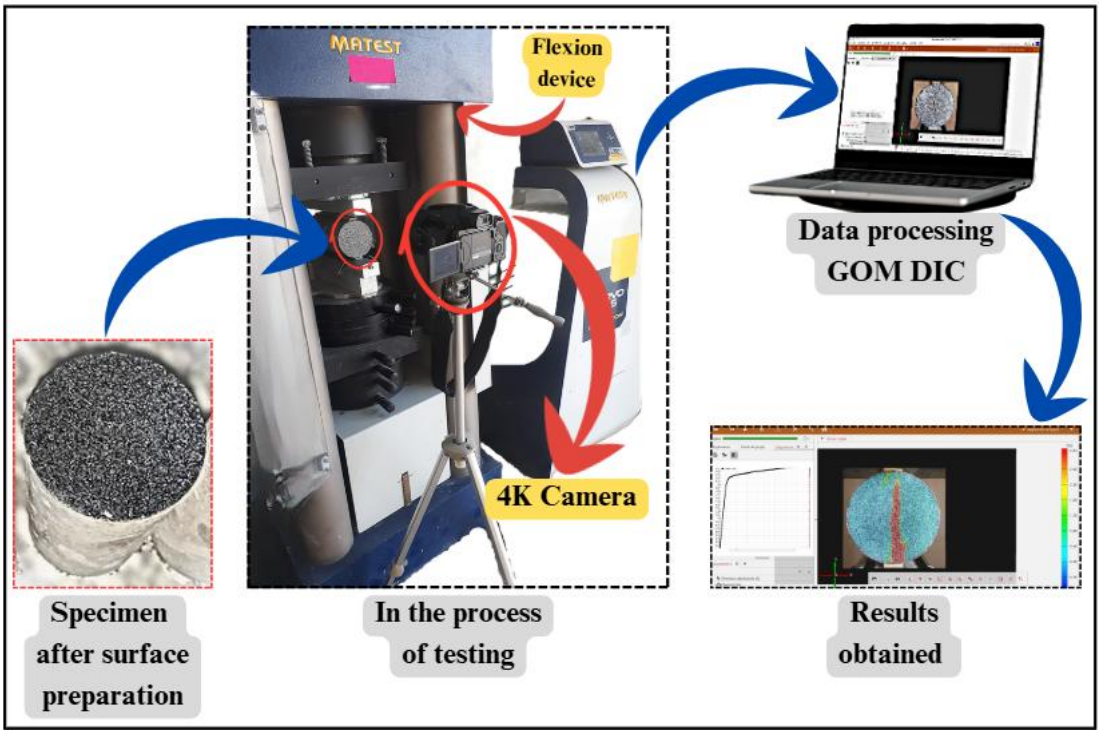

Figure 3.32 DIC phases.

3.9.2.10. Scanning Electron Microscopy (SEM)

There is a well-understood relationship between the microstructure of cement pastes and their physical and mechanical properties. As part of our study, a scanning electron microscope (SEM) microstructural analysis was carried out on FF and PP compositions at 28 days of age using a Zeiss Gemini SEM 300 is an imaging technique for observing and analysing the surface of a sample with high resolution and depth of field. This type of SEM, equipped with a field effect gun (FEG), offers very high quality images with sub-nanometric detail. The Environmental Scanning Electron Microscope (SEM), used to study the morphology, microstructure and cracking of concrete, is a material observation technique using an electron beam after evacuating the sample. Primary electrons from the electron gun strike the surface of the sample; they are scattered elastically and inelastically, and the area influenced takes on a pear shape.

Figure 3.33 The scanning electron microscope (SEM) used.

3.9.2.11. X-ray concrete CT

Computed Tomography (CT) is a non-destructive imaging technique that enables researchers to visualize the internal structure of concrete samples in two or three dimensions. This method operates by passing X-rays through the concrete and analyzing the resulting data to generate detailed images of its internal components. CT is particularly valuable for studying concrete's microstructure, identifying cracks and other damage, and understanding its behavior under various conditions. Originally developed for medical applications, X-ray CT has since been adapted for use in materials science, the chemical industry, and biology, among other fields. Recent advancements have successfully applied this technology to characterize the microstructure of concrete, signifying considerable progress in the field. Based on the technical capabilities demonstrated in medical CT, we are confident that our studies provide sufficient evidence for the successful application of CT in analyzing concrete and concrete elements to determine aggregate size and distribution, pore or void size and distribution, and fiber distribution. This is especially relevant for fiber-reinforced concrete, a composite material that offers superior performance characteristics compared to traditional concrete[134].

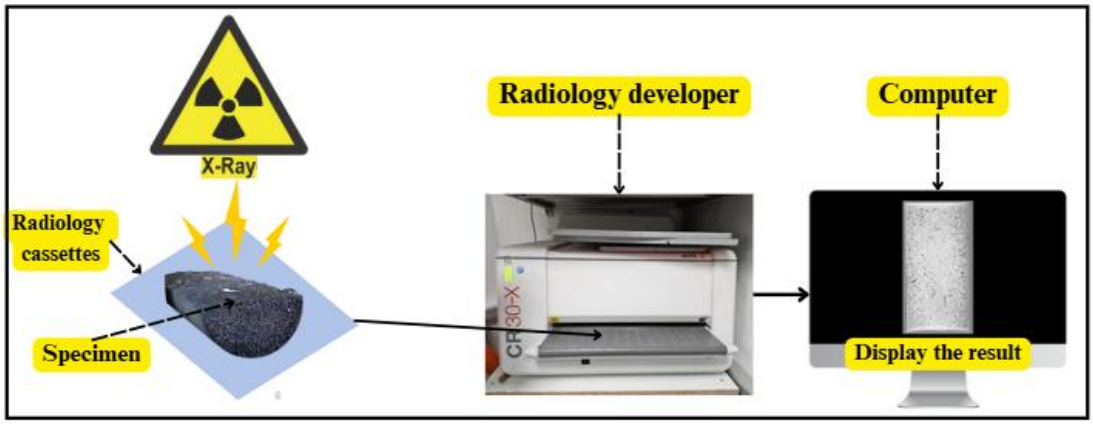

Figure 3.34 X-ray concrete CT steps

Chapter 04

Results and discussion

Chapter 04

RESULTS AND DISCUSSION

4.1. Introduction

This chapter is a synthesis of the results obtained for the various experiments we conducted in our study, starting with the fresh concrete experiments the workability and rheological behavior of high-performance concrete (HPC) reinforced with polypropylene (PP) and flax fibers (FF), focusing on their synergistic effects on workability, mechanical performance, and durability. The slump test results show that increasing fiber content reduces flowability due to heightened internal friction and fiber-matrix interactions. PP fibers induce greater slump reductions than plant-based fibers due to their finer diameter and higher filament density per unit volume. Despite these challenges, all mixtures retained sufficient workability for practical application, with the FF3050 blend showing the most pronounced impact. The rheological properties of fiber-reinforced concrete were rigorously evaluated using the ICAR Rheometer protocol, revealing a strong negative correlation between slump and yield stress. The chapter also explores hardened-state properties, linking microstructural changes to macro-scale performance. Alkali-treated flax fibers enhance crack resistance and load distribution. Digital Image Correlation analyses provide unprecedented spatial resolution of deformation mechanisms, while microstructural imaging validates the role of fiber-matrix adhesion in mitigating shrinkage and improving durability. This chapter advances the understanding of fiber-reinforced HPC, offering actionable insights for optimizing mix designs in sustainable construction.

4.2. Slump test

Figure 4.1 presents the slump test outcomes for various concrete mixtures incorporating distinct proportions of PP (polypropylene) and FF (flax fiber) fibers. The Figure 4.1 highlights how altering fiber content impacts the workability of fresh high-performance concrete (HPC). As fiber dosage increased, the mixtures exhibited reduced flowability. Specifically, compared to the baseline mix, slump values dropped by 2%, 15%, 8%, 26%, 11%, and 36% for PP1215/FF1515, PP1230/FF3030, FF1530, FF1550, FF3015, and FF3050, respectively.

This decline in workability stems from elevated fiber volume, which intensifies internal friction within the concrete matrix by increasing fiber-matrix interactions and hindering flow [135]. Higher fiber concentrations exacerbate entanglement between fibers, further diminishing slump. Notably, PP fibers caused greater reductions in flowability than plant-based fibers due to their finer diameter and shorter length, which heighten friction and interaction with the matrix. For equivalent fiber volumes, PP fibers have a denser filament count than plant fibers [136].

The FF3050 mixture, containing the highest fiber content and longest flax fibers, showed the most pronounced slump reduction (17 cm, a 36% decrease from the control HPC). Despite this, the concrete retained sufficient fluidity for practical application.

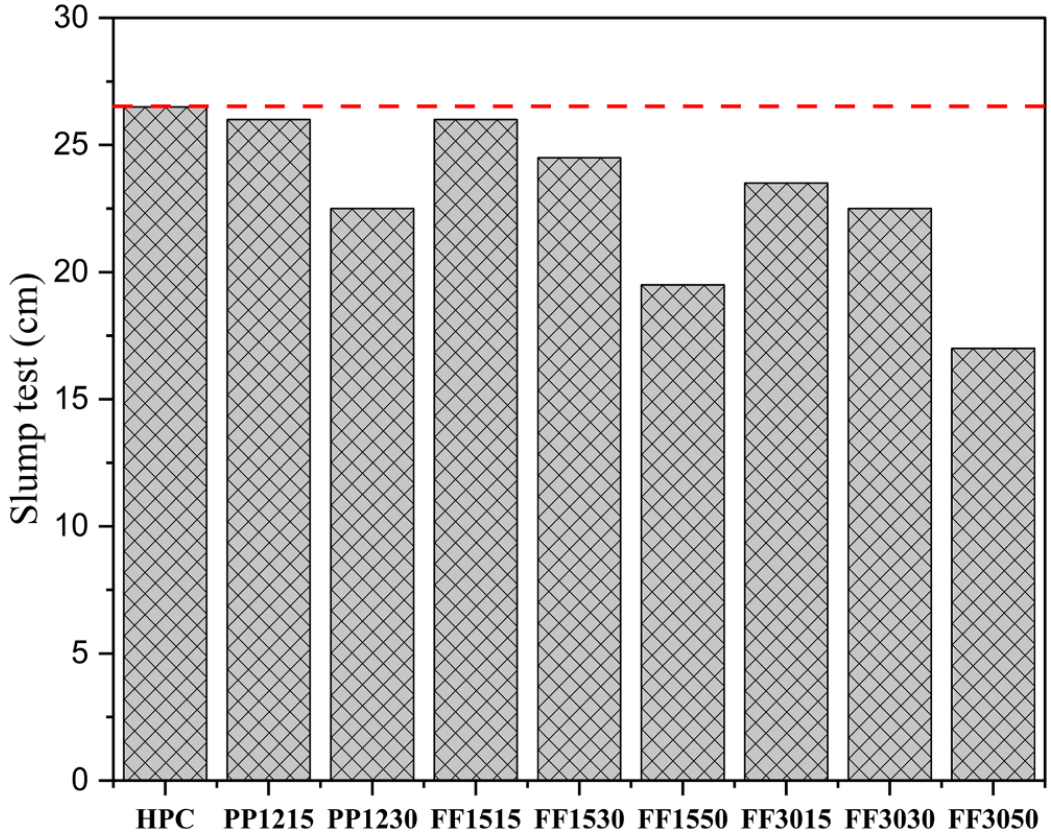

Figure 4.1 Workability test.

4.3. Rheological Properties Of Fiber-Reinforced Concrete

4.3.1. Testing Protocol and Methodology

The testing protocol for evaluating the rheological properties of fiber-reinforced concrete using the ICAR Rheometer involves precise calibration of the rheometer in accordance with manufacturer specifications, along with thorough cleaning of the vane and container. The testing procedure consists of two stages: **a pre-shear phase** of 100 seconds at 0.6 revolutions per second (rps) to standardize the initial state of the concrete, followed by **flow curve measurement** over 20-second intervals at seven decreasing rotational speeds ranging from 0.6 rps to 0.1 rps. This captures the relationship between shear stress and strain rate.

Data reporting includes tabulating results of mix design parameters (e.g., fiber type, dosage, length) and environmental conditions (temperature, humidity). Comparative analysis of measurements taken at 0 minutes (fresh concrete) and 30 minutes (aged concrete) assesses workability retention. After testing, equipment is sanitized, and concrete waste is disposed of in compliance with environmental regulations.

The rheological behavior of fiber-reinforced concrete is modeled using the **Reiner-Riwlin equation (4.1)**, which incorporates variables such as rotational speed (Ω), torque (M), vane dimensions (h, R1), plastic viscosity (μ), and yield stress (τ_0).

$$\Omega = \frac{\mathbf{M}}{\mathbf{4\pi h\mu}}\left(\frac{\mathbf{1}}{\mathbf{R_1^2}} - \frac{\mathbf{2\pi h\tau_0}}{\mathbf{M}}\right) - \frac{\boldsymbol{\tau_0}}{\mathbf{2\mu}}\ln\left(\frac{\mathbf{M}}{\mathbf{2\pi h\tau_0 R_1^2}}\right) \quad \textbf{(4.1)}$$

The mean squared error (MSE) quantifies discrepancies between calculated and measured rotational speeds :

$$\mathbf{MSE} = \sqrt{\frac{\sum(\Omega_{calculated} - \Omega_{measured})^2}{n}} \quad \textbf{(4.2)}$$

Critical assumptions regarding vane geometry (e.g., length, spacing) are essential for accurate modeling.

A strong negative correlation ($R^2 = 0.908$) exists between slump test results and yield stress, with higher slump values indicating greater flowability and lower yield stress. Fiber additions generally increase resistance to deformation. Polypropylene (PP) fibers (mixes PP1215, PP1230) show moderate increases in viscosity with rising fiber content. PP fibers, characterized by smooth surfaces and small diameters, generate lower friction compared to flax fibers. Flax fibers exhibit

significant viscosity variations. Mixes FF1515, FF1550, and FF3050 show higher viscosity, while FF1530 and FF3030 (0.3% fiber content, 30 mm length) display unexpectedly low viscosity, contradicting literature expectations that longer fibers increase viscosity [137, 138]. This anomaly suggests optimal fiber-matrix interaction at a 0.3% dosage.

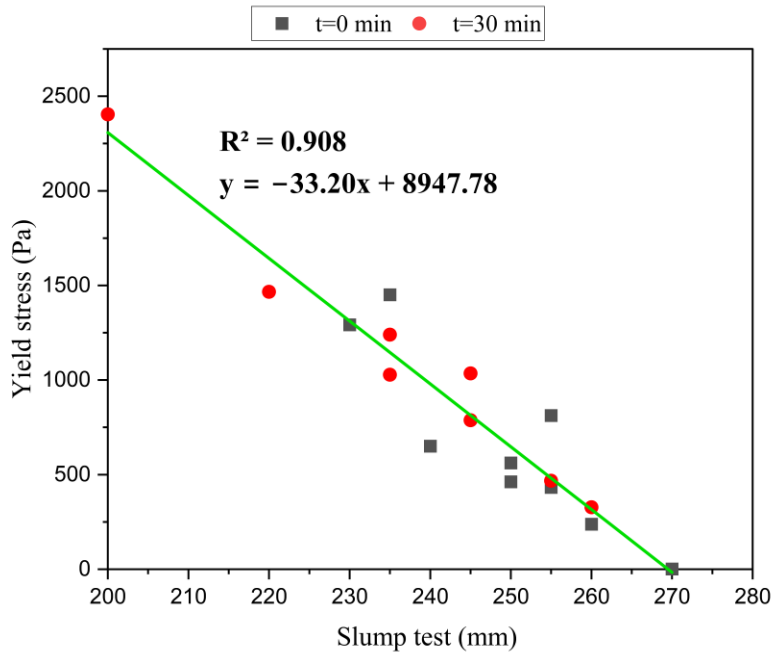

Figure 4.2 Yield stress and slump test.

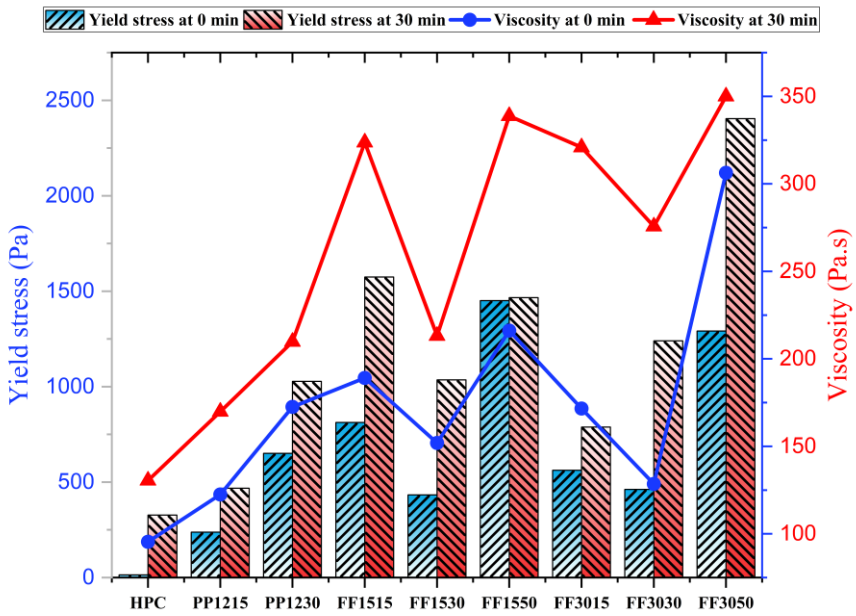

Figure 4.3 Yield stress and viscosity of different mixture types.

Figure 4.4 shows a moderate positive correlation (r = 0.78, R^2 = 0.553) exists between viscosity measurements at 0 minutes and 30 minutes. The linear regression (Y = 0.60X + 16.71) indicates non-proportional viscosity growth over time, highlighting dynamic matrix-fiber interactions. Fiber inclusion universally increases yield stress compared to plain high-performance concrete (HPC). PP fibers (PP1215, PP1230) cause smaller increases, while flax fibers (FF1550, FF3050) induce substantial rises. Notably, FF1530 and FF3030 exhibit the lowest yield stress among flax-reinforced mixes, reinforcing the 0.3% dosage as optimal. Natural fibers, with higher surface area and rough textures, demand greater stress for flow initiation due to enhanced matrix adhesion challenges [139].

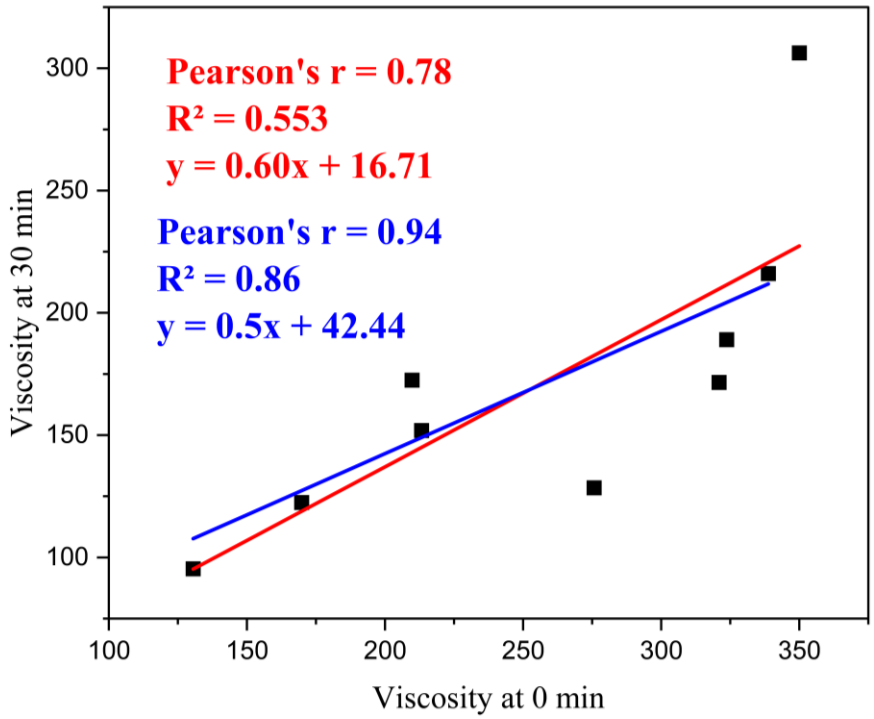

Figure 4.4 Viscosity comparison at 0 and 30 min.

The study underscores the complexity of fiber-reinforced concrete rheology. The low viscosity and yield stress of the FF3030 mixture, despite longer fibers, challenge conventional models, suggesting that factors such as fiber dispersion, orientation, or surface treatment may dominate. Current rheological frameworks inadequately capture these nuances, emphasizing the need for refined models integrating multi-scale interactions. The critical role of fiber type, dosage, and length in governing concrete rheology is highlighted. While PP fibers offer predictable behavior, flax fibers exhibit variability, with a 0.3% dosage (30 mm length) optimizing workability. Future research should explore surface modifications and dispersion techniques to enhance fiber-matrix synergy.

4.4. Tests in the hardened state

4.4.1. Porosity:

The porosity results, as shown in the Figure 4.5, indicate a clear trend of matrix densification over time, with all mixtures exhibiting lower porosity at 90 days compared to 28 days.

At 28 days, the control HPC mix had a porosity of approximately 6.0%. The addition of fibers at this stage showed varied results; some mixes like FF3015 showed a slight improvement, while others like PP1230 and FF3050 had slightly higher porosity, likely due to the initial matrix disruption by the fibers before hydration was more advanced.

By 90 days, the continued hydration process significantly reduced the porosity across all samples. The control HPC porosity decreased to 5.0%. At this later age, all fiber-reinforced mixes demonstrated a clear improvement, achieving lower porosity than the control. The most substantial improvement was observed in the FF3030 mix, which recorded the lowest porosity of approximately 3.0%, a 40% reduction compared to the 90-day control mix. Other mixes also showed significant gains; for example, the FF3015 and FF1550 mixes reduced porosity by approximately 30% and 26%, respectively. The polypropylene mixes also showed improved density, with PP1215 reducing porosity by 17% compared to the control.

This trend demonstrates that while the initial inclusion of fibers can have a mixed effect, their long-term presence contributes to a denser and less porous matrix. This is likely due to the fibers' ability to control the formation of microcracks and refine the pore structure during the extended hydration period, leading to enhanced durability and mechanical performance [140, 141].

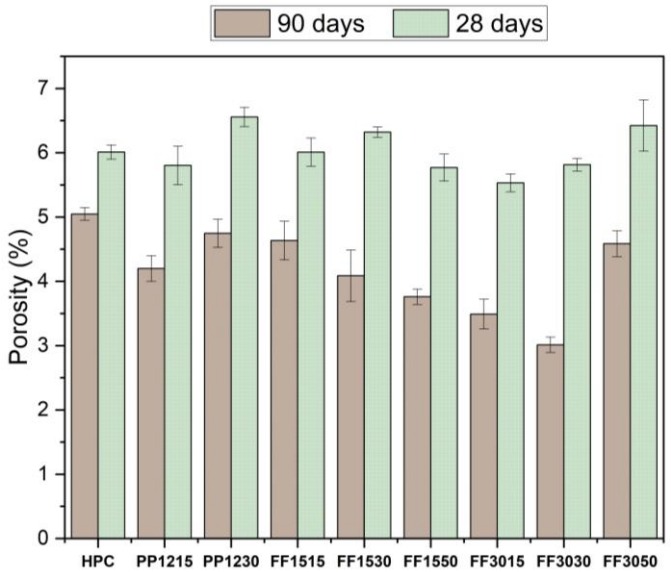

Figure 4.5 Porosity results for all mixtures.

4.4.2. Water absorption by capillary

Figure 4.6 depicts the water absorption by capillary values of the various mixes produced.

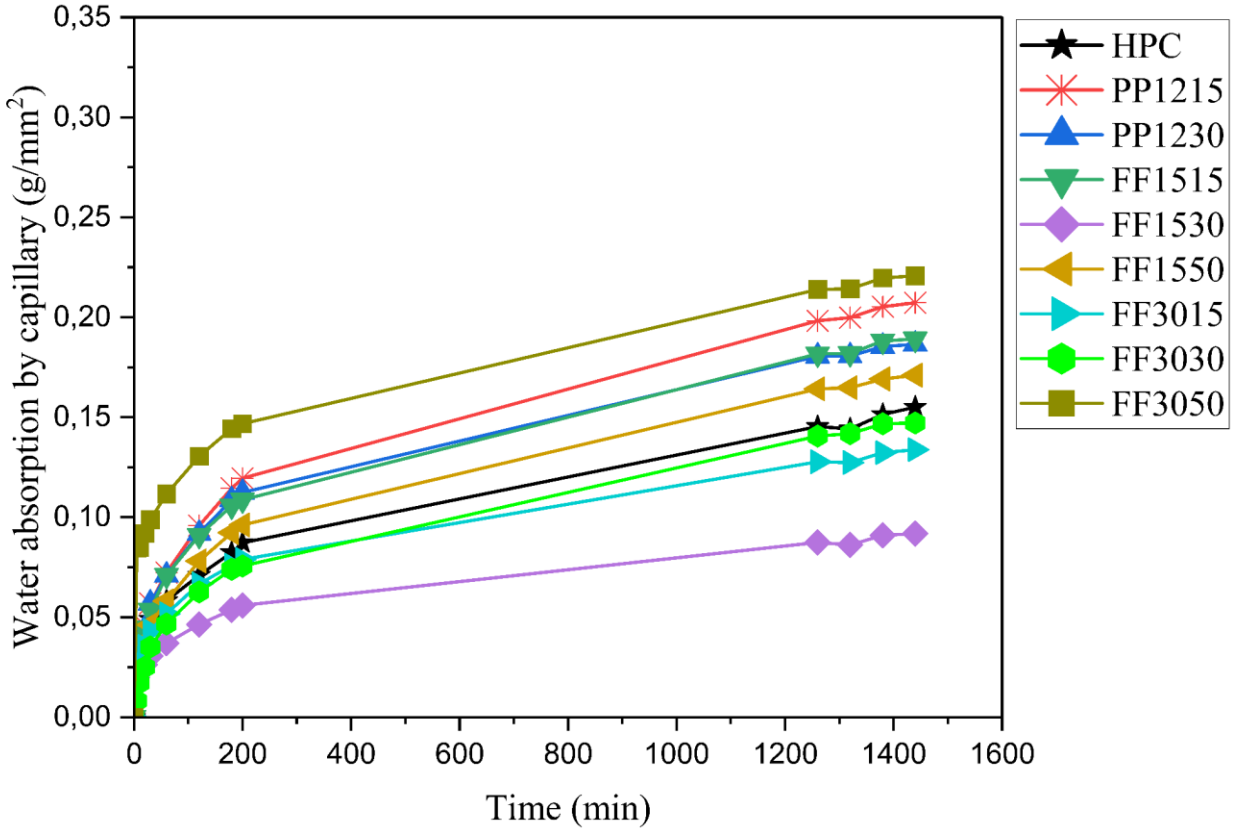

Figure 4.6 Water absorption by capillary.

Based on the water absorption by capillary measurements provided in Figure 4.6, it was noted that after 24 h, the HPC mix exhibited a water absorption of 0.16g/mm2. However, the inclusion of flax fibers at rates of 0.15% and 0.3% inhibited this capillary water absorption. Onuaguluchi and Panthia [142] proved that the injection of fibers into concrete, in particular proportions, effectively fills the holes within the matrix. Moreover, it not only fills these spaces but also contributes to the establishment of a more sophisticated internal network. The FF1515 and FF1550 mixes resulted to an increase in water absorption via capillarity of 22% and 10%, respectively. In contrast, FF1530 decreased water absorption by 41% compared to the HPC, while the FF3015 and FF3030 combinations exhibited reductions of 14% and 5%, respectively, with a further rise of 42% seen for FF3050. For polypropylene fibers, a rise of 34% and 22% was reported for PP1215 and PP1230, respectively. Notably, the most significant decrease in water absorption via capillarity was realized with FF1530, suggesting a large increase in matrix density and possibly in its strength and endurance. The findings demonstrate a general trend of decreased porosity with the inclusion of flax fibers, especially at a dose of 0.3%. This shows an improvement in the density

and mechanical qualities of the concrete. These decreases in porosity indicate a denser matrix, owing to the fibers' capacity to inhibit the development of microcracks and strengthen their adherence inside the composite, ultimately contributing to enhanced mechanical performance [140, 141].

4.4.3. Thermal conductivity

Figure 4.7 depicts the thermal conductivity values for the various generated combinations.

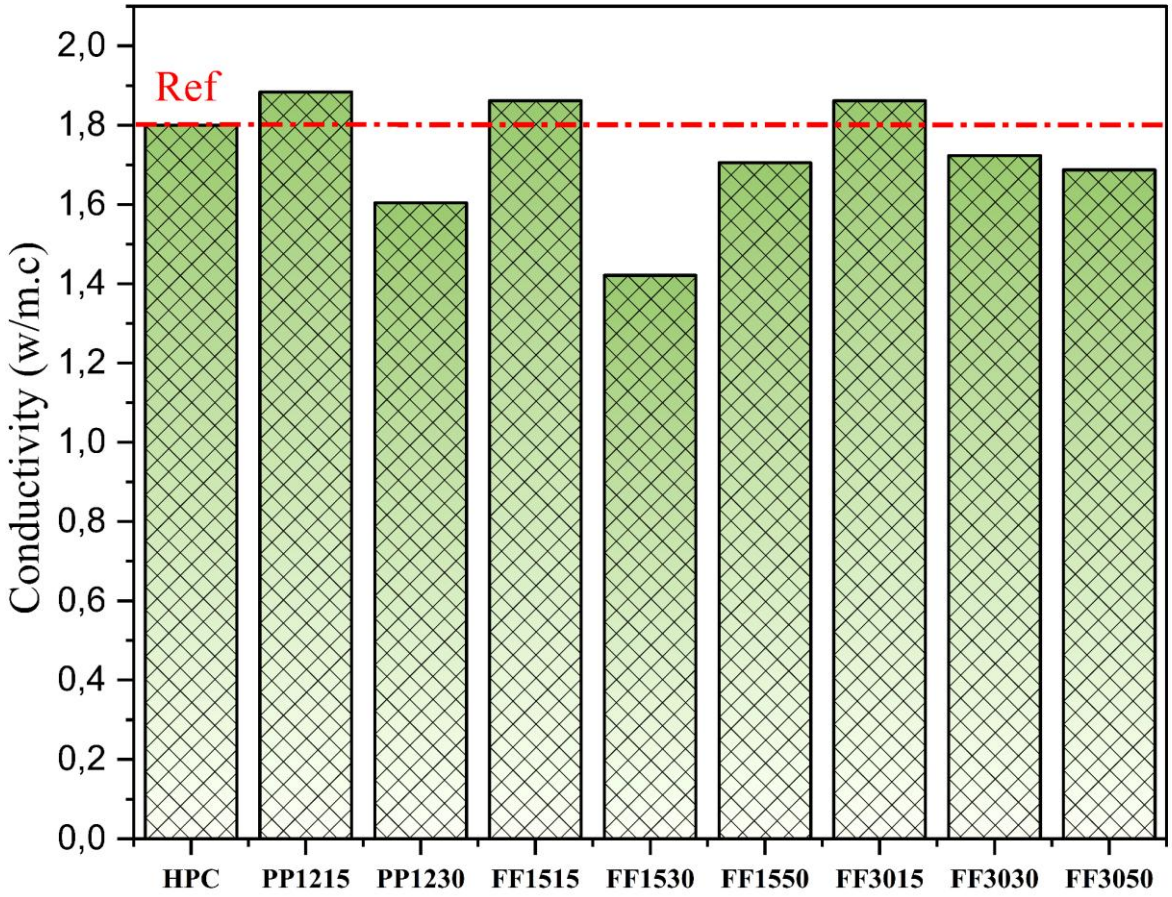

Figure 4.7 Thermal conductivity analysis of all mixtures.

According to Figure 4.7, the high-performance concrete mix PP1215 displays a thermal conductivity 4.6% larger than that of the control HPC mix. In contrast, the FF1530 mix, which has 0.3% of 15 mm flax fibers, drastically lowers heat conductivity by 21.1% compared to HPC. This large decline in conductivity is attributed to the lower density and thermal conductivity of flax fibers, as well as their potential to form barriers to heat transport within the concrete matrix. The incorporation of plant fibers into materials may diminish heat conductivity by up to 15%, according to Belkadi et al.[143], Zhao et al. [144] subsequently proved that this property may be amplified by

exposing the material to alkaline treatment. Thus, the addition of flax fibers looks as a plausible technique for decreasing the heat conductivity of concrete [145].

4.4.4. Compressive strength

The compressive strength results for all blends are reported in Figure 4.8.

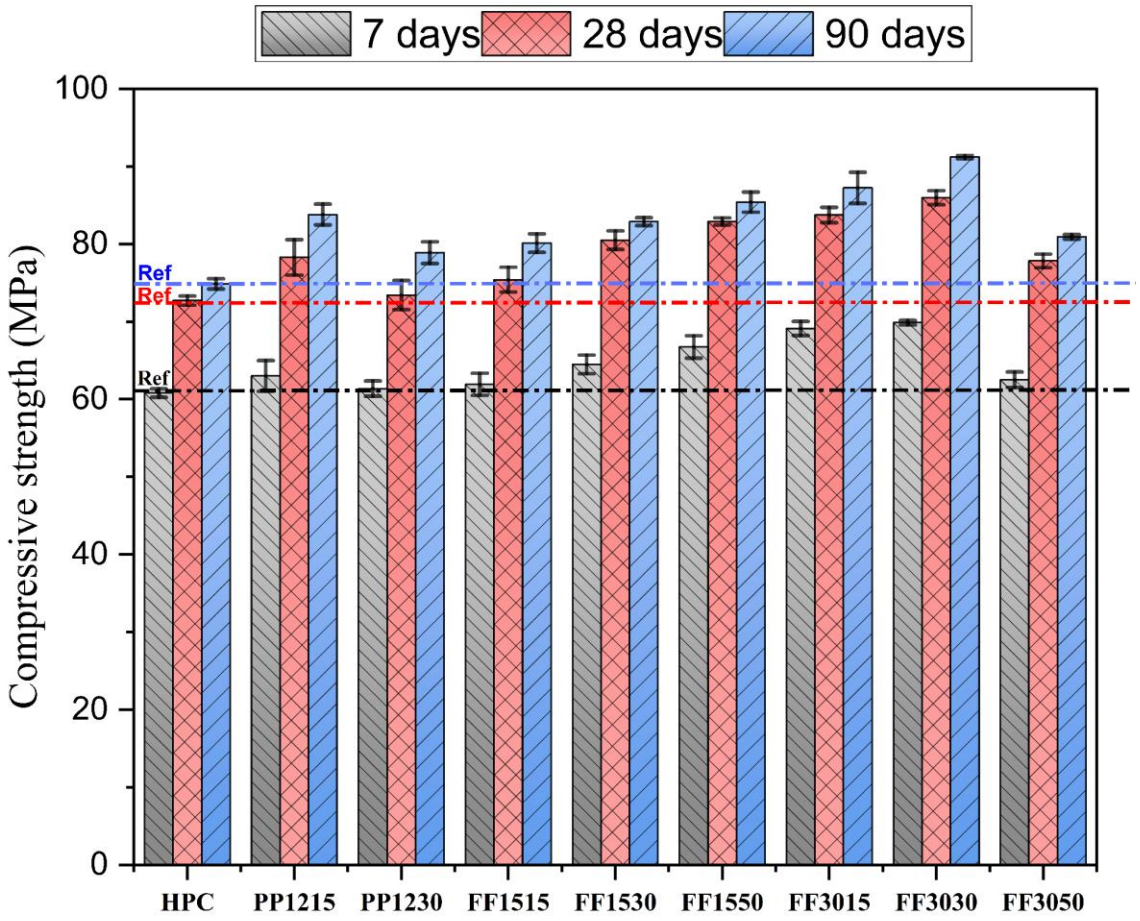

Figure 4.8 Compressive strength of the mixtures incorporating HPC, flax and polypropylene fibers.

While it is widely reported in the literature that fiber inclusion does not typically yield significant gains in compressive strength, the results from this investigation present a noteworthy exception. This study demonstrates that through specific surface treatments, such as the alkali treatment applied to the flax fibers, a substantial improvement in compressive strength can be achieved. This enhancement is attributed to the improved fiber-matrix interfacial bond and better fiber dispersion, factors that differentiate these findings from studies involving untreated natural fibers.

Figure 4.8 displays the compressive strength of all combinations relative to the control mix (HPC). While all fiber types initially demonstrated greater compressive strength with increasing

fiber content, this trend reversed at higher concentrations. The PP1215 mix demonstrated the largest strength gains: 4%, 8%, and 12% at 7, 28, and 90 days, respectively. Fibers strengthen fracture resistance and promote load distribution in concrete by dispersing and transferring compressive stresses [146, 147].

For the PP1230 mix, the compressive strength was identical to HPC at 7 and 28 days but demonstrated a modest increase of 5% at 90 days. This is due to a loss in concrete density from an excessive quantity of low-density filaments and increased porosity created by fiber insertion. The FF1515, FF1530, and FF1550 mixes performed similarly to or even better than HPC in numerous scenarios. Overall, a greater fraction of flax fibers frequently equates to a significant improvement in compressive strength. The strength of FF1515, FF1530, and FF1550 grew by 5% to 10% at 7 days, 3% to 14% at 28 days, and 7% to 14% at 90 days. Flax fibers increase concrete's compression strength and ductility by inducing multiple fracture forms within the material [148]. This contrasts with earlier studies demonstrating that natural fibers might reduce compressive strength due to microstructural defects, fiber clustering, and poor adhesion between fibers and the matrix [149-151]. However, the study by Rahimi et al. demonstrated that integration of alkali-treated fibers enhanced dispersion and outstanding adhesion within the matrix, resulting in an improvement in compressive strength of up to 12 % [152].

The FF3015 and FF3030 mixes displayed the biggest rise in compressive strength, with increments of roughly 13% at 7 days, 15% to 18% at 28 days, and 16% to 21% at 90 days. Conversely, the FF3050 mix did not reveal any notable improvement at 7 days. However, an increase of 7% was noted at 28 and 90 days. The use of longer fibers, together with a sufficient dosage, permits a more effective redistribution of stresses, which enhances resistance to fractures generated by the capillary pressure formed during the evaporation of internal water. This impact is largely associated with the strong hydration reaction of the cement. Furthermore, Nathalie et al. [148] stressed that fiber length plays a vital role in limiting capillary water pressure in clay concretes, particularly during the drying period.

Alkaline treatment, which dissolves lignin, pectin, and other incrusting components, breaks down the flax fibers, hence increasing their specific surface area and facilitating better dispersion within the cement matrix. [153, 154]. This surface modification greatly increases the fiber-cement interaction.

4.4.5. Split tensile strength

Figure 4.9 depicts the split tensile strength results for all the combinations.

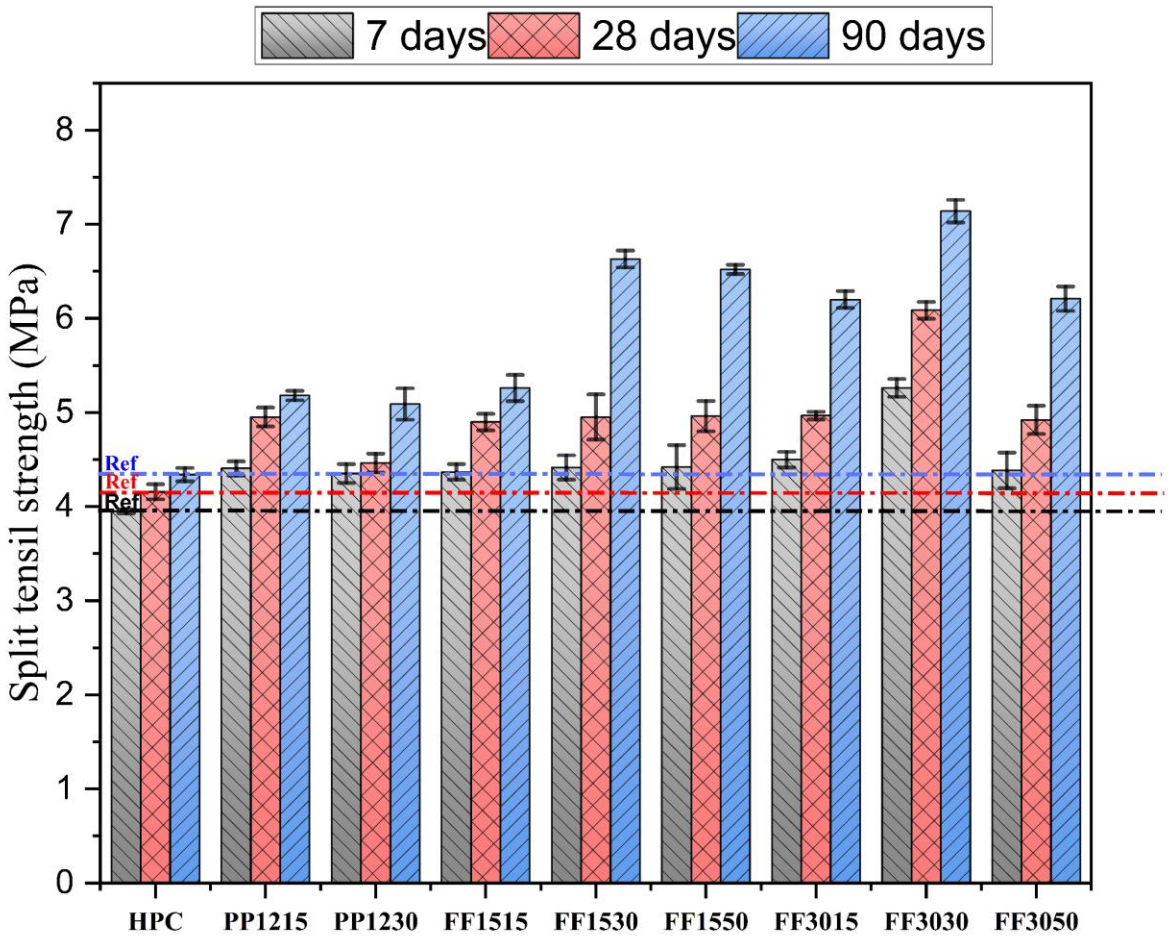

Figure 4.9 The split tensile strength of the mixtures incorporating HPC, flax, and polypropylene fibers.

Figure 4.9 depicts the evolution of split tensile strength over time (7, 28, and 90 days) for various blends. Both PP1215 and PP1230 combinations demonstrated greater split tensile strength compared to HPC. The PP1215 mix demonstrated the most notable gains: 12%, 19%, and 21% at 7, 28, and 90 days, respectively. However, higher fiber content led in a reduction in tensile strength. Polypropylene fibers are known to decrease fracture propagation and microcrack formation, thereby leading to improved tensile strength and durability [155, 156].

The FF1515 mix offers a performance improvement similar to that of the PP1215 mix compared to HPC. However, the FF1530 and FF1550 mixes exhibited a more considerable improvement, especially after 90 days, with corresponding increases of 53% and 50% compared to the HPC control mix. The expansion of the fibers significantly enhanced the results, as stated.

The FF3015, FF3030, and FF3050 mixes exhibited a rise in tensile strength, with values of 14%, 34%, and 11% at 7 days. At 28 days, the increases were 20%, 51%, and 19%, respectively,

and at 90 days, they reached 18%, 65%, and 43%. The high tensile strength of alkali-treated flax fibers enhances their interaction with the matrix and their efficacy in suppressing fracture formation, hence explaining the higher tensile strength values found in HPC [152].

The inferior performance of FF3050 relative to FF3030 is attributed to its larger fiber content and longer fiber lengths. These circumstances likely created fiber clumping and poor dispersion inside the concrete matrix, a process known as fiber agglomeration [73]. Agglomeration may cause flaws in the composite, leading to reduced overall tensile strength [157]. Achieving efficient fiber reinforcement involves a precise balance between fiber number, length, and dispersion to optimize mechanical performance [158]. While fiber aggregation is an issue, chemical treatments may increase fiber-matrix adhesion, thereby boosting the composite's overall performance [159, 160]. Moreover, fiber length is crucial in limiting crack propagation, resulting to increased fracture toughness [82].

4.4.6. Flexural strength

Figure 4.10 exhibits the flexural strength values for the various combinations.

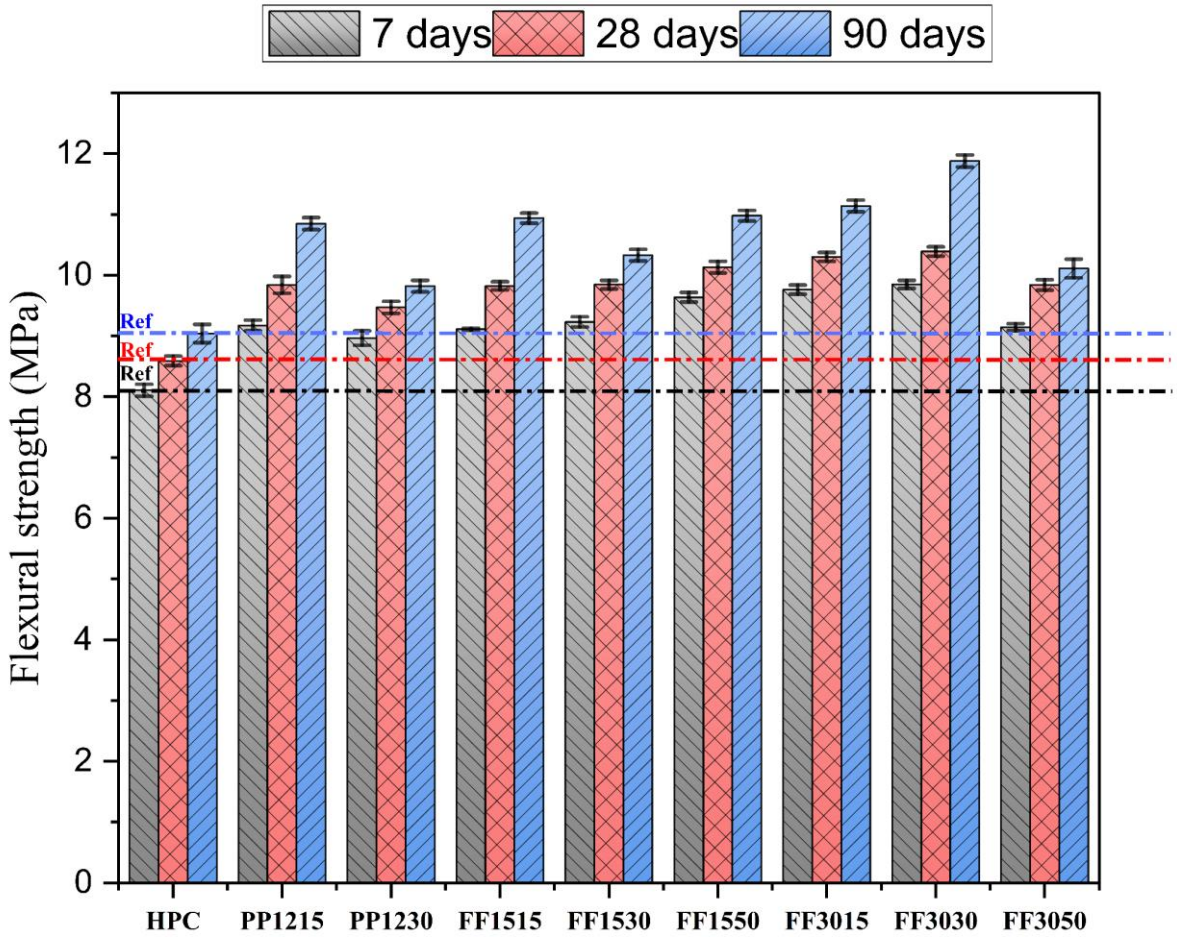

Figure 4.10 The flexural strength of the mixtures incorporating HPC, flax and polypropylene fibers.

Figure 4.10 displays the flexural strength of the various combinations. The PP1215 combination revealed improvements in flexural strength of 14%, 15%, and 21% at 7, 28, and 90 days, respectively, compared to the HPC mixture. The PP12330 combination also exhibited a 10% improvement in almost all time periods compared to the HPC mixture. Several studies have indicated that adding polypropylene (PP) fibers to concrete boosts its flexural strength, enhancing its resistance to bending stresses [161-165]. However, the right amount of these fibers is crucial: an excess of fibers could damage the concrete's strength and lifetime due to a reduction in its workability [155]. All combinations evaluated revealed flexural strength increases at all ages compared to HPC. The FF1515, FF1530, and FF1550 mixes indicated advantages at all ages, with increases of 12%, 14%, and 19% at 7 days, 14%, 15%, and 18% at 28 days, and 21%, 14%, and 22% at 90 days, respectively. Similarly, FF3015, FF3030, and FF3050 mixtures indicated advantages, with increases of 20%, 22%, and 13% after 7 days, 20%, 21%, and 15% after 28 days, and 23%, 31%, and 12% at 90 days. Both the length and arrangement of flax fibers are essential components in increasing the flexural strength of composite materials. The influence of fiber length on concrete's flexural strength has been well-documented, with longer fibers often delivering superior performance [166]. These longer fibers bridge fractures more effectively and enhance post-cracking behavior, contributing to increased flexural strength and toughness [82].

The FF3030 mix displayed better strength compared to the PP1215 mix, with superior percentages of 7%, 6%, and 10% at 7, 28, and 90 days, respectively.

4.4.7. Shrinkage endogenous

The findings of endogenous shrinkage for the varied combinations up to 100 days are displayed in Figure 4.11.

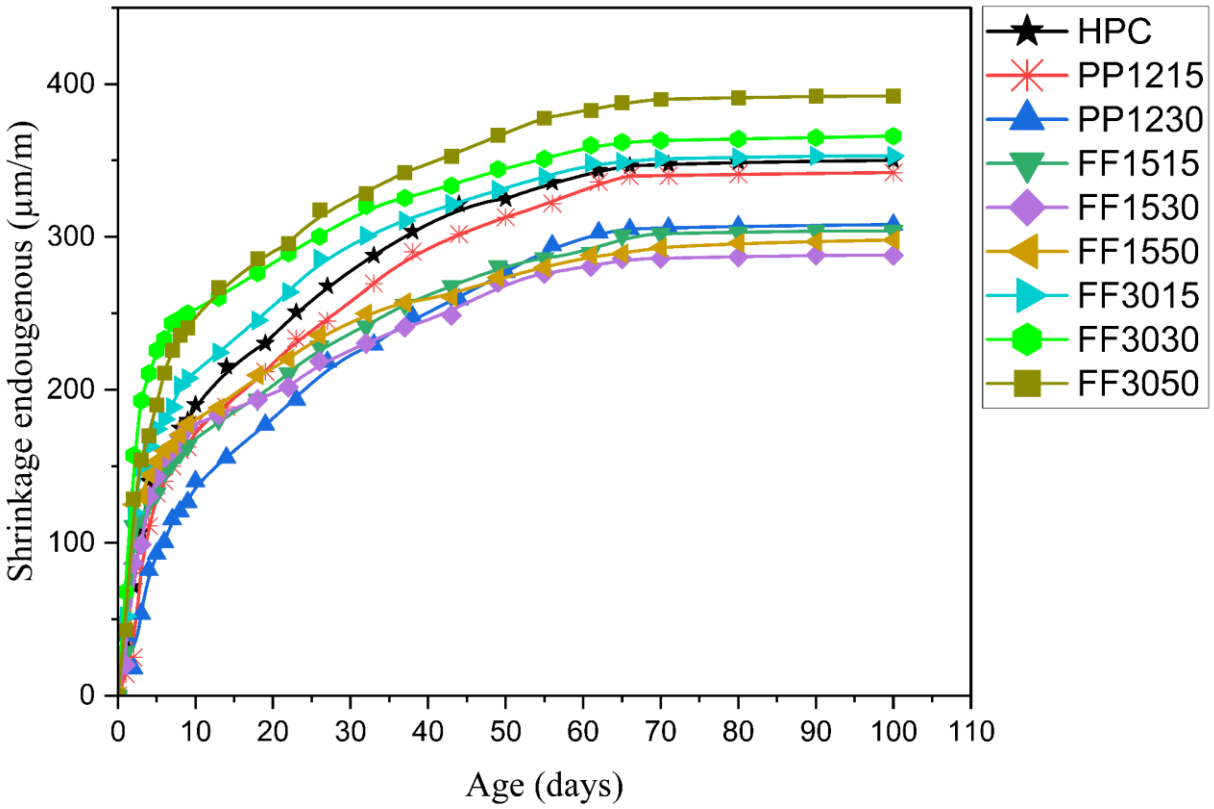

Figure 4.11 Shrinkage endogenous for all mixtures.

The total deformation during the first week for the control sample was approximately 150 µm, whereas the FF3050 mixture exhibited the highest deformation at 250 µm among all mixtures. The overall deformation during the first week for the control sample was roughly 150 µm, while the FF3050 combination demonstrated the maximum deformation at 250 µm among all mixes. The lowest deformation value was 120 µm for the PP1230 combination. After forty days, several combinations exhibited reduced deformation compared to the control sample, and this tendency remained up to 100 days. It is also found that deformation stabilized across all mixes. The control mixture exhibited a deformation of roughly 346 µm, with the maximum reported at 392 µm for the FF3050 combination, and the lowest at 285 µm for the FF1530 mixture. Mixtures reinforced with 15 mm flax fibers exhibited an improvement of around 27% compared to the control mixture. Polypropylene fiber-reinforced mixes also lowered the deformation rate and displayed excellent performance from the early days up to day 70, notably for PP1230. In contrast, mixes containing 30 mm flax fibers continually demonstrated higher values than the control combination from the early

days until day 100. However, the FF13015 and FF3030 combinations exhibited substantial improvement close to day 100, attaining deformation approximately the same as the control mixture, and sometimes even less

Both flax and polypropylene fibers play major roles in preventing self-shrinkage in concrete. Flax fibers, particularly when treated with alkali, have been found to significantly decrease self-shrinkage in high-performance concrete (HPC) while preserving increased flowability, compressive strength, and bending capacity [152, 167, 168]. On the other side, polypropylene fibers have been reported to prevent plastic shrinkage, delay fracture development, and boost bending strength [169].

The addition of damp flax fibers into concrete considerably minimizes deformation induced by shrinkage. This process is linked to an internal curing action, where water trapped in the fibers is progressively released, giving continual hydration to the cement matrix. This technique helps minimize fast desiccation of the concrete, a typical source of fracture formation [170].

Additionally, investigations, especially those by Rahimi et al [152] , reveal that oilseed flax fibers may delay the beginning of cracking, hence adding to shrinkage reduction.

As with cellulose fibers, their efficiency relies on their inherent qualities and applied treatments, such as crystallinity and alkaline processing. According to Shiho et al. [149], adding cellulose fibers boosts the concrete's resilience to fractures induced by autogenous shrinkage. However, high fiber content might affect the workability of the combination. The length of the fibers has a key impact, notably in the uniformity of the mix. Therefore, optimizing the dispersion of fibers inside the concrete is a vital method to enhance their performance.

4.5. Microstructures analyses

Scanning electron microscopy (SEM) and optical microscopy were conducted on the specimens following the flexural test at 28 days.

Figure 4.12 and Figure 4.13 demonstrates the influence of sodium hydroxide (NaOH) treatment on flax fibers (FF). This treatment alters the fiber surface by enhancing its roughness by the breakdown of hydrogen bonds and the partial dissolving of amorphous components such as hemicellulose. This chemical modification exposes cellulose microfibrils and increases fiber wettability and adherence to the matrix, as demonstrated by earlier research [143, 160, 171]. The research highlights that rougher fiber surfaces give additional anchoring locations for the cementitious matrix, enhancing the interfacial connection, energy dissipation under load, and fracture toughness [110, 172].

As illustrated in Figure 4.12 the Scanning electron microscopy (SEM) and Optique scanning in Figure 4.13 evaluations of the mixes containing FF fibers are presented.

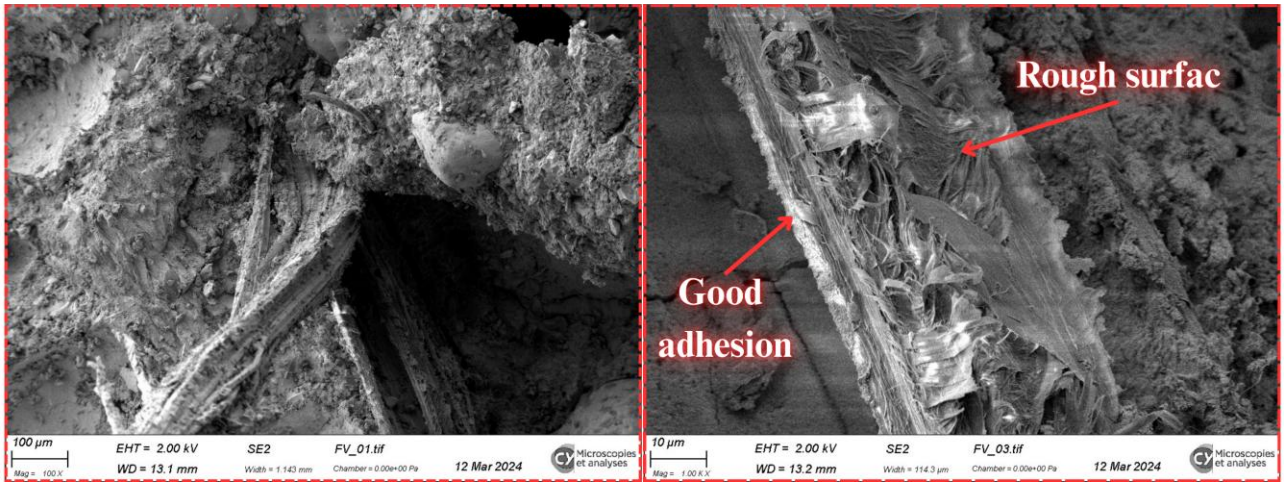

Figure 4.12 Flax fiber (FF) Scanning electron microscopy (SEM) images.

Figure 4.13 Flax fiber Optique scanning.

This increased adhesion eliminates microcracks around the fibers and decreases the porosity of the hardened composite. These results correlate with those of Rahimi et al. [152], who found that alkaline-treated natural fibers considerably enhance compressive and flexural strength in fiber-reinforced high-performance concrete (HPC).

Figure 4.14 shows the scanning electron microscopy (SEM) and optical scanning Figure 4.15 evaluations of the PP fibre blends.

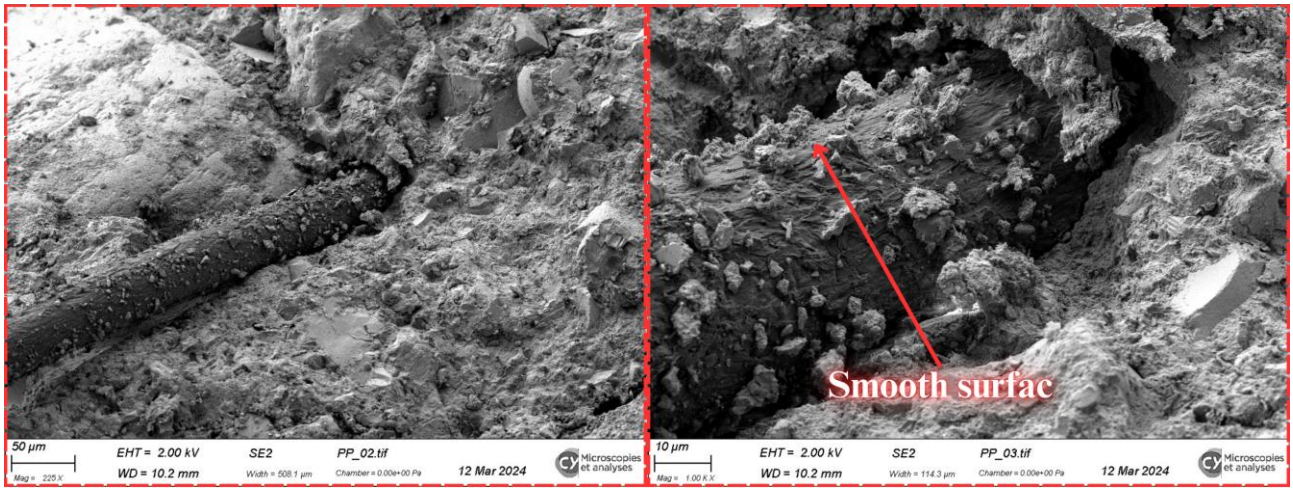

Figure 4.14 Polypropylene fiber Scanning electron microscopy (SEM) images.

Figure 4.15 Polypropylene fiber Optique scanning.

Figure 4.14 and Figure 4.15 demonstrates the smooth shape of polypropylene (PP) fibers is unchanged by the treatment. The hydrophobic and chemically inert character of PP fibers precludes efficient attachment to the matrix, limiting their crack-bridging ability and lowering the overall mechanical strength of the composite. These findings are verified by prior investigations. The research suggests that PP fibers largely help to minimizing plastic shrinkage and early-age cracking rather than increasing long-term mechanical properties [143].

These findings indicate the greater contribution of treated flax fibers to mechanical performance and microstructural integrity. The observed increases in fracture resistance and other performance indices, as detailed in previous sections, are comparable with reported advances ranging from 7% to 90% for reference composites, notably in terms of flexural and splitting tensile strength.

4.6. Digital image correlate

4.6.1. DIC compression strength

Figure 4.16 displays curve of deformation along the X-axis and Figure 4.17 the Digital Image Correlation (DIC) analysis of the compressive strength of the various blends.

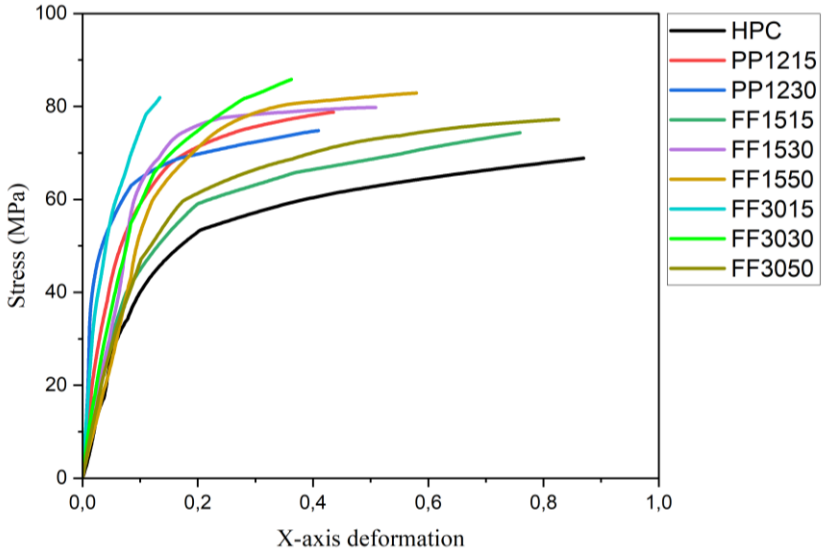

Figure 4.16 Compressive strength Deformation along the X-axis.

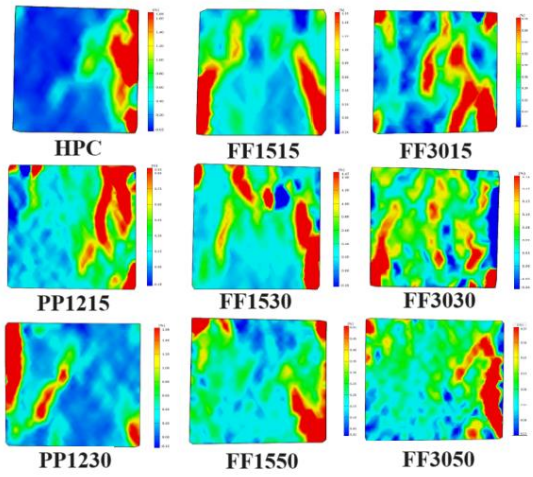

Figure 4.17 3D image of the deformation on the x-axis, extracted from the GOM software.

While the Figure 4.18 shows the displacement graph for all mixtures and Figure 4.19 displays 3D image of the displacement of the compressive strength on the x-axis, extracted from the GOM software.

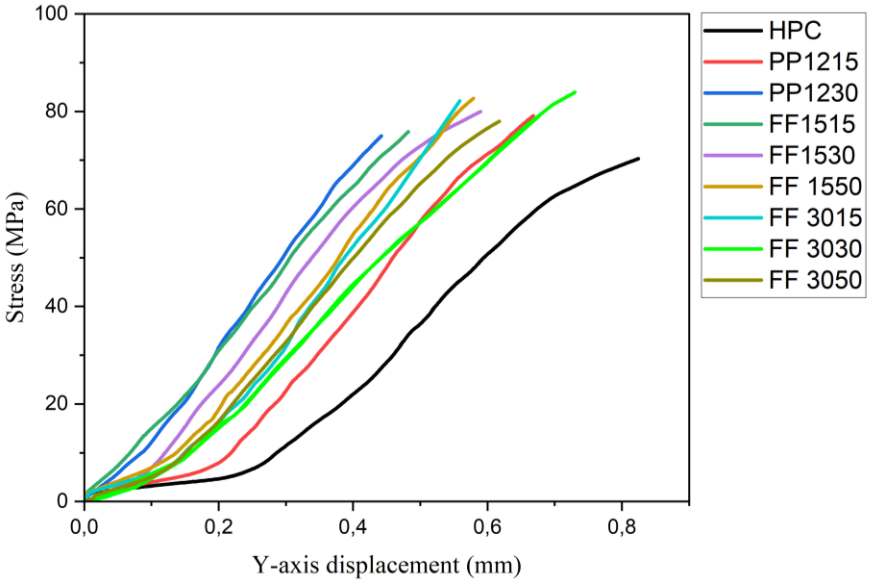

Figure 4.18 Compressive strength Displacement along the Y-axis.

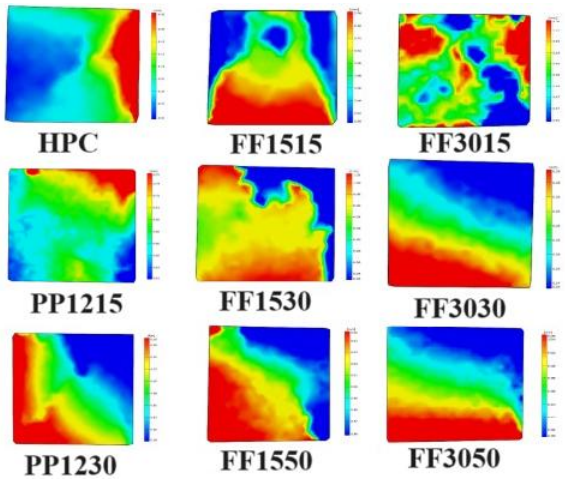

Figure 4.19 3D image of the displacement on the x-axis, extracted from the GOM software.

Based to Figure 4.16 and Figure 4.18 reveal that the control mixture demonstrated the largest displacement and deformation, computed at 0.82 mm and 1.16%, with a compressive strength of roughly 70 MPa, equivalent to the maximum load for HPC. For the fiber-reinforced mixtures at the same load, a substantial reduction in displacement was noted. The PP1215 and PP1230 mixes lowered displacement by roughly 0.60 mm and 0.41 mm, respectively. The distortion for both mixes was around 0.18% and 0.21%. At maximum loads of 79 MPa for PP1215 and 74

MPa for PP1530, displacements of 0.67 mm and 0.44 mm were found, with deformations of roughly 0.51% and 0.41%, respectively.

For the FF1515, FF1530, and FF1550 mixes, the displacements were 0.44 mm, 0.47 mm, and 0.50 mm, respectively, while the deformations were 0.59%, 0.14%, and 0.20% at a 70 MPa stress. At maximum loads of 75 MPa, 79 MPa, and 82 MPa, the displacements were 0.48 mm, 0.59 mm, and 0.58 mm, with deformations of 0.83%, 0.51%, and 0.68%. For the FF3015, FF3030, and FF3050 mixes, at a load of 70 MPa, the displacements were 0.50 mm, 0.61 mm, and 0.54 mm, respectively, with deformations of 0.10%, 0.15%, and 0.40%. At maximum loads of 82 MPa, 86 MPa, and 77 MPa, the displacements were 0.56 mm, 0.68 mm, and 0.62 mm, with deformations of 0.14%, 0.39%, and 0.83%.

Increasing fiber content and length often increased performance, as demonstrated in the gradually lower displacements reported in the fiber-reinforced mixes compared to the HPC control. Digital Image Correlation (DIC) technology played a significant role in getting the force-displacement data, providing for a complete investigation of the material's response to loading. The incorporation of fibers enhances the tensile strength and fracture resistance of concrete, as demonstrated in various studies [173-175]. Their presence helps distribute stress more uniformly and decreases fracture formation, thereby increasing the overall structural performance of the concrete [76, 141]. Incorporating fibers into concrete mixtures positively improves mechanical performance, especially by decreasing displacement under a given load

[176]. The interaction between fiber length, volume %, and the matrix dictates the fibers' crack-bridging capacity, which in turn affects displacement behavior under stress. Shorter fibers are anticipated to raise toughness and limit micro-crack propagation at lower loads, while longer fibers may improve crack-bridging effectiveness at greater displacements [177-179].

4.6.2. DIC split tensile strength

Figure 4.20 displays curve of deformation along the X-axis and Figure 4.21 the Digital Image Correlation (DIC) analysis of the split tensile strength of the various blends.

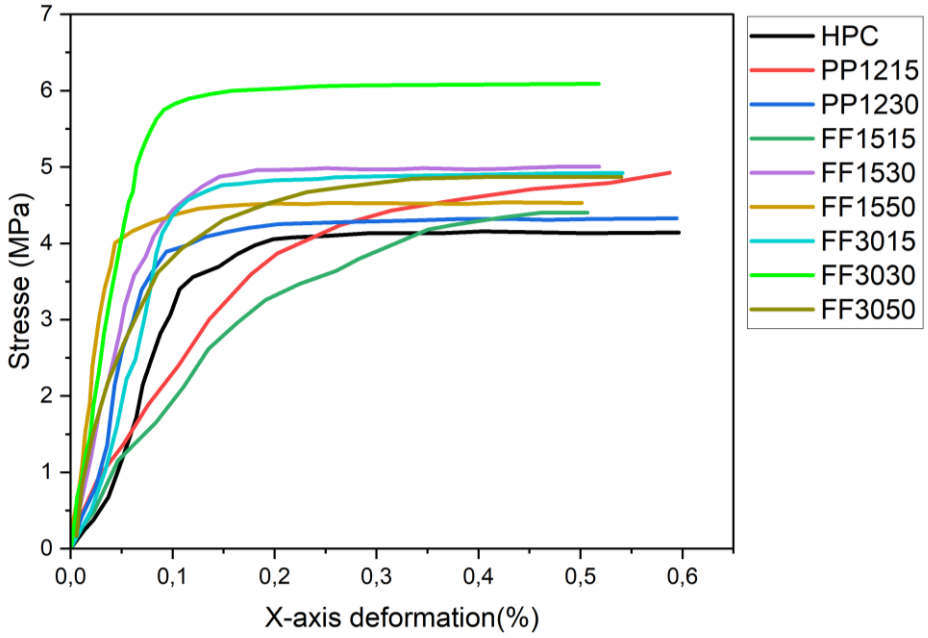

Figure 4.20 DIC Split Tensile Strength Deformation along the X-axis.

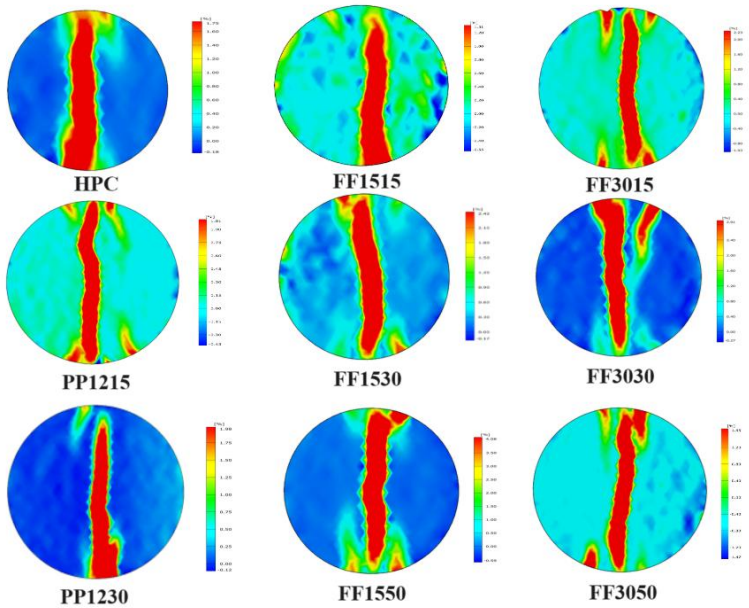

Figure 4.21 3D image of the deformation on the x-axis, extracted from the GOM software.

While the Figure 4.22 shows the displacement graph for all mixtures and Figure 4.23 displays 3D image of the displacement of the split tensile strength on the x-axis, extracted from the GOM software.

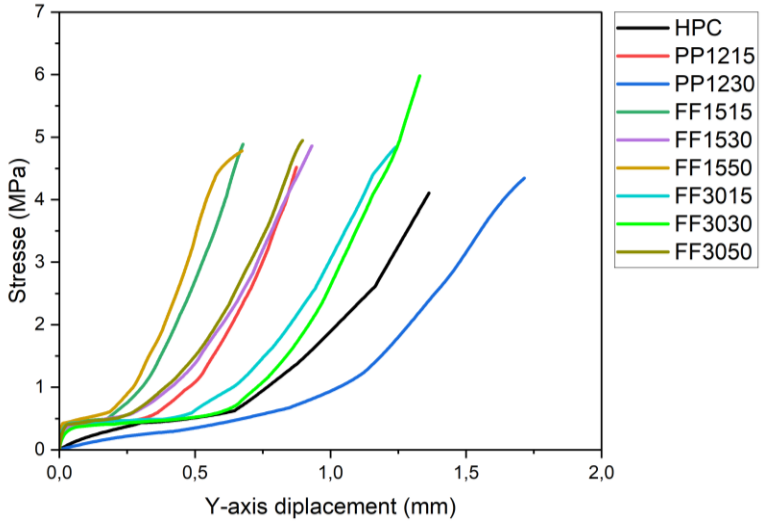

Figure 4.22 Split Tensile Strength displacement along the Y-axis.

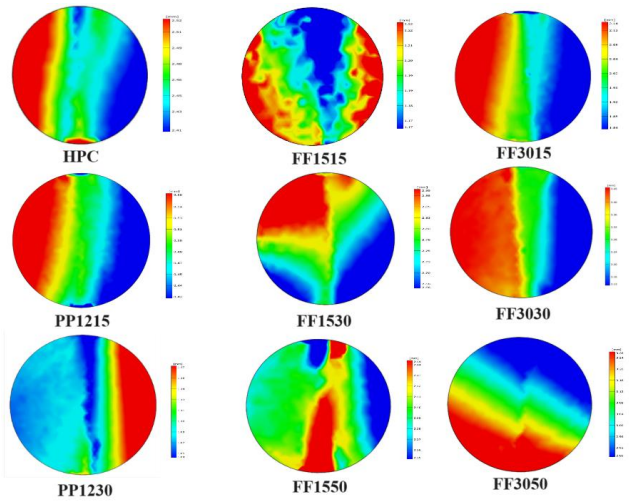

Figure 4.23 3D image of the displacement on the x-axis, extracted from the GOM software.

According to Figure 4.20 and Figure 4.22, the introduction of fibers, whether flax or polypropylene, generally contributed to a reduction in y-displacements and deformations (dx) compared to the control mixture (HPC). This indicates that adding fibers may boost the mechanical properties and deformation resistance of concrete mixtures, consistent with findings from past studies. According to the study by Saad et al. [180], incorporating fibers such as polypropylene and flax has consistently boosted the mechanical properties and deformation resistance of concrete mixes compared to control mixtures. Among the different fiber-reinforced mixes, FF1550 achieved

the lowest displacement (0.76 mm) and the lowest deformation (0.5%) at a stress level of 4.14 MPa. This implies that adding 0.5% of 15 mm long flax fibers supplied the greatest effective reinforcement in terms of controlling deflection and distortion under the tested loading conditions. Yan et al. [91], showed that incorporating flax fibers into concrete considerably enhanced both flexural behavior and post-crack performance. Additionally, flax fibers greatly boost the ductility of concrete, enabling it to sustain greater deformation before collapse. This feature is crucial for structures exposed to dynamic loads. Their findings reveal that inserting 0.5% flax fibers by weight of cement contributes to optimal increases in flexural strength and post-cracking behavior. These results coincide with the greater performance obtained for the FF1550 combo in this experiment.

4.6.3. DIC flexural strength

Figure 4.24 displays curve of deformation along the X-axis and Figure 4.25 the Digital Image Correlation (DIC) analysis of the flexural strength of the various blends.

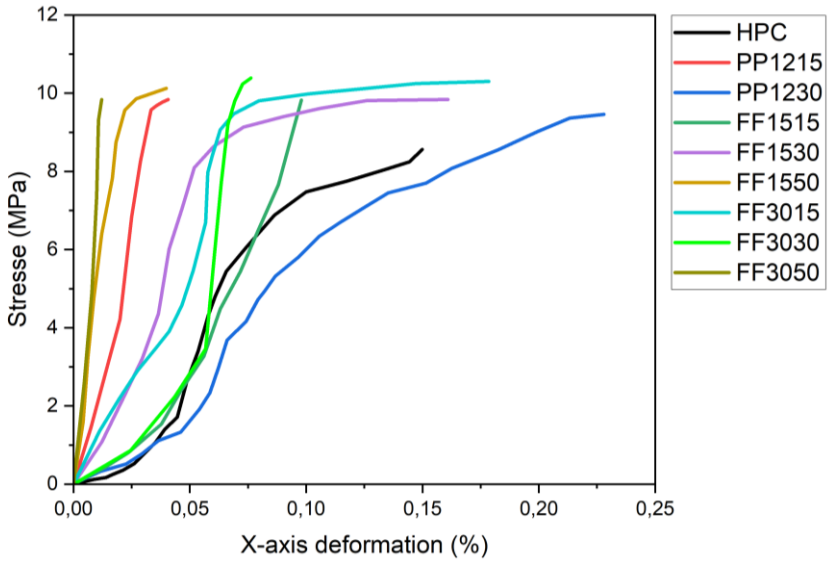

Figure 4.24 Flexural strength Deformation along the X-axis.

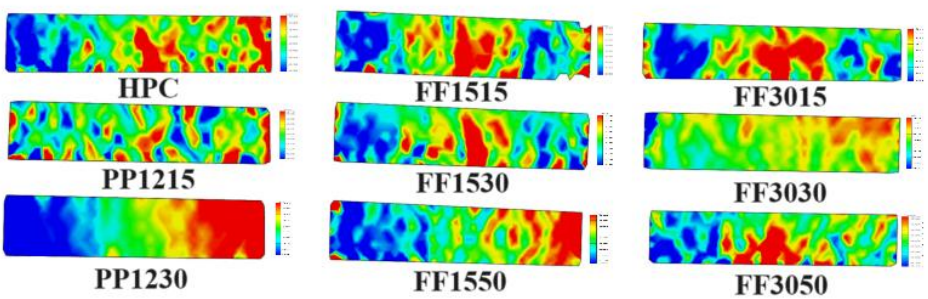

Figure 4.25 3D image of the deformation on the x-axis, extracted from the GOM software.

While the Figure 4.26 shows the displacement graph for all mixtures and Figure 4.27 displays 3D image of the displacement of the split tensile strength on the x-axis, extracted from the GOM software.

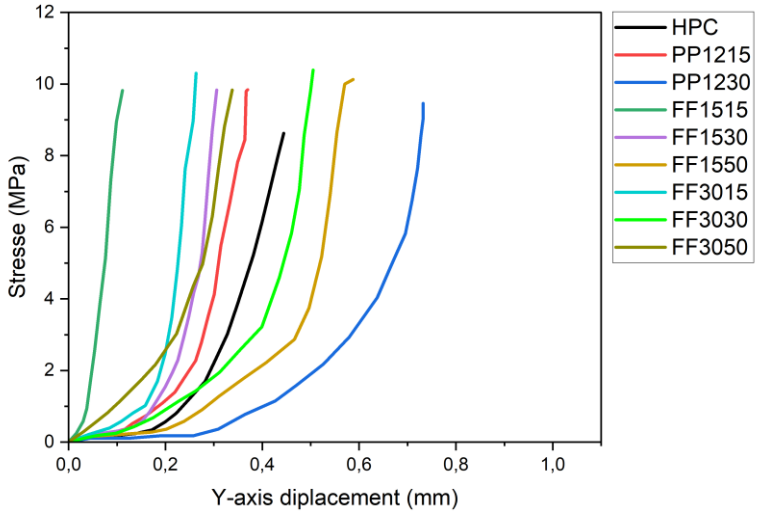

Figure 4.26 Flexural strength displacement along the Y-axis.

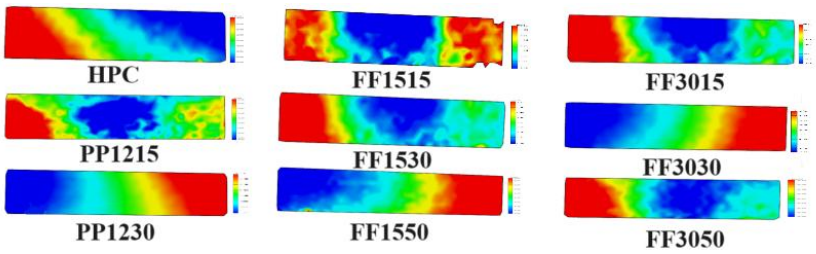

Figure 4.27 3D image of the displacement on the x-axis, extracted from the GOM software.

The data revealed that the inclusion of flax fibers at a content of 0.15% by weight of cement and a length of 15 mm (FF1515) demonstrated the least displacement (0.11 mm) and deformation (0.10%) among all mixtures at a stress level of 9.82 MPa. This combination outperformed the control HPC mixture and other fiber-reinforced mixes in terms of reducing deformations under flexural stress. The superior performance of the FF1515 combination may be attributed to the proper fiber content and aspect ratio (length-to-diameter ratio) of the flax fibers. At this dosage, the fibers were widely diffused throughout the cementitious matrix, successfully bridging and arresting microcracks, thereby enhancing the flexural resistance and lowering deformations. In contrast, combinations with larger fiber percentages (0.3% and 0.5%) displayed increased displacement and deformation, potentially owing to fiber aggregation and inadequate dispersion within the matrix, which might impair the fiber-matrix interfacial connection and lead to lower load transmission efficiency. The performance of polypropylene fiber-reinforced combinations (PP1215 and PP1230)

was considerably inferior than the best-performing flax fiber mixture (FF1515). This may be owing to the reduced aspect ratio and changed surface characteristics of polypropylene fibers, which may have culminated in worse fiber-matrix bonding and less resistance to fracture propagation under flexural stress.

4.7. X-ray analyses

The captured image consists of 256 levels of gray intensity that correspond to different densities within the specimen. Air voids and cracks (low density) in Figure 4.28 are shown in black. Aggregate (high density) are shown in white.

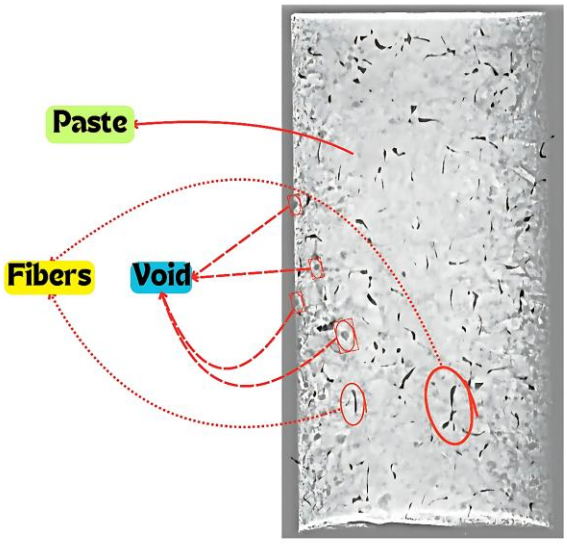

Figure 4.28 Air Void and Fiber Distribution in X-ray Images.

The X-ray image in Figure 4.28 presents a captivating visual narrative of the concrete's interior architecture, revealing a surprising degree of uniformity for a composite material. A significant remark derives from the distribution of voids, portrayed in colors of dark gray and black. Unlike a chaotic constellation of faults, these holes seem to be typically modest, relatively few in number, and carefully spaced. This spatial isolation is crucial for structural integrity; a dense clustering of voids offers preferred paths for fracture initiation and propagation, converting small flaws into catastrophic failures. The farther apart these internal discontinuities exist, the higher the material's resistance against subtle crack growth, hence maintaining its long-term performance and durability under stress. This regulated void structure is a mark of painstakingly planned and implemented high-performance concrete.

Furthermore, the picture precisely exposes the purposeful insertion of fibers, shown as thin, elongated black parts. Their dispersion is a tribute to efficient mixing techniques, exhibiting a remarkable consistency rather than damaging clumping. Fiber clumping, or 'balling,' is a persistent enemy in fiber-reinforced composites, generating localized stress concentrations and functioning as intrinsic weak places that significantly impair mechanical qualities. Such agglomerations may undermine the very advantages fibers are supposed to give, resulting to brittle failure. In sharp contrast, the obvious, even dispersion found here increases the fibers' potential to bridge nascent micro-cracks, redistribute stresses, and improve the concrete's post-cracking behavior. This optimal distribution translates directly into superior mechanical performance, most notably manifesting as significant improvements in both flexural and tensile strength – qualities that elevate this concrete beyond conventional formulations into the realm of high-performance materials capable of withstanding more demanding structural applications. The picture, therefore, is not only a snapshot of internal characteristics but a confirmation of effective material engineering, stressing tight control over two essential microstructural aspects that influence macroscopic performance.

4.8. Conclusion

This research has unveiled a transformative approach to enhancing high-performance concrete (HPC) through the strategic incorporation of flax and polypropylene fibers, coupled with advanced alkali treatment techniques. By meticulously evaluating the impact of fiber type, length, and dosage, we have demonstrated a significant improvement in mechanical properties, including compressive, tensile, and flexural strengths. Notably, the integration of alkali-treated flax fibers has proven to be a game-changer, reducing shrinkage-induced cracking by up to 27% and enhancing durability in harsh environments. The use of Digital Image Correlation (DIC) technology provided unprecedented insights into deformation mechanisms, revealing how fiber reinforcement optimizes strain distribution and mitigates structural weaknesses. These findings not only address critical challenges in HPC performance but also pave the way for sustainable construction practices. As we look to the future, the potential for further innovation is immense. Exploring hybrid fiber systems, advanced surface treatments, and eco-friendly binders could unlock new levels of performance and sustainability. This study invites the industry to reimagine HPC as a dynamic, resilient material one that not only meets the demands of modern infrastructure but also contributes to a greener, more durable built environment. The journey from lab to construction site holds promise for redefining what's possible in concrete technology, inspiring a new era of engineering solutions that are as imaginative as they are practical.

General conclusions and outlook

GENERAL CONCLUSIONS AND OUTLOOK

This thesis has provided a comprehensive exploration of the impact of various fiber types on the mechanical properties, durability, and microstructural characteristics of High-Performance Concrete (HPC). Through meticulous experimental analysis, the research has successfully addressed its key objectives, offering valuable insights into the optimization of fiber-reinforced HPC for enhanced structural performance and sustainability.

The findings of this study highlight the significant role of fiber reinforcement in improving the mechanical properties of HPC. The incorporation of fibers, particularly flax and polypropylene, has been shown to enhance compressive strength, flexural strength, and split tensile strength, with optimal results observed at specific fiber dosages and lengths. For instance, the FF1530 mixture, containing 0.3% flax fibers of 15 mm length, demonstrated superior performance in terms of reduced displacement and deformation under compressive and flexural loads, as analyzed through Digital Image Correlation (DIC). This indicates that the careful selection of fiber type, dosage, and length is crucial for maximizing the mechanical performance of fiber-reinforced HPC.

Durability is another critical aspect addressed in this research. The results indicate that fiber reinforcement significantly reduces porosity and water absorption, thereby enhancing the concrete's resistance to environmental degradation. Notably, the FF3030 mixture exhibited a substantial decrease in porosity and water absorption, suggesting improved matrix density and durability. These findings underscore the potential of fiber-reinforced HPC to withstand harsh environmental conditions, making it suitable for applications in marine environments and other aggressive settings.

The microstructural analysis conducted using Scanning Electron Microscopy (SEM) and optical microscopy revealed that the alkaline treatment of flax fibers enhances their adhesion to the cementitious matrix, resulting in improved interfacial bonding and fracture toughness. In contrast, polypropylene fibers, due to their smooth and hydrophobic nature, showed limited interaction with the matrix, highlighting the importance of fiber surface treatment in optimizing mechanical performance.

While the study has provided substantial insights, it is not without limitations. The research primarily focused on flax and polypropylene fibers, and the findings may not be directly applicable to other types of fibers. Additionally, the long-term durability and performance of fiber-reinforced HPC under various environmental conditions require further investigation. Future research should

explore the effects of different fiber types, such as glass and synthetic fibers, and investigate the long-term behavior of fiber-reinforced HPC in real-world applications. Furthermore, the development of advanced surface treatments for natural fibers could enhance their compatibility with the cementitious matrix, leading to improved mechanical properties and durability.

In conclusion, this thesis has demonstrated the significant potential of fiber reinforcement in enhancing the performance of HPC. The findings provide a solid foundation for the development of optimized fiber-reinforced HPC formulations, contributing to the advancement of sustainable and resilient construction materials. The insights gained from this research are expected to guide future studies and practical applications, promoting the use of high-performance concretes in modern infrastructure projects.

Appendices

Appendices

NOTICE TECHNIQUE *Version 03* *Edition février 2017* 2 1 1 9

MEDAFLOW 30

Conforme à la norme NA 774 , NA 5102 et NA 5075

Super plastifiant-haut réducteur d'eau

Mode D'emploi

Le **MEDAFLOW 30** ne doit pas être ajouté directement dans l'eau de gâchage, mais après un temps préalable de malaxage et après que 50 à 70% de l'eau de gâchage ait été ajoutée.

Le **MEDAFLOW 30** peut être aussi ajouté directement dans le camion malaxeur (toupie), et après introduction de la dose convenable, le malaxeur devra tourner à grande vitesse pendant 2 à 3 minutes après l'introduction du super plastifiant ;

Il est conseillé d'ajouter le **MEDAFLOW 30** à un béton qui ne soit pas trop ferme

Dosage :

Plage de dosage recommandée :
0,5 à 2,0 % du poids de ciment soit 0,46 à 1,85 litre pour 100 Kg de ciment.
Le dosage optimal doit être déterminé sur chantier en fonction du type de béton et des effets recherchés

Conditionnement Et Stockage

Le **MEDAFLOW 30** est conditionné en bidons de 10Kg, fûts de 210 Kg et 240 Kg, cubique 1100kg.

Délai de conservation :
Une année dans son emballage d'origine, à l'abri du gel et de la chaleur (5°C < t < 35°C).
Lors d'une exposition du produit au soleil, sa couleur est sujette à changer de ton.

Précautions D'emploi

Manipulation non dangereuse.

Se référer à la Fiche de Données de Sécurité disponible sur : **www.granitex-dz.com**

NB : La couleur des produits à base de Polycarboxylates d'Ether (PCE) lors d'une exposition aux UV, est sujette à changer de ton , mais qui n' a aucune incidence sur les propriétés et les effets de l'adjuvant.
PV d'essais conforme aux normes, établi par le **CNERIB** en 22 AVR 2012

NOTICE TECHNIQUE *Version 03* *Edition février 2017* 2 1 1 9

MEDAFLOW 30

Conforme à la norme NA 774 , NA 5102 et NA 5075

Super plastifiant-haut réducteur d'eau

Description

Le **MEDAFLOW 30** est un super plastifiant haut réducteur d'eau de la troisième génération. Il est conçu à base de Polycarboxylates d'Ether qui améliore considérablement les propriétés des bétons.
Le **MEDAFLOW 30** permet d'obtenir des bétons et mortiers de très haute qualité.
En plus de sa fonction principale de super plastifiant, il permet sans modifier la consistance, de réduire fortement la teneur en eau du béton.
Le MEDAFLOW 30 ne présente pas d'effet de retard de prise.

Domaines D'application

•Les bétons de préfabrication.
•Les bétons prêts à l'emploi.
•Les bétons lourds et légers.
•Les bétons d'ouvrages d'art.
•Les bétons de dallages industriels.
•Les bétons de bâtiment.
•Les bétons précontraints.
•Les bétons pompés.
•Les bétons pour fondations profondes.
•Les bétons pour ouvrages fortement ferraillés.
•Les bétons soumis à des milieux agressifs.
•Les BHP, BTHP,BUHP et BFUP
•Les bétons autonivelants - bétons autoplaçants.
•Les bétons architectoniques.

Propriétés

Grâce à ses propriétés le **MEDAFLOW 30** permet :
Sur béton frais :
- Obtention d'un rapport E/C très faible
- Amélioration considérable de la fluidité
- Une très bonne maniabilité
- Éviter la ségrégation
- Faciliter la mise en œuvre du béton

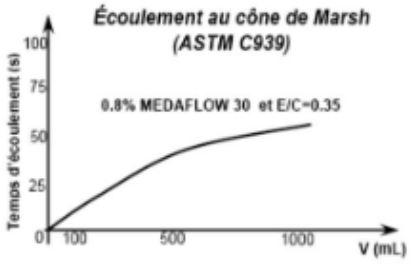

Sur béton durci :
- Augmenter les résistances mécaniques à jeune âge et à long terme (voir tableau).
- Diminuer la porosité
- Augmenter la durabilité
- Diminuer le retrait et le risque de fissuration

Désignation	Rc (MPa)		
	3J	7J	28J
MEDAFLOW 30 (1.4%)	39.2	54.7	62.2

Caractéristique

• Aspect ..... Liquide
• Couleur ..... Brun clair
• pH ..... 6 – 6,5
• Densité ..... 1, 07 ± 0,01
• Teneur en chlore ..... < 0,1 g/l
• Extrait sec 30%

Appendix A

Reference: Sample calculation

MIX DESIGN SHEET

Comp. Strength:	100 MPa

Table A	G_c	%
Cement	3.14	90
S.F.	2.2	10

		%		
Aggregate	G_{SSD}	w_{abs}	w_{tot}	w_h
Coarse	2.80	0.8	0.0	-0.8
Fine	2.65	1.2	3.5	2.3

$w_h = w_{tot} - w_{abs}$ $\quad M = M_{SSD}\ (1 + w_h)$

SUPERPLASTICIZER		$M_{sol} = C \times \frac{d}{100}$	$V_{liq} = \frac{M_{sol}}{s \times G_{sup}} \times 100$	$V_w = V_{liq} \times G_{sup} \times \left(\frac{100-s}{100}\right)$	$V_{sol} = V_{liq} - V_w = V_{liq}\left[1 - \left(\frac{100-s}{100}\right) \times G_{sup}\right]$
Spec. gravity (G_{sup})	Solids dosage s (%)	15 E	24 F	21 G	11 H
1.21	40	5	10.7	8.0	3.0

	1	2	3	4	5	6
MATERIALS	Content kg/m³	Volume l/m³	Dosage SSD conditions kg/m³	Water correction l/m³	Composition 1 m³	Composition Trial batch
WATER	2 140	2 140	2 140		23 124	25 11.5
$\frac{W}{B} = 0.27$ (1)						
CEMENT	3 520 — 4-1 470	8-1 150	4-1 470		4-1 470	26-1 43.7
SILICA FUME	4-2 50	8-2 23	4-2 50		4-2 50	26-2 4.7
	4-3 —	8-3 —	4-3 —		4-3 —	26-3 —
COARSE AGGREGATE	5 1075	9 384	5 1075	18 + 9	17 1066	27 99
FINE AGGREGATE		13 285	14 755	20 - 17	19 772	28 72
AIR	PERCENT 6 1.5 %	10 15	0			
SUPER-PLASTICIZER	7 1.0 %	11	15 5	21 - 8	24 V_{liq} 10.7	29 V_{liq} 1
TOTAL		12 715	16 2495	22 - 16		30 231

Box 1 Record the water/binder ratio

Box 2 Record the amount of water required, and report it in columns 1, 2 and 3 where box 2 appears.

Box 3 From the values appearing in boxes 1 and 2 calculate the necessary mass of binder.

Boxes 4–1, 4–2, 4–3 Calculate the mass of each of the different cementitious materials according to the cementitious composition selected appearing in Table A on the top part of the mix design sheet

and report it in columns 1, 3 and 5 where these boxes are found.

Box 5 Fill in the mass of coarse aggregate, and report it in columns 1 and 3 in box 5.

Box 6 Record the assumed air content.

Box 7 Record the amount of superplasticizer needed, obtained from the saturation point value.

At this stage, the only missing information is the mass of fine aggregate in the mix. This value is found by the absolute volume method, i.e. the volumes of all the ingredients already selected are calculated in order to find the volume of fine aggregate needed to make 1 m3 of concrete. This is done in column 2.

Boxes 8–1, 8–2, 8–3 The volumes of the different cementitious materials are calculated by dividing their masses, appearing in boxes 4–1, 4–2 and 4–3, by their respective specific gravities that have

been reported in the top part of the mix design sheet.

Box 9 The volume of coarse aggregate is calculated by dividing its mass (appearing in box 5) by its SSD specific gravity.

Box 10 The volume of entrapped air, in l/m3, is obtained by multiplying the air content (box 6) by 10.

Box 11 Calculate the volume Vsol (the volume of the solids contained in the superplasticizer) using the formulae presented in the middle part of the mix design sheet.

Box 12 The total mix volume (1000 l/m3) appears here.

Box 13 The volume of the fine aggregate in l/m3 is calculated by subtracting the volumes of all of the other ingredients (boxes 2, 8, 9, 10 and 11) from 1000.

The mass of fine aggregate and the unit mass of concrete can now be calculated. This is done in column 3.

Box 14 The mass of fine aggregate is calculated by multiplying its volume appearing in box 13 by its SSD specific gravity.

Box 15 The mass of solid in the superplasticizer Msol is reported here.

Box 16 All the masses appearing in column 3 are summed here to give the unit mass of the concrete.

Up to now the aggregate contents have been calculated on an SSD basis.

Next, the water dosage has to be corrected, taking into account the actual total water contents of the aggregates and the water brought into the mix by the liquid superplasticizer. These corrections are made in columns 4 and 5, in boxes 18, 20 and 21 with the following arbitrary sign convention: if aggregate brings water to the mix (i.e. if its moisture content is greater than its absorption with SSD state), its water content has to be subtracted from the water dosage, hence a negative sign will be used in the corresponding box, whereas a positive sign will be used when the aggregate will absorb some water from the mix.

Box 17 Multiply the SSD mass of coarse aggregate by (1+wh/100).

Box 18 Subtract the value in box 17 from that in box 5 and enter the result here.

Box 19 Calculate the SSD mass of the fine aggregate.

Box 20 Subtract the value in box 19 from that in box 14 and enter the result here.

Box 21 Write the amount of water brought to the mix by the superplasticizer from box G; the negative sign already appears in this box.

Box 22 Add algebraically all the water corrections.

The final composition of 1 m3 of concrete with the wet aggregates is now calculated in column 5.

Bibliographical references

Bibliographical references

1. Mehta, P.K. and P.J.M. Monteiro, *Concrete: Microstructure, Properties, and Materials*. 4th Edition ed. 2014, New York: McGraw-Hill Education.
2. Aïtcin, P.-C., *High Performance Concrete*. 1998: CRC Press.
3. Shah, S.P. and S. Ahmad, *High performance concretes and applications*. 1st Edition ed. 1994, Boca Raton, FL: CRC Press. 416.
4. De Larrard, F., *Concrete mixture proportioning*. 1999: CRC Press.
5. Malhotra, V.M. and P.K. Mehta, *Pozzolanic and Cementitious Materials*. 2014, London, England: CRC Press. 208.
6. *ACI 363R-10: Report on High-Strength Concrete.* ACI Committee, 2018. **363**.
7. Neville, A.M., *Properties of concrete*. 1995, Longman.
8. Mindess, S., J.F. Young, and D. Darwin, *Concrete*. 2003: Prentice Hall.
9. Bentur, A. and S. Mindess, *Fibre Reinforced Cementitious Composites, Second Edition*. 2 ed. Modern Concrete Technology. 2014, London, England: CRC Press. 624.
10. Brandt, A.M., *Fibre reinforced cement-based (FRC) composites after over 40 years of development in building and civil engineering.* Composite Structures, 2008. **86**(1): p. 3-9.
11. Richard, P. and M. Cheyrezy, *Composition of reactive powder concretes.* Cem. Concr. Res., 1995. **25**(7): p. 1501-1511.
12. Georges Dreux, J.F., *Nouveau guide du beton et de ses constituants*, Eyrolles, Editor. 1998.
13. D.BENAMARA, *Formulation et étude d''un béton à haute performance (BHP)*. 2011, Université de Biskra.
14. Xie, J., A. Elwi, and J. MacGregor, *Mechanical properties of three high-strength concretes containing silica fume.* Materials Journal, 1995. **92**(2): p. 135-145.
15. Neville, A.M., *Properties of Concrete*. 5 ed. 2011, London, England: Prentice-Hall. 872.
16. Tang, S., D. Huang, and Z. He, *A review of autogenous shrinkage models of concrete.* J. Build. Eng., 2021. **44**(103412): p. 103412.
17. *Proceedings of the Fifth International RILEM Symposium on Self-Compacting Concrete*. 2004: RILEM Publications.
18. Persson, B., *Experimental studies on shrinkage of high-performance concrete.* Cement and Concrete Research, 1998. **28**(7): p. 1023-1036.
19. Sicard, V., *Creep and shrinkage of high-strength concrete*, in *Proceedings of the Fifth International RILEM Symposium in*. 1993: Barcelona. p. 500-508.
20. *Fifth International Symposium on Creep and Shrinkage of Concrete (ConCreep-5).* Materials and Structures, 1994. **27**: p. 370-372.
21. *Technical guidelines for the design of concrete structures*. 1991.
22. Chaid, R., *Creep and shrinkage behavior of high-performance concrete with supplementary cementitious materials*, in *Proceedings of the Fifth International RILEM Symposium*. 1993: Barcelona, Spain.
23. *Report on high-performance concrete.* ACI Committee, 2010. **363**.
24. Bentur, A., S. Diamond, and N.S. Berke, *Steel corrosion in concrete: Fundamentals and applications. E & FN Spon*. 1997.
25. Elahi, A., et al., *Mechanical and durability properties of high performance concretes containing supplementary cementitious materials.* Construction and Building Materials, 2010. **24**(3): p. 292-299.
26. Taylor, H.F.W., *Cement Chemistry*. 1997: Emerald Publishing Limited.
27. Bentur, A., N. Berke, and S. Diamond, *Steel Corrosion in Concrete*. Modern Concrete

Technology. 2014, London, England: CRC Press.
28. Regourd, M., *Durabilité des bétons à hautes performances : réaction alcalis-granulats et carbonatation [Durability of high-performance concrete: Alkali-aggregate reaction and carbonation*, in *Les bétons à hautes performances : caractérisation, durabilité, application*, Y. Malier, Editor. 1992. p. 255-269.
29. Scrivener, K.L., A.K. Crumbie, and P. Laugesen, *The interfacial transition zone (ITZ) between cement paste and aggregate in concrete.* Interface Science, 2004. **12**(4): p. 411-421.
30. Richardson, I.G., *The nature of C-S-H in hardened cements.* Cement and Concrete Research, 1999. **29**(8): p. 1131-1147.
31. Agostini, F., et al., *Experimental study of accelerated leaching on hollow cylinders of mortar.* Cement and Concrete Research, 2007. **37**(1): p. 71-78.
32. Chatterji, S., N. Thaulow, and P. Christensen, *Puzzolanic activity of byproduct silica-fume from ferro-silicom production.* Cement and Concrete Research, 1982. **12**: p. 781-784.
33. Maiza, S., *Contribution À L'étude Des Propriétés Physico-mécaniques Des Bétons À Hautes Performances [Mémoire de Magister, Université M'hamed Bougara - Boumerdes*. 2012.
34. Ma, L., *The application of high performance in our lives.* Science and Technology of Engineering, Chemistry and Environmental Protection, 2023. **1**(2).
35. Wang, W., et al., *Application of high-performance Concrete in civil engineering.* Academic Journal of Science and Technology, 2024. **9**(2): p. 105-110.
36. Rashno, A., et al., *Investigation of Microstructure and Performance of Ultra-High-Performance Concrete for Transportation Infrastructure.* Transportation Research Record, 2024. **2678**(7): p. 819-834.
37. Wang, S., et al., *Ultra-high performance concrete: Mix design, raw materials and curing regimes-A review.* Materials Today Communications, 2023. **35**: p. 105468.
38. Laszlo, D., *High-Performance Concrete in the Confederation Bridge.* Concrete International. **20**(4).
39. Aïtcin, P.C., S. Mindess, and W.S. Langley, *8 - The Confederation Bridge*, in *Marine Concrete Structures*, M.G. Alexander, Editor. 2016, Woodhead Publishing. p. 199-214.
40. Naaman, A.E., *High performance fiber reinforced cement composites.* High-performance construction materials: Science and applications, 2008: p. 91-153.
41. *Report on Fiber-Reinforced Concrete (ACI 544.1R-96)*. 2018: American Concrete Institute.
42. *Report on Fiber-Reinforced Concrete*. 2018: American Concrete Institute.
43. Li, V.C., *Large volume, high-performance applications of fibers in civil engineering.* Journal of Applied Polymer Science, 2002. **83**(3): p. 660-686.
44. Shah, S.P., S.E. Swartz, and C. Ouyang, *Fracture mechanics of concrete*. 1995, Nashville, TN: John Wiley & Sons. 588.
45. Zollo, R.F., *Fiber-reinforced concrete: an overview after 30 years of development.* Cement and Concrete Composites, 1997. **19**(2): p. 107-122.
46. Johnston, C.D., *Fiber-reinforced cements and concretes*. 2014: Crc Press.
47. Naaman, A.E., *Engineered Steel Fibers with Optimal Properties for Reinforcement of Cement Composites.* Journal of Advanced Concrete Technology, 2003. **1**(3): p. 241-252.
48. Peled, A., A. Bentur, and B. Mobasher, *Textile reinforced concrete*. Modern Concrete Technology. 2019, London, England: CRC Press. 492.
49. Majumdar, A.J. and V. Laws, *Glass Fibre Reinforced Cement*. 1991, Philadelphia, PA: Blackwell Science. 208.
50. Bentur, A. and S. Mindess, *Fibre reinforced cementitious composites*. 2006: Crc Press.
51. Yin, S., et al., *Use of macro plastic fibres in concrete: A review.* Construction and Building Materials, 2015. **93**: p. 180-188.

52. Zhang, P. and Q.-f. Li, *Effect of polypropylene fiber on durability of concrete composite containing fly ash and silica fume.* Composites Part B: Engineering, 2013. **45**(1): p. 1587-1594.
53. Richardson, A.E., *Compressive strength of concrete with polypropylene fibre additions.* Structural Survey, 2006. **24**(2): p. 138-153.
54. Pacheco-Torgal, F. and S. Jalali, *Cementitious building materials reinforced with vegetable fibres: A review.* Construction and Building Materials, 2011. **25**(2): p. 575-581.
55. Aziz, M.A., P. Paramasivam, and S.L. Lee, *Prospects for natural fibre reinforced concretes in construction.* International Journal of Cement Composites and Lightweight Concrete, 1981. **3**(2): p. 123-132.
56. Yan, L., N. Chouw, and K. Jayaraman, *Effect of UV and water spraying on the mechanical properties of flax fabric reinforced polymer composites used for civil engineering applications.* Materials & Design, 2015. **71**: p. 17-25.
57. de Andrade Silva, F., et al., *Strain rate effect on the tensile behaviour of textile-reinforced concrete under static and dynamic loading.* Materials Science and Engineering: A, 2011. **528**(3): p. 1727-1734.
58. Brandt, A.M., *Fibre Reinforced Cement-Based (FRC) Composites After Over 40 Years of Development in Building and Civil Engineering.* Composite Structures, 2008. **86**(1-3): p. 3-9.
59. John, V.M. and V. Agopyan, *Durability of Natural Fibers in Concrete.* Cement and Concrete Composites, 2000. **22**: p. 127-136.
60. Shah, S.P. and Y. Ribakov, *Recent Trends in Steel Fibered High-Strength Concrete.* Materials and Structures, 2011. **44**(1): p. 107-119.
61. Ferrara, L., et al., *A comprehensive methodology to test the performance of steel fibre reinforced self-compacting concrete (SFR-SCC).* Construction and Building Materials, 2012. **37**: p. 406-424.
62. Shen, J. and Y. Zhang, *Fiber-reinforced Mechanism and Mechanical Performance of Composite Fibers Reinforced Concrete.* Journal of Wuhan University of Technology-Mater. Sci. Ed., 2020. **35**(1): p. 121-130.
63. Mena-Alonso, Á., et al., *Mechanical behavior of high-strength steel fiber-reinforced concrete*, in *Fiber-Reinforced Composites - Recent Advances, New Perspectives and Applications [Working Title]*. 2024, IntechOpen.
64. Kalifa, P., G. Chene, and C. Galle, *High-temperature behaviour of HPC with polypropylene fibres: From spalling to microstructure.* Cement and concrete research, 2001. **31**(10): p. 1487-1499.
65. Chen, Z., et al. *Influence of Modified PVA Fiber on Ultra-High Performance Concrete and Its Enhancing Mechanism*. Polymers, 2024. **16**, DOI: 10.3390/polym16233449.
66. Savastano Jr, H., et al., *Fracture and fatigue of natural fiber-reinforced cementitious composites.* Cement and Concrete Composites, 2009. **31**(4): p. 232-243.
67. Ali, M., et al., *Mechanical and dynamic properties of coconut fibre reinforced concrete.* Construction and Building Materials, 2012. **30**: p. 814-825.
68. Scott, D.A., et al., *New energy dissipation mechanisms for steel fiber reinforcement in ultra high-performance concrete.* Adv. Civ. Eng. Mater., 2019. **8**(3): p. 454-468.
69. Sanya, O.T. and J. Shi, *Ultra-high-performance fiber reinforced concrete review: constituents, properties, and applications.* Innovative Infrastructure Solutions, 2023. **8**(7): p. 188.
70. Wille, K., et al., *Ultra-high performance concrete and fiber reinforced concrete: achieving strength and ductility without heat curing.* Materials and structures, 2012. **45**: p. 309-324.
71. Toledo Filho, R.D., et al., *Free, restrained and drying shrinkage of cement mortar*

composites reinforced with vegetable fibres. Cement and concrete composites, 2005. **27**(5): p. 537-546.
72. Sonar, K. and S. Sathe, *Exploring fiber reinforcements in concrete and its challenges: a comprehensive review.* Multiscale and Multidisciplinary Modeling, Experiments and Design, 2024. **7**(4): p. 3099-3131.
73. Pickering, K.L., M.G.A. Efendy, and T.M. Le, *A review of recent developments in natural fibre composites and their mechanical performance.* Composites Part A: Applied Science and Manufacturing, 2016. **83**: p. 98-112.
74. Rady, M. and A.M. Soliman *Performance of Fiber-Reinforced Ultra-High-Performance Concrete Incorporated with Microencapsulated Phase Change Materials*. Fibers, 2023. **11**, DOI: 10.3390/fib11110094.
75. Turgut, P. and H. Murat Algin, *Limestone dust and wood sawdust as brick material.* Building and Environment, 2007. **42**(9): p. 3399-3403.
76. Afroughsabet, V., L. Biolzi, and T. Ozbakkaloglu, *High-performance fiber-reinforced concrete: a review.* Journal of Materials Science, 2016. **51**(14): p. 6517-6551.
77. Grunewald, S. and J.C. Walraven, *Parameter-study on the influence of steel fibers and coarse aggregate content of the fresh properties of self-compacting concrete.* Cement and Concrete Research, 2001. **31**: p. 1793-1798.
78. Khayat, K.H. and Y. Roussel, *Testing and performance of fiber-reinforced, self-consolidating concrete.* Materials and Structures, 2000. **33**(6): p. 391-397.
79. Martinie, L., P. Rossi, and N. Roussel, *Rheology of fiber reinforced cementitious materials: Classification and prediction.* Cement and Concrete Research, 2010. **40**: p. 226-234.
80. Markovic, I., *High-performance hybrid-fibre concrete: Development and utilisation (Doctoral dissertation)*. 2006.
81. Swamy, R., *The technology of steel fibre reinforced concrete for practical applications.* Proceedings of the Institution of Civil Engineers, 1974. **56**(2): p. 143-159.
82. Banthia, N. and M. Sappakittipakorn, *Toughness enhancement in steel fiber reinforced concrete through fiber hybridization.* Cement and Concrete Research, 2007. **37**(9): p. 1366-1372.
83. Li, V.C. and H.C. Wu, *Conditions for pseudo strain-hardening in fiber reinforced brittle matrix composites.* Applied Mechanics Reviews, 2018. **45**(8): p. 390-398.
84. Yoo, D.Y., S.T. Kang, and Y.S. Yoon, *Effect of fiber length and placement method on flexural behavior, tension-softening curve, and fiber distribution characteristics of UHPFRC.* Construction and Building Materials, 2015. **64**: p. 67-81.
85. Park, J.J., et al., *Benefits of using expansive and shrinkage-reducing agents in UHPC for volume stability.* Magazine of Concrete Research, 2012. **64**(3): p. 245-256.
86. Abbas, Y.M. and M.I. Khan, *Fiber-matrix interactions in fiber-reinforced high-performance concrete: A review.* Construction and Building Materials, 2016. **120**: p. 71-88.
87. Hsie, M., C. Tu, and P.S. Song, *Mechanical properties of polypropylene hybrid fiber-reinforced concrete.* Materials Science and Engineering: A, 2008. **494**(1): p. 153-157.
88. Qian, C.X. and P. Stroeven, *Development of hybrid polypropylene-steel fibre-reinforced concrete.* Cement and Concrete Research, 2000. **30**(1): p. 63-69.
89. Silva, F.d.A., N. Chawla, and R.D. de Toledo Filho, *An experimental investigation of the fatigue behavior of sisal fibers.* Materials Science and Engineering: A, 2009. **516**(1): p. 90-95.
90. Bos, H.L., M.J.A. Van Den Oever, and O.C.J.J. Peters, *Tensile and compressive properties of flax fibres for natural fibre reinforced composites.* Journal of Materials Science, 2002. **37**(8): p. 1683-1692.
91. Yan, L., N. Chouw, and K. Jayaraman, *Flax fibre and its composites – A review.*

Composites Part B: Engineering, 2014. **56**: p. 296-317.
92. Kayali, O., M.N. Haque, and B. Zhu, *Drying shrinkage of fibre-reinforced lightweight aggregate concrete containing fly ash.* Cement and Concrete Research, 1999. **29**(11): p. 1835-1840.
93. Wongtanakitcharoen, T. and A.E. Naaman, *Unrestrained early age shrinkage of concrete with polypropylene, PVA, and carbon fibers.* Materials and Structures, 2007. **40**(3): p. 289-300.
94. Zhang, J. and V.C. Li, *Effect of inclination angle on fiber rupture load in fiber reinforced cementitious composites.* Composites Science and Technology, 2002. **62**(6): p. 775-781.
95. Neville, A.M. and J.J. Brooks, *Concrete technology*. 2010: Prentice Hall.
96. Shen, D., et al., *Early-age behavior and cracking resistance of high-strength concrete reinforced with Dramix 3D steel fiber.* Construction and Building Materials, 2019. **196**: p. 307-316.
97. Thomas, J. and A. Ramaswamy, *Mechanical Properties of Steel Fiber-Reinforced Concrete.* Journal of Materials in Civil Engineering, 2007. **19**(5): p. 385-392.
98. Li, V.C. and T. Kanda, *Engineered Cementitious Composites for Structural Applications.* ASCE Journal of Materials in Civil Engineering, 1998. **10**(2): p. 66-69.
99. Zhang, P., Q. Li, and Z. Sun, *Influence of silica fume and polypropylene fiber on fracture properties of concrete composite containing fly ash.* J. Reinf. Plast. Compos., 2011. **30**(24): p. 1977-1988.
100. Ganesan, N., R. Abraham, and S. Deepa Raj, *Durability characteristics of steel fibre reinforced geopolymer concrete.* Construction and Building Materials, 2015. **93**: p. 471-476.
101. Meson, M., *Durability of steel fibre reinforced concrete in corrosive environments*. 2019.
102. Wang, H., et al., *Abrasion resistance of milling steel fibre-reinforced ultrahigh-performance concrete.* Mag. Concr. Res., 2024. **76**(13): p. 696-706.
103. Wang, W., et al., *Long-term performance of fiber reinforced cementitious composites with high ductility under seawater attack with different salinities.* Construction and Building Materials, 2022. **317**: p. 126164.
104. Hamzaoui, R., et al., *Microstructure and mechanical performance of modified mortar using hemp fibres and carbon nanotubes.* Materials & Design (1980-2015), 2014. **56**: p. 60-68.
105. Kriker, A., et al., *Mechanical properties of date palm fibres and concrete reinforced with date palm fibres in hot-dry climate.* Cement and Concrete Composites, 2005. **27**(5): p. 554-564.
106. Tolêdo Filho, R.D., et al., *Durability of alkali-sensitive sisal and coconut fibres in cement mortar composites.* Cement and Concrete Composites, 2000. **22**(2): p. 127-143.
107. Ali, M., X. Li, and N. Chouw, *Experimental investigations on bond strength between coconut fibre and concrete.* Materials & Design, 2013. **44**: p. 596-605.
108. Laifa, W., et al., *Caractérisation d'un béton autoplaçant avec addition de laitier cristallisé et renforcé par des fibres de polypropylène et de diss.* Synthèse: Revue des Sciences et de la Technologie, 2014. **29**(1): p. 100-110.
109. Pimentel, L.L., A.L. Beraldo, and H. Savastano Júnior, *Durability of cellulose-cement composites modified by polymer.* Engenharia Agrícola, 2006. **26**(2): p. 344-353.
110. Awwad, E., et al., *Studies on fiber-reinforced concrete using industrial hemp fibers.* Construction and Building Materials, 2012. **35**: p. 710-717.
111. Bahloul, O., A. Bourzam, and A. Bahloul, *Utilisation des fibres végétales dans le renforcement de mortiers de ciment (cas de l'alfa)*, in *sbeidco. 1st International Conference on Sustainable Built Environment Infrastructures in Developing Countries, ENSET*. 2009: Oran (Algeria.
112. Ozerkan, N.G., et al., *Mechanical performance and durability of treated palm fiber*

reinforced mortars. International Journal of Sustainable Built Environment, 2013. **2**(2): p. 131-142.
113. Gram, H.E., *Swedish Agency for Research Cooperation with Developing Countries*. 1984.
114. Ramli, M., W.H. Kwan, and N.F. Abas, *Strength and durability of coconut-fiber-reinforced concrete in aggressive environments.* Construction and Building Materials, 2013. **38**: p. 554-566.
115. Almeida Filho, F., et al., *Hardened properties of self-compacting concrete a statistical approach.* Construction and Building Materials, 2010. **24**(9): p. 1608-1615.
116. Mohr, B., J. Biernacki, and K. Kurtis, *Supplementary cementitious materials for mitigating degradation of kraft pulp fiber-cement composites.* Cement and Concrete Research, 2007. **37**(11): p. 1531-1543.
117. Agopyan, V., et al., *Developments on vegetable fibre-cement based materials in São Paulo, Brazil: an overview.* Cement and Concrete Composites, 2005. **27**(5): p. 527-536.
118. Toledo Filho, R.D., et al., *Development of vegetable fibre-mortar composites of improved durability.* Cement and concrete composites, 2003. **25**(2): p. 185-196.
119. Sedan, D., et al., *Mechanical properties of hemp fibre reinforced cement: Influence of the fibre/matrix interaction.* Journal of the European Ceramic Society, 2008. **28**(1): p. 183-192.
120. Rahimi, M., A. Omran, and A. Tagnit-Hamou, *Role of homogenization and surface treatment of flax fiber on performance of cement-based composites.* Cleaner Materials, 2022. **3**: p. 100037.
121. Lucile, *European flax fiber: quality and sustainability*. 2024.
122. Li, Q., et al., *Treatment methods for plant fibers for use as reinforcement in cement-based materials.* Cellulose, 2021. **28**(9): p. 5257-5268.
123. C39, A., *Standard Test Method for Compressive Strength of Cylindrical Concrete Specimens.* ASTM International, 2018.
124. C496, A., *Standard Test Method for Splitting Tensile Strength of Cylindrical Concrete Specimens.* ASTM International, 2011.
125. C78, A., *Standard Test Method for Flexural Strength of Concrete (Using Simple Beam with Third-Point Loading).* American Society for Testing and Materials, 2018.
126. C830, A., *Standard Test Methods for Apparent Porosity, Liquid Absorption, Apparent Specific Gravity, and Bulk Density of Refractory Shapes by Vacuum Pressure.* ASTM International, 2016.
127. C1585-20, A., *Standard Test Method for Measurement of Rate of Absorption of Water by Hydraulic-Cement Concretes*. 2020, ASTM International: West Conshohocken, PA.
128. C1784, A., *Standard Test Method for Using a Heat Flow Meter Apparatus for Measuring Thermal Transmission Properties of Insulations.* ASTM International, 2014.
129. P18-427, N., *Béton - Détermination des variations dimensionnelles entre deux faces opposées d'éprouvettes de béton durci.* Normes nationales et documents normatifs nationaux, 1996.
130. C143, A., *Standard Test Method for Slump of Hydraulic-Cement Concrete.* American Society for Testing and Materials. **vol. 15**.
131. *Norme Européenne NF EN 12350-6*, in *Essai pour béton frais -Partie*. 1999, Masse.
132. Française, N., *béton-Auscultation sonique, Éditions AFNOR*. Vol. 18. 1989, Paris.
133. Belkadi, A.A., *Contribution à l'étude de la durabilité et les performances des bétons autoplaçants (fibres végétales, milieu agressif, formulation, modélisation*, in *Génie Civil et Hydraulique*. 2018, UNIVERSITE MOHAMED KHIDER BISKRA.
134. Guehlouz, I., et al., *Experimental analysis of mechanical behavior, rheology, and endogenous shrinkage in high-performance concrete with flax and polypropylene fibers.* Construction and Building Materials, 2025. **460**: p. 139856.

135. Ren, G., et al., *Influence of sisal fibers on the mechanical performance of ultra-high performance concretes.* Construction and Building Materials, 2021. **286**: p. 122958.
136. Wu, Z., et al., *Static and dynamic compressive properties of ultra-high performance concrete (UHPC) with hybrid steel fiber reinforcements.* Cement and Concrete Composites, 2017. **79**: p. 148-157.
137. Gerland, F., et al., *Analysing the Influence of Fibers on Fresh Concrete Rheometry by the Use of Numerical Simulation.* Construction Materials, 2024. **4**(1): p. 128-153.
138. Zhang, K., C. Lin, and L. Pan, *Investigation of the Effect of Sisal Fibers on Rheological Properties of Cement Paste.* Journal of Materials in Civil Engineering, 2023. **35**(12): p. 04023463.
139. Ermeydan, M.A., *New Methodologies to Improve the Interfacial Interaction in Natural Fibre Polymer Composites*, in *Interfacial Bonding Characteristics in Natural Fiber Reinforced Polymer Composites: Fiber-matrix Interface In Biocomposites*, S. Krishnasamy, et al., Editors. 2024, Springer Nature Singapore: Singapore. p. 23-45.
140. Akeed, M.H., et al., *Ultra-high-performance fiber-reinforced concrete. Part I: Developments, principles, raw materials.* Case Studies in Construction Materials, 2022. **17**: p. e01290.
141. Gong, J., et al., *Utilization of fibers in ultra-high performance concrete: A review.* Composites Part B: Engineering, 2022. **241**: p. 109995.
142. Onuaguluchi, O. and N. Banthia, *Plant-based natural fibre reinforced cement composites: A review.* Cement and Concrete Composites, 2016. **68**: p. 96-108.
143. Belkadi, A.A., et al., *Effect of vegetable and synthetic fibers on mechanical performance and durability of Metakaolin-based mortars.* Journal of Adhesion Science and Technology, 2018. **32**(15): p. 1670-1686.
144. Zhao, R., et al., *Optimization Research of Sodium Hydroxide Pretreatment to Enhance the Thermal Properties of Straw–Mortar Composite Materials.* Sustainability, 2024. **16**(12): p. 5239.
145. Li, Z., et al., *Mechanical Performance and Strengthening Mechanism of Polymer Concretes Reinforced with Carbon Nanofiber and Epoxy Resin.* Coatings, 2023. **13**(11): p. 1964.
146. Nili, M. and V. Afroughsabet, *The effects of silica fume and polypropylene fibers on the impact resistance and mechanical properties of concrete.* Construction and Building Materials, 2010. **24**(6): p. 927-933.
147. Das, C.S., et al., *Performance evaluation of polypropylene fibre reinforced recycled aggregate concrete.* Construction and Building Materials, 2018. **189**: p. 649-659.
148. Kouta, N., J. Saliba, and N. Saiyouri, *Effect of flax fibers on early age shrinkage and cracking of earth concrete.* Construction and Building Materials, 2020. **254**: p. 119315.
149. Kawashima, S. and S.P. Shah, *Early-age autogenous and drying shrinkage behavior of cellulose fiber-reinforced cementitious materials.* Cement and Concrete Composites, 2011. **33**(2): p. 201-208.
150. Li, Z., X. Wang, and L. Wang, *Properties of hemp fibre reinforced concrete composites.* Composites Part A: Applied Science and Manufacturing, 2006. **37**(3): p. 497-505.
151. Tonoli, G.H.D., et al., *Cellulose modified fibres in cement based composites.* Composites Part A: Applied Science and Manufacturing, 2009. **40**(12): p. 2046-2053.
152. Rahimi, M., O.A. Hisseine, and A. Tagnit-Hamou, *Effectiveness of treated flax fibers in improving the early age behavior of high-performance concrete.* Journal of Building Engineering, 2022. **45**: p. 103448.
153. Wang, B., et al., *Pre-treatment of Flax Fibers for use in Rotationally Molded Biocomposites.* Journal of Reinforced Plastics and Composites, 2007. **26**(5): p. 447-463.
154. Page, J., et al., *Enhancement of the long-term mechanical performance of flax fiber-*

reinforced cementitious composites by using alternative binders. Journal of Building Engineering, 2021. **40**: p. 102323.
155. Ahmad, J., et al., *A Review on Failure Modes and Cracking Behaviors of Polypropylene Fibers Reinforced Concrete.* Buildings, 2022. **12**(11): p. 1951.
156. Ahmed, T.W., A.A.M. Ali, and R.S. Zidan, *Properties of high strength polypropylene fiber concrete containing recycled aggregate.* Construction and Building Materials, 2020. **241**: p. 118010.
157. Saba, N., et al., *A review on dynamic mechanical properties of natural fibre reinforced polymer composites.* Construction and Building Materials, 2016. **106**: p. 149-159.
158. Faruk, O., et al., *Biocomposites reinforced with natural fibers: 2000–2010.* Progress in Polymer Science, 2012. **37**(11): p. 1552-1596.
159. Li, X., L.G. Tabil, and S. Panigrahi, *Chemical Treatments of Natural Fiber for Use in Natural Fiber-Reinforced Composites: A Review.* Journal of Polymers and the Environment, 2007. **15**(1): p. 25-33.
160. Chiker, T., A.A. Belkadi, and S. Aggoun, *Physico-chemical and microstructural fire-induced alterations into metakaolin-based vegetable and polypropylene fibred mortars.* Construction and Building Materials, 2021. **276**: p. 122225.
161. Alhozaimy, A.M., P. Soroushian, and F. Mirza, *Mechanical properties of polypropylene fiber reinforced concrete and the effects of pozzolanic materials.* Cement and Concrete Composites, 1996. **18**(2): p. 85-92.
162. Anas, M., et al., *Fiber Reinforced Concrete: A Review.* Engineering Proceedings, 2022. **22**(1): p. 3.
163. Blazy, J. and R. Blazy, *Polypropylene fiber reinforced concrete and its application in creating architectural forms of public spaces.* Case Studies in Construction Materials, 2021. **14**: p. e00549.
164. Ahmad, J., et al., *Mechanical performance of concrete reinforced with polypropylene fibers (PPFs).* Journal of Engineered Fibers and Fabrics, 2021. **16**: p. 15589250211060399.
165. Khan, S.Z., et al., *Effect of Polypropylene Fibers and Cement on the Strength Improvement of Subgrade Lying on Expansive Soil.* Iranian Journal of Science and Technology, Transactions of Civil Engineering, 2022. **46**(1): p. 343-352.
166. Yoo, D.-Y., S.-T. Kang, and Y.-S. Yoon, *Effect of fiber length and placement method on flexural behavior, tension-softening curve, and fiber distribution characteristics of UHPFRC.* Construction and Building Materials, 2014. **64**: p. 67-81.
167. Derdour, D., M. Behim, and M. Benzerara, *Effect of date palm and polypropylene fibers on the characteristics of self-compacting concretes: comparative study.* Frattura ed Integrità Strutturale, 2023. **17**(64): p. 31-50.
168. Nassif, H., et al., *Restrained Shrinkage of High-Performance Ready-Mix Concrete Reinforced with Low Volume Fraction of Hybrid Fibers.* Polymers, 2022. **14**(22): p. 4934.
169. Statkauskas, M., A. GRINYS, and D. Vaičiukynienė, *Investigation of Concrete Shrinkage Reducing Additives.* Materials, 2022. **15**(9): p. 3407.
170. Saad, M., et al., *Potential of oleaginous flax fibre as mortar reinforcement.* Academic Journal of Civil Engineering, 2019. **37**(2): p. 263-269.
171. Dridi, M., S. Hachemi, and A.A. Belkadi, *Influence of styrene-butadiene rubber and pretreated hemp fibers on the properties of cement-based repair mortars.* European Journal of Environmental and Civil Engineering, 2023. **27**(1): p. 538-557.
172. Kessal, O., et al., *Bio-fiber reinforced roller compacted concrete designed for road construction: feasibility of date palm fibers in pavements.* European Journal of Environmental and Civil Engineering, 2023. **27**(3): p. 1224-1246.
173. Wang, D., et al., *Mechanical properties of high performance concrete reinforced with basalt*

fiber and polypropylene fiber. Construction and Building Materials, 2019. **197**: p. 464-473.
174. Tahwia, A.M., M. Mokhles, and W.E. Elemam, *Optimizing characteristics of high-performance concrete incorporating hybrid polypropylene fibers.* Innovative Infrastructure Solutions, 2023. **8**(11): p. 297.
175. Grzesiak, S., et al., *Influence of Fiber Addition on the Properties of High-Performance Concrete.* Materials, 2021. **14**(13): p. 3736.
176. Xu, D., et al., *Analysis of the hybrid composite materials reinforced with natural fibers considering digital image correlation (DIC) measurements.* Mechanics of Materials, 2019. **135**: p. 46-56.
177. del Rey Castillo, E., et al., *Digital image correlation (DIC) for measurement of strains and displacements in coarse, low volume-fraction FRP composites used in civil infrastructure.* Composite Structures, 2019. **212**: p. 43-57.
178. Pereira, E.B., G. Fischer, and J.A.O. Barros, *Effect of hybrid fiber reinforcement on the cracking process in fiber reinforced cementitious composites.* Cement and Concrete Composites, 2012. **34**(10): p. 1114-1123.
179. Berkouche, A., et al., *Enhancing Sustainable Construction Practices: Utilizing Heat-Treated Recycled Concrete Fines for Improving Slag-Based Geopolymer Materials.* Arabian Journal for Science and Engineering, 2024.
180. Saad, M., et al., *Effect of Natural and Polypropylene Fibers on early Age Cracking of Mortars.* Construction Technologies and Architecture, 2022. **1**: p. 103-112.